Exploration of medulloblastoma tumorigenesis engenders a mouse model of the rare tumor variant medullomyoblastoma

Shannon Swikert

Integrated Program in Neuroscience (IPN)

McGill University, Montreal

October 2020

A thesis submitted to McGill University in partial fulfillment of the requirements of the degree of Doctor of Philosophy

Table of Contents

Abstract

Understanding the molecular mechanisms underlying tumorigenesis not only provides insights into putative, targeted therapies but also elucidates key elements of normal development. Medulloblastoma (MB), the most common pediatric brain malignancy, can originate from cerebellar granule cell precursors (GCPs). This neoplastic transformation of GCPs is a multistep process, in which sustained activation of Sonic hedgehog (Shh) signaling is a key early event that is accompanied by collaborative mutations.

In the third chapter of this thesis, I focus on the Shh co-receptor Brother-of-Cdo (Boc). Previous work from our lab has demonstrated that Boc is necessary for Shh-induced DNA damage and that deletion of *Boc* drastically reduces tumor incidence in the *Patched1* heterozygous ($Ptch1^{+/-}$) mouse model of MB. As Boc is strongly expressed in human and mouse MB tumors, we wanted to probe the link between high Boc expression and DNA damage in GCPs. Specifically, we modeled upregulation of Boc through transient transfection of dissociated cerebellar cultures and showed that high levels of Boc in GCPs and non-GCPs are associated, at least temporarily, with phosphorylation of H2AX, a marker of DNA damage. Due to technical limitations of our experimental paradigm (namely the inefficient expression of Boc in GCPs), our efforts to uncover the molecular mechanism upstream of H2AX phosphorylation and to describe the activation of the DNA damage response (DDR) network are too ambiguous to make firm conclusions. Overall, the data provided suggest that electroporation of Boc in early postnatal cerebellar cells is genotoxic, likely leading to cell death; however, further work utilizing an alternative method to express Boc in GCPs is needed to verify this finding.

While exploring the role of Boc in MB tumorigenesis, our lab performed deep sequencing on mouse $Ptch1^{+/-}$ tumors with or without Boc expression. The fortuitous discovery of a spontaneous H1047R substitution within the *phosphoinositol 3-kinase catalytic subunit*

(*Pik3ca*), which encodes a constitutively active kinase, instigated the work depicted in chapter four. Hotspot activating mutations of *PIK3CA* such as the H1047R, known to be oncogenic, have been identified in human MB. Shockingly, generating mice with germline $Ptch1^{+/-}$ and spatially restricted $Pik3ca^{H1047R}$ ($Ptch1^{+/-}$;$Pik3ca^{H1047R}$) engenders tumors exhibiting elevated expression of genes associated with muscle identity and function. The presence of myogenic cells within MB tumors is characteristic of the rare variant medullomyoblastoma (MMB), and we show that MMB and $Ptch1^{+/-}$;$Pik3ca^{H1047R}$ tumors share transcriptional similarities. The effect of mutant PI3K on muscle marker expression occurs independent of *Ptch1* loss in the early postnatal cerebellum. Intriguingly, deletion of *Ptch1* and *Enhancer-of-Zeste 2* (*Ezh2*), the catalytic component of polycomb repressive complex 2 (PRC2), also produces a muscular phenotype in advanced tumors. Inhibition of Ezh2 enzymatic activity along with Shh stimulation was able to trigger muscle marker expression in GCPs *in vitro*. This phenotype seems to be linked to changes in the activity rather than the expression of Myoblast determination 1 (MyoD) – the myogenesis regulating factor endogenously expressed in a population of proliferating GCPs. Finally, we found that myogenic cells do not express the GCP transcription factor Paired box 6 (Pax6) but do express MyoD, implying that muscle marker expression represents a change in identity. In conclusion, manipulation of either PI3K or Ezh2 signaling in the developing cerebellum induces a myogenic phenotype that signifies a fate change of GCPs, likely the result of MyoD-dependent transcription. This work provides both important insights into a cell-of-origin of MMB, a poorly characterized MB variant, and novel tools for future work that could reveal therapeutic targets for MMB.

Résumé

Comprendre les mécanismes moléculaires responsables de la tumorigenèse permet non seulement d'identifier de nouvelles thérapies ciblées, mais aussi d'élucider les éléments clés du développement normal. Le médulloblastome (MB), la tumeur maligne cérébrale pédiatrique la plus courante, peut provenir de précurseurs de cellules granulaires cérébelleuses (GCP). Cette transformation néoplasique des GCP est un processus en plusieurs étapes, dans lequel l'activation prolongée de la signalisation Sonic Hedgehog (Shh) est un événement précoce et crucial, et qui par ailleurs s'accompagne de mutations collaboratives.

Dans le troisième chapitre de cette thèse, je me concentre sur le co-récepteur de Shh, Brother-of-Cdo (Boc). Des travaux antérieurs de notre laboratoire ont démontré que la suppression de Boc, qui est nécessaire à l'induction par Shh de dommages à l'ADN, réduit considérablement l'incidence des tumeurs dans le modèle de souris hétérozygote *Patched1* (*Ptch1*$^{+/-}$) de MB. Comme Boc est fortement exprimé dans les tumeurs MB humaines et murines, nous avons voulu comprendre le lien entre une expression élevée de Boc et les dommages à l'ADN induits dans les GCP. Plus précisément, nous avons modélisé la surexpression de Boc par transfection transitoire de cultures de cellules du cervelet dissociées et avons montré que des niveaux élevés de Boc dans les GCP et les non-GCP sont associés, au moins temporairement, à la phosphorylation de H2AX, un marqueur de dommages à l'ADN. En raison des limites techniques de notre paradigme expérimental (à savoir l'expression inefficace de Boc dans les GCP), nos résultats obtenus pour découvrir le mécanisme moléculaire en amont de la phosphorylation de H2AX ainsi que pour décrire l'activation de la réponse aux dommages à l'ADN, sont trop ambigus pour établir des conclusions formelles. Dans l'ensemble, les données fournies suggèrent que l'électroporation de Boc dans les cellules cérébelleuses postnatales

précoces est génotoxique, conduisant probablement à la mort cellulaire. Cependant, des travaux supplémentaires utilisant une méthode alternative pour exprimer Boc dans les GCP seront nécessaires pour vérifier ce résultat.

Tout en explorant le rôle de Boc dans la tumorigenèse des MB, notre laboratoire a effectué le séquençage de tumeurs de souris *Ptch1*$^{+/-}$ avec ou sans expression de Boc. La découverte fortuite d'une substitution (H1047R) spontanée au sein de la sous-unité catalytique du gène de l'enzyme phosphoinositol 3-kinase (*Pik3ca*), codant pour une kinase constitutivement active, nous a conduit à mener les travaux décrits au chapitre quatre. Des mutations activatrices de PIK3CA, telles que H1047R, connues pour être oncogéniques, ont été identifiées dans le MB humain. De manière surprenante, la génération de la lignée de souris *Ptch1*$^{+/-}$ associée avec l'expression localisée de *Pik3ca*^{H1047R} (*Ptch1*$^{+/-}$*; Pik3ca*^{H1047R}) engendre des tumeurs présentant une expression élevée de gènes associés à l'identité et à la fonction musculaires. La présence de cellules myogéniques dans les tumeurs MB est caractéristique de la variante rare du médullomyoblastome (MMB), et nous montrons que les tumeurs issues de MMB et les tumeurs issues des animaux *Ptch1*$^{+/-}$*; Pik3ca*^{H1047R} partagent des similitudes transcriptionnelles. L'effet du mutant PI3K sur l'expression des marqueurs musculaires se produit indépendamment de la perte de *Ptch1* dans le cervelet postnatal précoce. De façon intéressante, la suppression de *Ptch1* et *Enhancer-of-Zeste 2* (Ezh2), le composant enzymatique du complexe répressif polycomb 2 (PRC2), produit également un phénotype musculaire dans les tumeurs avancées. L'inhibition de l'activité enzymatique d'Ezh2 en combinaison avec la stimulation par Shh déclenche l'expression de marqueurs musculaires dans les GCP *in vitro*. Ce phénotype semble être lié à des changements d'activité du facteur de régulation de la myogenèse Myoblast determination 1 (MyoD), qui est exprimé de manière endogène chez certain GCP en prolifération. Enfin, nous

avons constaté que les cellules myogéniques n'expriment pas Paired box 6 (Pax6), un facteur de transcription typique des GCP, mais expriment MyoD. Cela implique que l'expression des marqueurs musculaires représente un changement d'identité. En conclusion, la manipulation de la signalisation PI3K ou d'Ezh2 dans le cervelet en développement induit un phénotype myogénique qui signifie un changement de destin des GCP, ce qui est probablement le résultat d'une transcription dépendante de MyoD. Ce travail fournit à la fois des informations importantes sur la cellule d'origine MMB, un type de cancer extrêmement méconnu, et de nouveau outils qui pourraient permettre de découvrir de nouvelles approches thérapeutiques contre le MMB.

Acknowledgments

First, I would like to thank my supervisor Frédéric Charron. At the outset, I asked each potential supervisor if they had space, funding, and interest in a new student. Two projects, seven years of stipends, and many meetings later, Dr. Charron has followed through with his assent.

The work presented in this thesis is a testament to the collaborative nature of research. Many thanks to Lukas Tamayo-Orrego, Chia-Lun Wu, and Amandine Bemmo for both their efforts and for guiding me along the way; to Ahmed Khedher, Moheb Ghobrial, Nicolas Bouchard, Frédéric Mille, Samer Salameh, Jean-Francois Michaud, and Francois Depault for their contributions (a detailed description follows); to our collaborators Maxime Uriarte and El Bachir Affar along with Hamza Farooq, Florence Cavalli, Sorana Morissy, and Michael Taylor; and to Cynthia Hawkins, Jean-Francois Coté, Jacques Drouin, and Vahab Soleimani for tissue and reagents. The IRCM provides a superb set of core facilities. Thanks to Dominic Fillion for all his microscopy assistance; to Odile Neyret, Myriam Rondeau and the members of the molecular biology platform for the RNA sequencing; to Simone Terouz of the histology platform for her advice; and most especially to the Animal Care facility including Jessica Barthe, Constantin Androne, Manon Laprise, Caroline Dube, Sara Demontigny, and Marie-Anne Riquelme Jacob.

I am heartily grateful to my advisory committee: Drs. El Bachir Affar, Javier Di Noia, and Stefano Stifani. I benefited both from their engaging and constructive feedback at my annual meetings and from their moral support during this last year. I would also like to thank my mentor, Dr. Adam Hendricks, for his advice and advocacy.

During my graduate training, I have received external funding from both McGill University's IPN and Faculty of Medicine and the IRCM Foundation that I appreciate.

I have worked with wonderful colleagues. Thank you to former members: Nicolas Bouchard, Julie Cardin, Tiphaine Dolique, Julien Ferent, Heather Keightly, Ahmed Khedher, Jeanne Madranges, Shirin Makihara, Steves Morin, Jimmy Peng, Samer Salameh, Tyler Sloan, Lukas Tamayo-Orrego, Michael Verwey and Cornelia Zorca. The last few months have been extra challenging, so I would like to especially thank current lab members: Nursen Balekoglu, Amandine Bemmo, Sara Calabretta, Francois Depault, Jean-Francois Michaud, Sushmetha Mohan, Frederic Racicot, Rachelle Sauve, Sabrina Schlienger, Chia-Lun Wu, and Patricia Yam. Every single member of this lab has taught me something; hence, they have each informed this thesis even if they did not directly contribute to the data. Most importantly, they are a jovial bunch, and we shared so many memorable activities. We laughed. We cried. We ate ice cream.

I have been lucky enough to be a part of both the IPN and IRCM communities. I would like to specifically recognize Drs. Josephine Nalbantoglu, Joe Rochford, Ed Ruthazer, Carl Ernst, and Joe Makkerh for their role in the IPN rotation program. I would also like to thank the members of the Takahashi, Kania, and Cayouette labs for their collaboration and camaraderie.

My time in Montreal has been sweetened by a stellar support network that is too many to enumerate. However, I would like to acknowledge my colleague, friend, and boxing buddy Camille Boudreau-Pinsonnault for all those Wednesdays of stress relief. Also, I am indebted to my Montreal family – Dipto, Basil, Eva, Fiona, and the rest of the VanChar clan.

I would like to thank my own crazy family for providing me a place of respite, love, and laughter during my trips home. Finally, and most importantly, this thesis is dedicated to my parents, Terri and Dennis Swikert, who always believed in me even when I did not believe in myself. Getting to this point took every ounce of strength, persistence, and resilience that I could muster, yet I would not have made it here without their unwavering love and support.

Preface and Contribution of Authors

This thesis was prepared by Shannon Swikert in accordance with McGill University "Thesis Guidelines" and is written in the traditional monograph style. Chapter 2 contains the methodology for the work depicted in Chapters 3 and 4, which represent original scholarship. Specifically, the data presented in Chapter 4 (and **Figure 1**-**7**) are part of an ongoing manuscript. The specific contribution of individual authors is detailed below:

Chapter 3 – "Probing the link between high expression of the Shh receptor Boc and DNA damage in GCPs" Swikert SM, Tamayo-Orrego L, Khedher A, and Charron F

The initial hypothesis and project conception – L. Tamayo-Orrego and F. Charron.

Experimental Design – S. Swikert, L. Tamayo-Orrego, and F. Charron

- *Figure 3-1:* All experiments conducted by S. Swikert. Similar results were obtained by L. Tamayo-Orrego and A. Kheder
- *Figure 3-2*: All experiments conducted by S. Swikert. Similar overnight SANT1 and GANT58 experiments were also conducted by L. Tamayo-Orrego and A. Khedher
- *Figure 3-3*: All experiments conducted by S. Swikert. Cytoplasmic deletion experiments (in Boc WT GCP cultures) were also performed by A. Khedher.
- *Figures 3-4, 3-5, 3-6*: All experiment were conducted by S. Swikert.

Data analysis, figure compilation, and chapter writing – S. Swikert with input from F. Charron

Chapter 4 – "Manipulation of PI3K or Ezh2 signaling in the developing mouse cerebellum induces a myogenic phenotype: Insights into a rare medulloblastoma variant" Swikert SM,

Bemmo A, Wu CL, Tamayo-Orrego L, Gobrial M, Bouchard N, Salameh S, Uriarte M, Michaud JF, Depault F, Affar EB, and Charron F

*JF Michaud and M. Uriate (EB Affar) performed experiments for the manuscript in preparation that are not included in this thesis

The initial hypothesis (MMB) – S. Swikert

Project conception – S. Swikert and F. Charron.

- Figure 1-7: Experimental design by F. Mille and F. Charron. Animal crossing and RNA sample preparation was done by F. Mille. Data analysis was conducted by N. Bouchard and A. Bemmo.
- Figure 4-1: Experimental design by L. Tamayo-Orrego and F. Charron. Animal crossing, RNA sample preparation, generation of tissue, and survival analysis was performed by L. Tamayo-Orrego. Bioinformatic analysis was conducted by N. Bouchard and A. Bemmo with input from S. Swikert and F. Charron. Immunostaining experiments conducted by M. Ghobrial and S. Swikert.
- Figure 4-2: Experimental design by A. Bemmo and F. Charron. Bioinformatics analysis by A. Bemmo with input by S. Swikert and F. Charron. Immunohistochemistry performed by S. Swikert.
- Figure 4-3: Experimental design by S. Swikert, M. Ghobrial, and F. Charron. Tissue generated by L. Tamayo-Orrego and S. Swikert. Experiments performed by M. Ghobrial and S. Salameh.
- Figure 4-4: Initial *ASXL3* mutation uncovered by A. Bemmo. Asxl3 CRISPR experiments were designed by C-L. Wu and F. Charron. Asxl3 CRISPR construct designed and

validated by F. Depault. Ezh2 experiments were designed by S. Swikert and F. Charron with input from C-L. Wu. *In utero* electroporation and tissue preparation was conducted by C-L Wu. Immunofluorescence performed by S. Swikert (panel B) and S. Salameh (panel C).

- *Figure 4-5*: Experimental design by S. Swikert and F. Charron. Experiments conducted and analyzed by S. Swikert with input from F. Charron.
- Figure 4-6: Experimental design by S. Swikert and F. Charron. Experiments conducted and analyzed by S. Salameh (panels C,D with input by S. Swikert) and S. Swikert (panels E,F,G). Lentivirus optimization and quality control was performed by C-L. Wu.
- *Figure 4-7*: Experimental design, execution, and analysis by S. Swikert with input from F. Charron.

Figure compilation – S. Swikert and A. Bemmo (bioinformatic graphs) with input from F. Charron

Chapter writing – S. Swikert with input from A. Bemmo, C-L. Wu, and F. Charron

Thesis editing: J. Ferent (who also translated the abstract into French), C-L Wu, A. Bemmo, and F. Charron

List of Figures and Tables

Chapter 1

Chapter 2

Chapter 3

List of Abbreviations

ACTA1	Skeletal muscle α-actin
APC	Adenomatous polyposis coli
ARID1A	AT-rich interacting domain-containing protein 1A
ASXL3	Additional sex combs-like 3
ATM	*Ataxia telangiectasia* mutated
ATR	*Ataxia telangiectasia* and Rad3-related
BAP1	BRCA1 associated protein 1
bHLH	Basic helix-loop-helix
BOC	Brother-of-Cdo
BOS	Bohring-Opitz syndrome
BPRS	Bainbridge-Ropers syndrome
BRCA2	Breast cancer 2
CDK6	Cyclin dependent kinase 6
CDO	CAM-related/downregulated by oncogenes
CHK1(2)	Checkpoint kinase 1(2)
CKM	Creatine muscle kinase
CMV	Cytomegalovirus
CNA	Copy Number Alteration
CNS	Central nervous system
CREBBP	CREB-binding protein
CRISPR	Clustered regularly interspaced short palindromic repeats
DDR	DNA damage response
DDX3X	DEAD-box helicase 3X-linked
DIV#	Day # *in vitro*
DMEM	Dulbecco's Modified Eagle Medium
DMSO	Dimethyl sulfoxide
DNA	Deoxyribonucleic acid
DOCK	Dedicator of cytokinesis
DSBs	Double-stranded breaks
e#	Embryonic day #
EGL	External granule layer
ELMO	Engulfment and Cell Motility
ENU	N-ethyl-N-nitrosourea
EZH2	Enhancer of Zeste 2
FBS	Fetal Bovine Serum
FC	Fold change
FNIII	Fibronectin II
G3/4-MB	Group 3/4 medulloblastoma
GAB1	GRB2-associated binding protein 1
GAS1	Growth arrest specific 1
GCPs	Granule cell precursors
GEF	Guanine nucleotide exchange factor
GFI1/1B	Growth factor independent 1/1B
GFP	Green fluorescent protein
GLI	Glioma-associated oncogene
GSEA	Gene set enrichment analysis
GSK-3β	glycogen synthase kinase 3β
H3K27(me^3/ac)	Trimethylation/acetylation of lysine 27 on histone 3
H3K4	Histone 3 lysine 4
HBSS	Hank's balanced salt solution
HEK293T	Human embryonic kidney 293T
hESC	Human embryonic stem cell
Hh	Hedgehog
hIPSC	Human induced pluripotent stem cells
hUBC	Human ubiquitin C
Ig	Immunoglobin
IGF1/2	Insulin-like growth factor 1/2
IGF1R	IGF1 Receptor
IGL	Internal granule layer
IRES	Internal ribosome entry site
KDM6A	Lysine-specific demethylase 6a

KMT2D	Lysine-specific methyltransferase 2D	**PR-DUB**	Polycomb repressive deubiquitinase
MAPK	Mitogen-activated protein kinase	**PTCH1**	Patched1
Math1	Mouse atonal homologue 1	**PTEN**	Phosphatase and tensin homolog
MB	Medulloblastoma	**PTF1A**	Pancreatic transcription factor 1a
MBEN	Medulloblastoma with extensive nodularity	**PWM**	Prospective white matter
MEF2	Myocyte enhancing factor 2	**RMS**	Rhabdomyosarcoma
MMB	Medullomyoblastoma	**RNA**	Ribonucleic acid
MRF	Myogenic regulatory factor	**RPM**	Rotations per minute
mTOR	mouse Target of rapamycin	**RT**	Room temperature
MYF5	Myogenic factor 5	**SERCA1**	Sarcoplasmic/endoplasmic reticulum calcium ATPase 1
MYOD	Myoblast determination 1	**SFK**	Src-famliy kinase
NOS	Not-otherwise-specified	**SHH**	Sonic hedgehog
NSC	Neural stem cell	**SMARCA4**	SWI/SNF-related matrix-associated actin-dependent regulator of chromatin subfamily A member 4
OTX2	Orthodenticle homeobox 2	**SMO**	Smoothened
p-	Phosphorylated	**Sox2**	SRY-box 2
P#	Post-natal day #	**SUFU**	Suppressor of fused
PALB2	Partner and localizer of BRCA2	**SWI/SNF**	Switch/Sucrose Non-Fermentable
PAX6	Paired box 6	**TBR2**	T-box brain 2
PBS	Phosphate buffered saline	**TERT**	Telomerase reverse transcriptase
PC1	Principal component 1	**TNNI2**	Troponin I2
PCA	Principal component analysis	**TNNT3**	Troponin T3
PDL	Poly-D-lysine	**TP53**	Tumor protein p53
PDX	Patient-derived xenograft	**TPM2**	Tropomyosin 2
PFA	Paraformaldehyde	**tSNE**	t-distributed stochastic neighbor embedding
PI3K	Phosphoinositol-3-kinase	**UBC**	Unipolar brush cell
PIK3CA	Phosphatidylinositol-3-kinase catalytic subunit A	**UV**	Ultraviolet
PIP_2	Phosphatidylinositol (4,5)-bisphosphate	**VZ**	Ventricular zone
PIP_3	Phosphatidylinositol (3,4,5)-triphosphate	**WNT**	Wingless-related integration site
PRC2	Polycomb repressive complex 2	**γ-H2AX**	Phosphorylated (serine 139) Histone 2A.X
PRDM6	PR/Set domain 6		

Chapter 1

Introduction

1.1 Exploring tumor initiation: two birds, one stone

The study of tumor initiating mechanisms, particularly in pediatric malignancies, lies at the interface of developmental and cancer biology. Cancer, a major public health concern, carries a lifetime risk of nearly 40% in the United States (Howlader et al., 2019). Given its wide impact, the identification of potential therapeutic targets is one important goal of exploring mechanisms of tumorigenesis. For medulloblastoma (MB), the most common brain malignancy of childhood, current treatments combine surgery, radiation, and/or chemotherapy, and though overall survival rates have improved to upwards of 70%, these therapies carry significant sequelae, such as secondary malignancies and neurodevelopmental deficits (Hovestadt et al., 2019a). Thus, the drive in the field is to cultivate more targeted treatments with less severe side effects.

Research into tumor formation can also provide a window into the world of normal development. Cancer predisposition syndromes – an umbrella term denoting those congenital mutations associated with an elevated risk of developing cancer – account for roughly 8% of pediatric tumors and 6% of MBs (Waszak et al., 2018; Zhang et al., 2015). Similar to early work in *Drosophila*, where mutagenesis was used to link genes such as *Hedgehog* (*Hh*) with their developmental function, the cancer phenotype resulting from germline mutations provides key clues about the normal function of those gene products (Nüsslein-Volhard and Wieschaus, 1980). For instance, Gorlin's syndrome, also known as nevoid basal cell carcinoma syndrome, is linked to multiple cancer types including MB and is caused by loss-of-function mutations in *Patched1* (*PTCH1*) (Gorlin, 1987; Hahn et al., 1996; Johnson et al., 1996). PTCH1 is a receptor for and negative regulator of Hh and its mammalian orthologue Sonic hedgehog (SHH) (Briscoe and Thérond, 2013; Chen and Struhl, 1996; Echelard et al., 1993), and subsequent studies showed that SHH signaling is mitogenic for cerebellar granule cell precursors (GCPs), an MB cell-of-

origin (Dahmane and Ruiz-i-Altaba, 1999; Schüller et al., 2008; Wallace, 1999; Wechsler-Reya and Scott, 1999; Yang et al., 2008).

As illustrated in the example above, one key element in the examination of neoplastic transformation is the tumor-initiating-cell because it focuses functional studies through the lens of context. While the anatomical location, morphology, and gene expression of tumor cells can provide strong evidence for the cell-of-origin, model systems like genetically engineered mice are powerful tools not only for delivering direct evidence of tumor-initiating-cells but also for documenting the process of tumor development. Contained in this thesis is the tale of how my interest in understanding the molecular mechanisms of MB tumorigenesis steered me towards the rare variant medullomyoblastoma (MMB) and its cell-of-origin.

1.2 Medulloblastoma

Bailey and Cushing originally coined the term "medulloblastoma" to define a specific type of brain tumor, often diagnosed in the first decade of life, that was composed of rounded cells with scanty cytoplasm – now referred to as classic histology (1925). Because these tumors were located in the cerebellum and extended to the roof 4th ventricle, they postulated that medulloblastomas derived from the "undifferentiated cells of the developing cerebellum."

As additional histology types were described, initial attempts to predict survival outcomes based on histopathology had mixed results (Bloom et al., 1969; Chatty and Earle, 1971; Miles et al., 1970). In general, large cell/anaplastic (LCA) tumors are associated with poor prognosis while the correlation of medulloblastoma with extensive nodularity (MBEN) with better outcomes depends on context (Cavalli et al., 2017; Eberhart et al., 2002; Giangaspero et al., 1999; Giangaspero et al., 1992; Korshunov et al., 2018; Rutkowski et al., 2010).

Interestingly, both desmoplastic medulloblastoma and MBEN are linked to SHH signaling and its components (Brugières et al., 2012; Garrè et al., 2009; Pietsch et al., 1997; Pomeroy et al., 2002).

Early work into the cytogenetic and molecular information of medulloblastoma revealed multiple recurrent events, of which the most common is isochromosome 17q (i17q) and/or loss of 17p (Albrecht et al., 1994; Bigner et al., 1988; Cogen et al., 1990). Other alterations include gain of chromosome 7, loss of 8p, and loss of 10q (Bayani et al., 2000; Eberhart et al., 2002; Nishizaki et al., 1999; Reardon et al., 1997). Of course, there is also loss of 9q, identified in both Gorlin's syndrome and sporadic MBs, which we now know contains the *PTCH1* locus (Farndon et al., 1992; Gailani et al., 1992; Hahn et al., 1996; Johnson et al., 1996; Schofield et al., 1995). In addition to comparative genomic hybridization, focal amplifications were also revealed through *in situ* hybridization for targets like MYC and MYCN (Aldosari et al., 2002; Bayani et al., 2000; Eberhart et al., 2002). Studies of the receptor tyrosine kinase ERBB2 (HER2), whose gene is located at 17q12, found that increased protein expression correlated with worse outcomes resulting in the launch of phase I and phase II clinical trials with the ERBB1 (EGFR)/ERBB2 dual inhibitor lapatinib (Bautista et al., 2017; Fouladi et al., 2010; Gilbertson et al., 1992; Gilbertson et al., 1997; Gilbertson, 2005). Unfortunately, the drug, which had limited side effects, did not display any significant anti-tumor activity possibly due to inefficient central nervous system (CNS) penetration, so the study was closed midway (Fouladi et al., 2013).

Starting in the early 2000s, an outpouring of large scale, deep sequencing studies have improved the molecular characterizations of MB from which a consensus of the scientific community established four molecular subgroups: Wingless Int-1 (WNT), Sonic Hedgehog (SHH), Group 3 (G3), and Group 4 (G4) (Cho et al., 2011; Diede et al., 2010; Jones et al., 2012;

Northcott et al., 2012; Parsons et al., 2011; Pugh et al., 2012; Robinson et al., 2012). Recent efforts have sought to address heterogeneity within the larger subgroups by further subdividing tumors (Cavalli et al., 2017; Northcott et al., 2017; Schwalbe et al., 2017; Sharma et al., 2019). To incorporate subgroup information into clinical oncology without abandoning the previous histology-based diagnostic system, the current World Health Organization (WHO) classification of CNS tumors aimed for an integrated approach (Louis et al., 2016). Ironically for MB, the result is two separate classification categories: one molecular – where the SHH subgroup is split by *TP53* (Tumor protein p53) status – and one histological – where variants other than classic, LCA, desmosplastic/nodular, and MBEN are lumped together as not-otherwise-specified. This two-tiered organization highlights an open question about the relationship, if any, that exists between histology and gene expression in MB tumors, and one way that current research has approached this is to analyze whether histology is predictive of outcome when accounting for molecular identity. For example, LCA tumors correlate with decreased survival in children with SHH-MB but are not prognostically significant in either G3- or G4-MB (Schwalbe et al., 2017).

1.2.1 Medullomyoblastoma

For more rare tumor variants, the scarcity of human tumor samples has hindered researchers' ability to conclusively extrapolate prognosis and molecular profile generalizations. For example, MMB, later re-named medulloblastoma with myogenic differentiation, is a rare variant that occurs mainly in the cerebellar vermis of children with a slight bias towards males and that is characterized by regions of differentiated muscle cells (Louis et al., 2007). It is most often diagnosed by histopathology and immunohistochemistry against muscle-specific antigens like desmin, myoglobin, or smooth muscle actin (**Table 1-1**). First described in 1933 by

Table 1-1. MMB case studies since 2004

No	Age, Sex	Tumor Location	Histologies (subgroup)	Muscle Marker IHC	Cytogenetics	Reference
1	15y, M	Left CPA; auditory canal	MMB	desmin; myoglobin		(Park et al., 2004)
2	7y, M	4th V	MMB; cartilage; tubular/glandular	SMA	i17q	(Ismail et al., 2005)
3	8y, M	Vermis (4th V)	MMB	myoglobin		(Jaiswal et al., 2005)
4	2y, M	Cb (4th V)	MMB; focal melanotic	muscle specific actin, myogenin, MyoD		(Nozza et al., 2008)
5	3.5y, F	PF midline (4th V)	MMB; melanotic	desmin		(Mehta et al., 2006)
6	3y, M	PF midline (4th V)	MMB	muscle specific actin, desmin	Trisomy 5 and 13, MYC gain, 1:17 translocation; i17q; loss of 9	(Lindberg et al., 2007)
7	7y, M	4th V	MMB; calcification	desmin		(Patel et al., 2007)
8	9y, M	Vermis (4th V)	MMB; calcification	desmin		(Chaturvedi et al., 2008)
9	7y, F	Vermis*	MMB	myogenin		(Er et al., 2008)
10	2.5y, M	Cb (4th V)	MMB; melanotic; focal LCA	desmin		(Granese et al., 2008)
11	49y, M	right Cb hemisphere, Vermis	MMB	SMA (neg); desmin, MyoD		(Ke et al., 2008)
12	2y, M	Vermis	MMB; melanotic; LCA	muscle specific actin, desmin, myogenin	MYC amp; i17q	(Polydorides et al., 2008)
13	28y, M	PF	MMB; melanotic; cartilage	SMA, desmin		
14	0.5y, F	PF	MMB; melanotic; cartilage foci	SMA (neg), desmin		
15	4y, M	PF	MMB; rare melanotic cells	SMA (neg), desmin		(Sachdeva et al., 2008)
16	3y, M	PF	MMB	SMA (neg), desmin		
17	4y, M	PF	MMB	SMA (neg), desmin		
18	8y, M	PF	MMB	SMA (neg), desmin		
19	4y, M	PF	MMB	SMA (neg), desmin		
20	6y, M	Vermis	MMB; melanotic; classic	desmin, myoglobin		(Sakata et al., 2008)
21	3y, F	Vermis; spinal metastasis	MMB; LCA	SMA; muscle specific actin; desmin; myoglobin		(Kido et al., 2009; Yoshino et al., 2011)
22	4y, M	4th V	MMB; melanotic	muscle specific actin; desmin; myogenin		(Borcek et al., 2011)
23	21y, M	PF	MMB	SMA; desmin		(Rattenberry et al., 2011)
24	1y, F	Vermis	MMB; LCA	SMA, myoglobin	Few cells with MYCN gains	(Smolle et al., 2012)
25	4y, F	4th V	MMB; focal LCA (SHH)	desmin, myogenin	MYC amp, i17q	(Wright et al., 2012)

26	7y, M	Cb (4thV)	MMB nodule; melanotic; cartilage; calcification; LCA	desmin		(Majumdar et al., 2013)
27	3y, M	4th V	MMB; melanotic; LCA		No MYC amp	(Fathaddin et al., 2014)
28	3.9y, M	4th V; spinal metastasis	MMB; focal LCA; melanotic; cartilage; bone (G3/4)	SMA; desmin	No MYC/MYCN amp; No CTNNB1 mutation; gain 1q, 17q; loss of 8, 21q	(Stefanits et al., 2014)
29	3y, F	PF	MMB; LCA	Myogenin	No MYCN; MYC amp (8 polyploidy)	(Crawford and Levy, 2015)
30	2y, M	Vermis (4th V)	MMB; melanotic (WNT)	desmin, myogenin	No MYC amp	(Rajeshwari et al., 2016)
31	3y, F	PF	MMB	desmin myogenin		(Sarkar et al., 2017)
32	8y, M	PF	MMB	desmin, myogenin		
33	4y, F	Vermis	MMB; classic (U)	SMA, desmin, myogenin		
34	7y, M	4th V	MMB; classic (U)	SMA, desmin (neg), myogenin (neg)		
35	15y, F	4th V	MMB; classic (U)	SMA, desmin (neg), myogenin (neg)		
36	5y, M	PF	MMB; classic; focal LCA (U)	SMA, desmin (neg), myogenin (neg)		(Gupta et al., 2018)
37	40y, F	Vermis	MMB; melanotic; desmoplastic; focal LCA (U)	SMA, desmin, myogenin (neg)		
38	2y, M	Vermis	MMB; classic (U)	SMA, desmin, myogenin		
39	3.6y, M	4th V	MMB; classic (U)	SMA (neg), desmin, myogenin		
40	7y, F	left Cb hemisphere	MMB; LCA (SHH TP53 mutant)	desmin	No MYC amp	(Rao et al., 2020)

Abbreviations: y, years; Cb, cerebellum; CPA, cerebellopontine angle; PF, posterior fossa; V, ventricle; LCA, large cell/anaplastic; U, unknown; SMA, smooth muscle actin; neg, negative; amp, amplification
, * indicates invasion hemispheres and brain stem

Marinesco and Goldstein, MMB research has mostly been confined to studies of individual or small sets of cases (Helton et al., 2004). Thus, the prognosis of an MMB diagnosis is still unclear with some groups reporting worse outcome compared to MB while others report no difference (Helton et al., 2004; Mahapatra et al., 1998), and in contrast to MB subgroups, almost nothing is known about the molecular drivers of the muscle phenotype.

In 2004, Helton *et al.* stated that 47 cases of MMB had been recorded in the literature. This number, which does not even include the 6 cases presented in that article, is still the standard reference point more than 15 years later (Rao et al., 2020). To fill this lacuna, **Table 1-1** provides a list of case studies since that publication, raising the current number of documented MMB cases to 93 (47+6+40).

Speculation about the source of the myogenic cells has dominated the discussion of MMB case studies, and four main hypotheses have been put forth with varying amounts of support. One is that MMBs are actually teratoid tumors, which implies that the cell-of-origin is an early multipotent stem cell (Er et al., 2008; Mahapatra et al., 1998). A defining feature of teratomas is the existence of cells from all three germ layers, and only rare examples of MMBs meet this criterion while most lack an endodermal component (Chowdhury et al., 1985; Ismail et al., 2005; Mahapatra et al., 1998). Another theory is that myogenic cells arise from multipotent mesenchymal/endothelial-derived stem cells that reside within the tumor; proponents of this theory focus on cases where myogenic cells were located near blood vessels (Lewis, 1973; Walter and Brucher, 1979). For others, the co-existence of myogenic and melanotic cells in a subset of tumors suggests that these cells derive from neural crest cells, which generate oculocutaneous melanin pigmented cells, that improperly migrated to the posterior fossa (**Table 1-1**) (Gupta et al., 2018; Rajeshwari et al., 2016).

The fourth, and most compelling, hypothesis is that the tumor-initiating-cell is also the source of the myoblastic cells (Helton et al., 2004; Kido et al., 2009; Lindberg et al., 2007). In those cases where cytogenetic information was extracted including one case with teratoma-like features, many of the alterations revealed, such as *MYC* amplifications and/or i17q, are typical of MB (**Table 1-1**) (Ismail et al., 2005). Crucially, *MYC* amplifications have been identified both in the tumor and myogenic cells, suggesting a common origin (Bai et al., 2012; Lindberg et al., 2007). Furthermore, in one instance, a subset of myoglobin-positive cells also expressed the neuronal marker synaptophysin, implying that the myogenic cells are neuronally-derived (Kido et al., 2009). The capacity of neuronal cells to undergo myogenic differentiation is also supported by examples where MB cell lines, rat cerebellar cell lines, and neural stem cells (NSCs) have been induced to express muscle-related genes (Bai et al., 2012; Galli et al., 2000; Valtz et al., 1991).

As mentioned above, some cases have been evaluated for genetic alterations, which led to one MMB being defined as a G3/4-MB (Stefanits et al., 2014). However, most attempts to classify MMBs into molecular subgroups have relied upon immunohistochemistry (Gupta et al., 2018; Rajeshwari et al., 2016; Rao et al., 2020; Wright et al., 2012). Although three tumors were diagnosed as either WNT- or SHH-MBs, seven other cases – all in the same study – did not meet clear subgroup criteria. Like other histology types, it is probable that MMBs appear in more than one molecular subgroup although the possibility that MMB is an independent molecular entity cannot be excluded. Deeper investigation into the molecular identity of MMBs will shed light on the potential heterogeneity of these tumors and be enhanced by the wealth of information uncovered in the last decade about MB molecular subgroups.

1.2.2 WNT-MB

The least frequent subgroup, WNT-MB (~10% of MB cases) is associated with the best outcomes and is rarely metastatic at diagnosis, thus encouraging new clinical trials to adopt de-escalated treatment protocols for this subgroup (**Figure 1-1**) (Ellison et al., 2005; Hovestadt et al., 2019a; NCT01878617; NCT02724579). Most cases of WNT-MB occur in children between the ages of 3 and 17 years with an equal distribution between males and females. It is the most homogenous of the four subgroups both in terms of histology, which is almost exclusively classic, and molecular profile, as it is mostly considered a single subtype (Hovestadt et al., 2019a; Northcott et al., 2017; Schwalbe et al., 2017).

Like Gorlin's syndrome and SHH-MB, early evidence for enhanced WNT signaling in MB came from studies of Turcot syndrome patients, specifically those with germline mutations in *Adenomatous polyposis coli* (*APC*) (Groden, 1995; Hamilton et al., 1995; Turcot et al., 1959; Van Meir, 1998). APC functions as part of a complex that retains β-catenin in the cytoplasm and triggers its degradation (Polakis, 2000; Taylor et al., 2000). Binding of the WNT ligand to its receptor induces release and nuclear translocation of β-catenin where it acts as a transcriptional co-activator. In WNT-MB, *APC* mutations (germline or somatic) are less common than and mutually exclusive with mutations in *CTNNB1*, the gene encoding β-catenin (Northcott et al., 2017; Zurawel et al., 1998). Together, mutations in these two driver genes account for more than 97% of all WNT-MBs (Northcott et al., 2017; Waszak et al., 2018). Other common co-driver events include mutations in *DEAD-box helicase 3X-linked* (*DDX3X*), an RNA helicase; mutations in members of the SWI/SNF (Switch/Sucrose Non-Fermentable) chromatin remodeling complex, specifically *SMARCA4* (*SWI/SNF-related matrix-associated actin-*

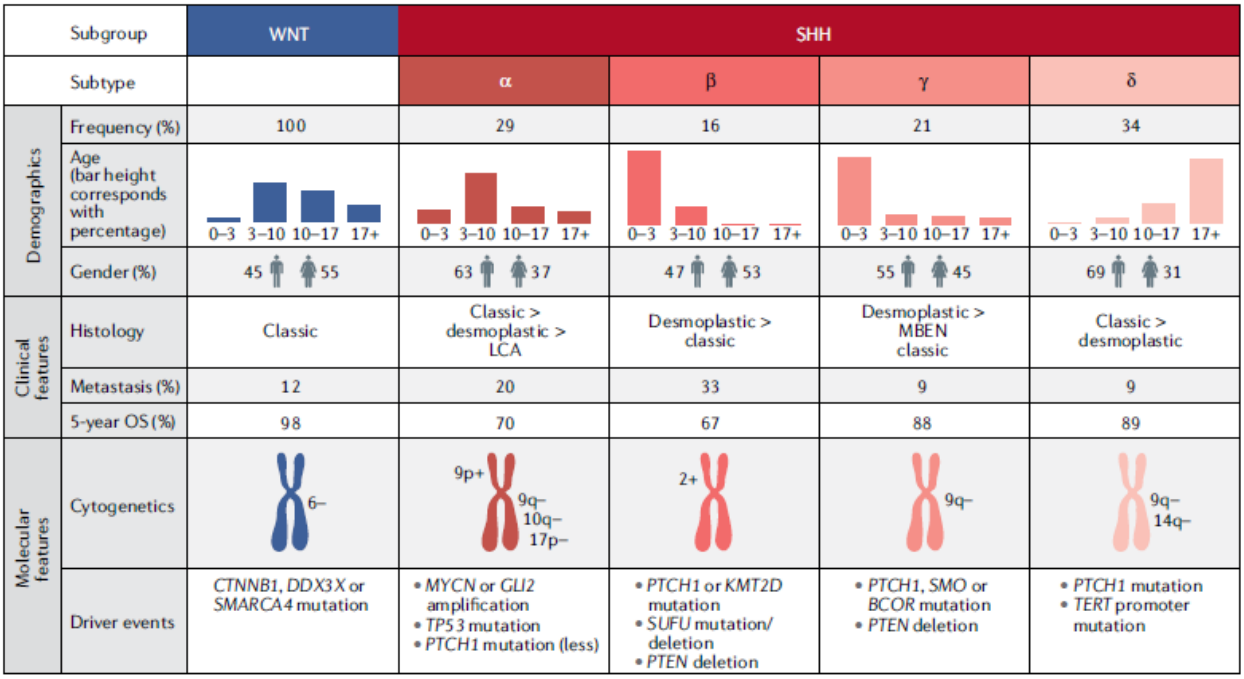

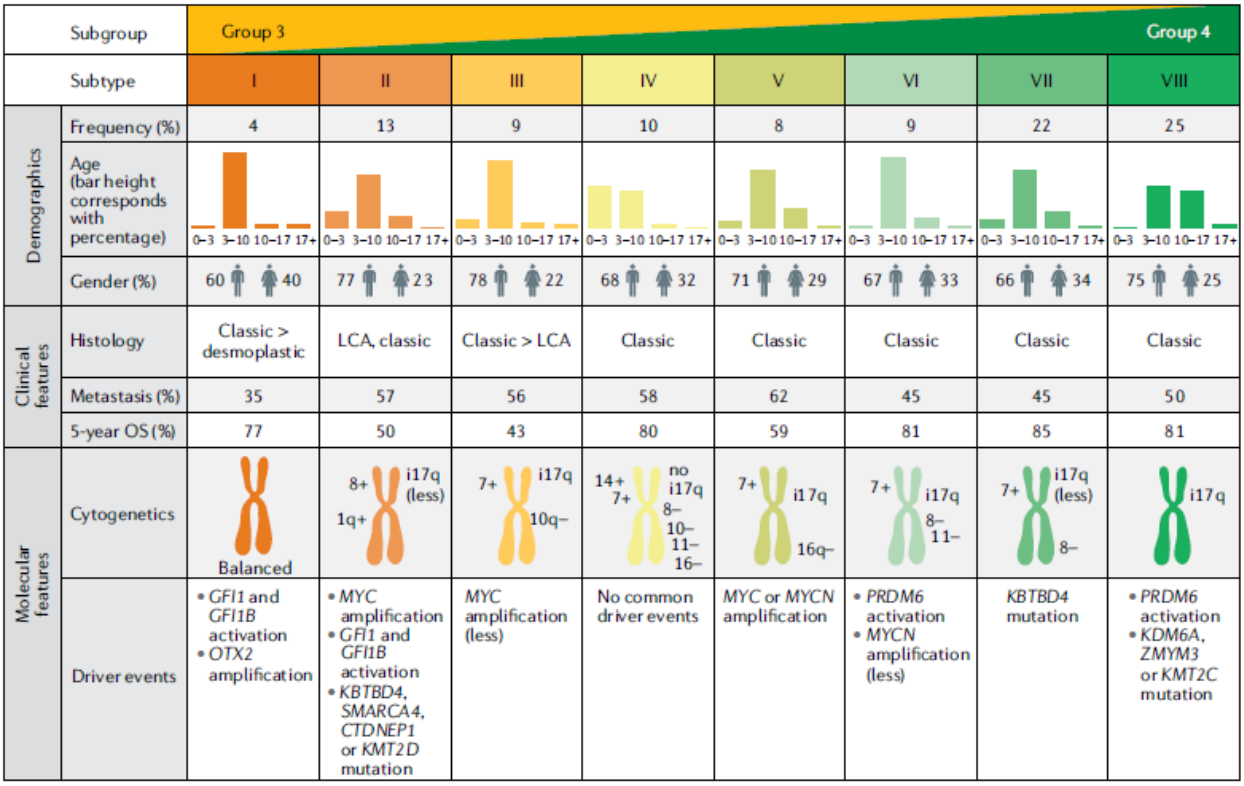

Figure 1-1. Overview of MB subgroups

Infographic of MB subgroups with subtype-specific patient, clinical, and molecular features. OS, overall survival. Subtype classifications for SHH are derived from Cavalli *et al.* (2017) while WNT is based on Scwhalbe *et al.* (2017) and the G3 and G4 subtypes come from both Northcott *et al.* (2017) and Sharma *et al.* (2019). Figure from (Hovestadt et al., 2019a).

dependent regulator of chromatin subfamily A member 4), *ARID1A* (*AT-rich interacting domain-containing protein 1A*), and *ARID2*; and loss of chromosome 6, which is the only recurrent copy number alteration (CNA) in WNT-MB (Hovestadt et al., 2019a; Jones et al., 2012; Northcott et al., 2017; Pugh et al., 2012; Robinson et al., 2012).

1.2.3 SHH-MB

SHH-MB accounts for about 30% of all MBs and is generally considered to be of intermediate risk (**Figure 1-1**) (Hovestadt et al., 2019a). It is the most common type of MB in infants, where it is evenly diagnosed in males and females, and in adults, where the male-to-female ratio is 2:1. Like its variable age distribution, all four major histology types are represented in SHH-MB. Age is a key factor in delineating SHH subtypes; SHHα encompasses most of the SHH-MBs in young children (3-10 years), whereas adults make up most of the SHHδ subtype and infants comprise the patients with SHHβ and SHHγ (Cavalli et al., 2017). Interestingly, MBEN tumors have better overall survival compared to other SHH-MBs correlating well with the fact that most of these tumors are within SHHγ, a subtype associated with better prognosis (Cavalli et al., 2017; Korshunov et al., 2018). However, MBEN is not a significant predictor of outcome within SHHγ (Cavalli et al., 2017).

The role of cancer predisposition syndromes has perhaps been best studied in SHH-MBs, yet the extent to which germline mutations drive tumorigenesis is still surprising. In one recent study, nearly 20% of all SHH-MBs contained germline mutations, including one infant with a germline *APC* mutation normally associated with WNT-MB and one infant with a germline *PTEN* (phosphatase and tensin homolog) mutation (Waszak et al., 2018). As expected, germline mutations in *PTCH1* and *SUFU* (Suppressor of fused), another mediator of SHH signaling, were

identified (Taylor et al., 2002; Waszak et al., 2018). In addition, germline *TP53* mutations, which cause Li-Fraumeni syndrome, are associated with SHH-MB (Rausch et al., 2012). Unlike *PTCH1*, *SUFU* and *TP53*, germline mutations in *BRCA2* (*Breast cancer 2*), previously linked with MB, and *PALB2* (*Partner and localizer of BRCA2*) were not exclusive to SHH-MB and were also discovered in G3- and G4-MBs (Alter et al., 2007; Waszak et al., 2018). Mutations of these two genes, both of which are Fanconi-Anemia genes, are associated with deficiencies in a specific type of DNA damage repair known as homologous recombination and are linked to breast cancer predisposition (Patel, 2007).

While germline *PTCH1* mutations or deletions are more prevalent in infants, somatic alterations occur at all ages (**Figure 1-1**) (Kool et al., 2014; Schwalbe et al., 2017; Waszak et al., 2018). Genetic aberrations in other SHH pathway components often occur in a more subtype-restricted manner; for example, *MYCN* and *GLI2* amplifications are associated with SHHα while *SUFU* and *SMO* (Smoothened) mutations are more frequent in SHHβ and SHHγ, respectively. Similarly, other driver mutations show a subtype preference. *TP53* mutations, more common in SHHα, are also associated with poor prognosis and as mentioned earlier, define a distinct subset of SHH-MBs recognized by the WHO (Cavalli et al., 2017; Louis et al., 2016; Schwalbe et al., 2017). *PTEN* deletions occur mostly in infants while *TERT* (*Telomerase reverse transcriptase*) promoter mutations are frequent in adults (Cavalli et al., 2017; Hovestadt et al., 2019a; Kool et al., 2014). Furthermore, *KMT2D* (*Lysine-specific methyltransferase 2D*; formerly *MLL2/4*) mutations are associated with SHHβ and *BCOR* (*BCL-6 corepressor*) mutations with SHHγ (Hovestadt et al., 2019a; Northcott et al., 2017).

The development of SMO inhibitors, such as vismodegib, presented an exciting opportunity to specifically target SHH-MB that was fueled by initial success in preclinical

models (Romer et al., 2004). However, prolonged treatment produces premature growth plate fusion in young mice and humans, so current trials restrict usage to "skeletally mature" participants (Kimura et al., 2008b; NCT01878617; Robinson et al., 2017). Even in these cases, drug efficacy is transient often due to acquired resistance through *de novo* mutations (Robinson et al., 2015; Rudin et al., 2009; Yauch et al., 2009).

1.2.4 Group 3- and Group 4-MB

Although distinct subgroups, G3-MB and G4-MB share the most molecular overlap, and as expected from their generic names, these are the least well understood MB categories. G3-MB accounts for ~25% of all cases, is more common in males (2:1), mainly occurs in young children (3-10) with some cases in infants, and is the subgroup most frequently associated with LCA histology although more G3-MBs have a classic phenotype (**Figure 1-1**) (Hovestadt et al., 2019a; Northcott et al., 2012). G4-MB is the most frequent (~35%) yet least understood subgroup. It is strongly biased towards males (3:1), is the most common subgroup among adolescents (10-17) and is mostly coupled with classic histology.

Among the first three seminal papers on subtyping, there was little consensus for G3- and G4-MBs (Cavalli et al., 2017; Northcott et al., 2017; Schwalbe et al., 2017). Hence, an additional round of analysis on 1501 G3/G4-MBs was conducted and produced an 8-subtype grouping that matched those of Northcott and company (**Figure 1-1**) (2017; Sharma et al., 2019). Although slightly counter-intuitive based on the diagram, subtypes II-IV are exclusively composed of G3-MBs, and subtype VIII is a G4 subtype; on the other hand, subtypes I and V-VII are a mixture of the two subgroups composed of more G4-MBs than G3-MBs.

Unlike WNT- and SHH-MBs, there are no clear associations between G3- or G4-MBs and cancer predisposition syndromes. Medulloblastoma cases in patients with Rubenstein-Taybi Syndrome, caused by deletions in the *CREBBP* (*CREB-binding protein*) locus located on chromosome 16p, have been reported in the literature (Taylor et al., 2001). More recently, germline *CREBBP* mutations have been identified in G3/G4-MBs, and loss of chromosome 16 recurrently occurs in subtype IV (Bourdeaut et al., 2014; Northcott et al., 2017; Waszak et al., 2018). Somatic *CREBBP* mutations, on the other hand, are more frequent in adults with SHH-MB (Merk et al., 2018). In general, CNAs rather than somatic mutations drive G3/4 tumors, including the highly prevalent i17q (Gröbner et al., 2018; Northcott et al., 2017). Additionally, amplification of *MYCN* and *OTX2* (*Orthodenticle homeobox 2*) drive shared subtypes (Hovestadt et al., 2019a). *MYC* amplifications, however, are restricted to G3-MBs. More recent studies have pinpointed structural changes that activate genes such as *Growth factor independent 1/1B* (*GFI1*/*GFI1B*) and *PR/Set domain 6* (*PRDM6*) via a phenomenon known as enhancer-hijacking, where the coding sequence of an oncogene is placed proximal to active [super] enhancers (Northcott et al., 2017; Northcott et al., 2014).

1.3 Cerebellar development

1.3.1 Cerebellar neurogenesis

Medulloblastoma is a disease of neuronal development; therefore, understanding the mechanisms fundamental to its formation requires knowledge of normal neurogenesis – specifically but not exclusively of the cerebellum. Cerebellar neuronal populations arise from two discrete germinal centers: the ventricular zone (VZ) (the source of inhibitory interneurons and glia) and the rhombic lip (the source of excitatory glutamatergic neurons) **(Figure 1-2A)**

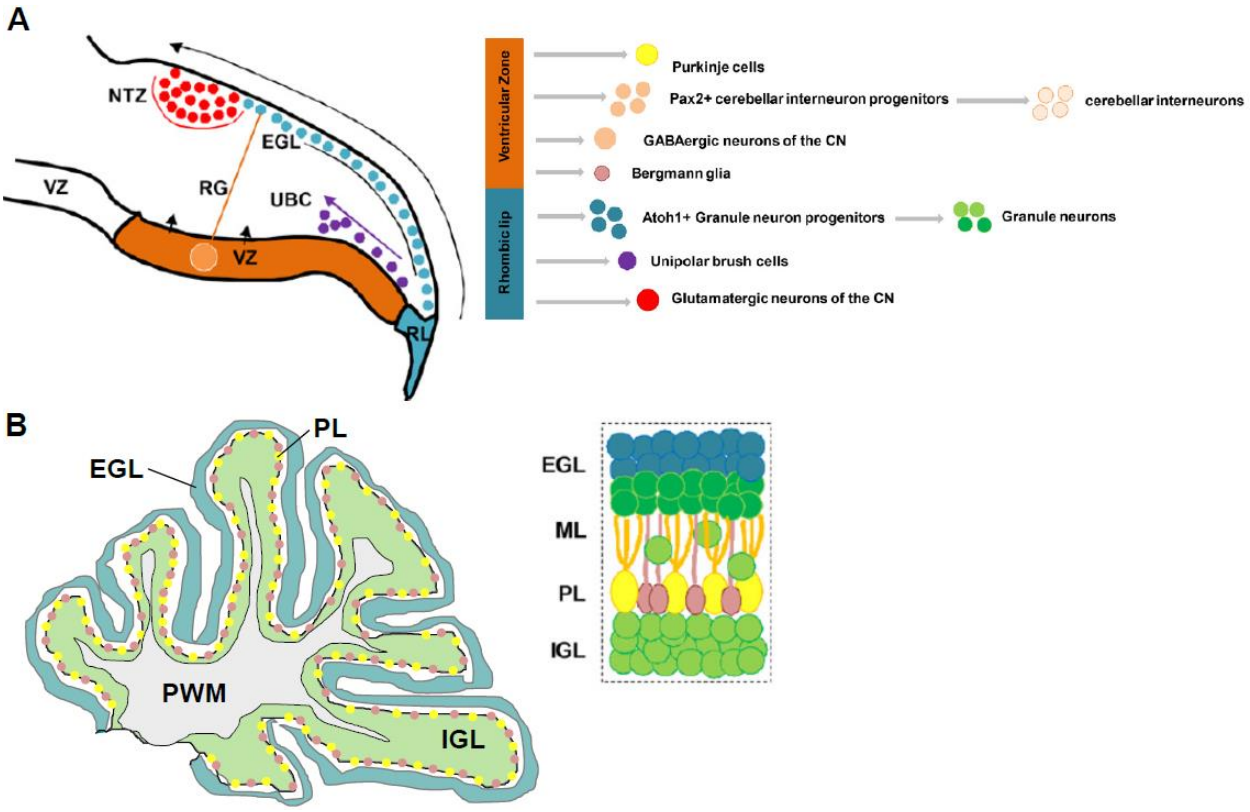

Figure 1-2. Schematic of embryonic and early postnatal cerebellar development
A) Embryonic neurogenesis arises from two zones as illustrated in this sagittal view of the cerebellar primordium (left) with detailed visualization of discrete pools of cell specification (right). The ventricular zone gives rise to glial cell populations and inhibitory neurons, including the Purkinje cells and interneurons, of the cerebellum. These cells then migrate along radial glia. The rhombic lip is the source of cerebellar glutamatergic neurons: cerebellar nuclei neurons, granule neuron progenitors (aka GCPs), and unipolar brush cells. These populations migrate tangentially into the cerebellar anlage. NTZ, nuclear transitory zone; EGL, external granule layer, RG, radial glia; UBC, unipolar brush cell; VZ, ventricular zone; RL, rhombic lip. Figure from (Haldipur and Millen, 2019).
B) GCP expansion in the EGL at the early postnatal stage. Sagittal view of P7 cerebellum (left) color coded to match the lamination schematic on the right. GCPs residing in the outer EGL (blue) will proliferate in response to Shh secreted from Purkinje cells (yellow). As the GCPs exit the cell cycle (dark green), they will migrate through the molecular and Purkinje layers into the IGL where they will reside as granule neurons (light green). ML, molecular layer; PL, Purkinje layer; IGL, internal granule layer; PWM, prospective white matter. Figure adapted from (Haldipur and Millen, 2019).

(Leto et al 2016). Current evidence from single cell RNA sequencing implicates early neural stem cells (NSCs) in the formation of G3-MB as the tumor bulk is mostly comprised of cells that align transcriptionally with undifferentiated progenitors which are interspersed with rare inhibitory and excitatory neuronal populations (Hovestadt et al., 2019b; Vladoiu et al., 2019).

The two neurogenic zones are specified between embryonic day 8.5 and 9.5 (e8.5-e9.5) in mouse via multiple morphogens orchestrated by a transient structure known as the Isthmic Organizer (Leto et al., 2016). Proper ventricular zone patterning of the cerebellum requires Pancreatic transcription factor 1a (*Ptf1a*), identified as the causative mutation in the *cerebelless* mouse line (Hoshino et al., 2005; Millen et al., 2014), and homozygous mutations engender rare cases of cerebellar agenesis in humans (Leto et al., 2016). Specification of deep cerebellar nuclei inhibitory interneurons initiates around e10.5, is brief (ending around e11.5), and partially overlaps with early born Purkinje cells (Haldipur and Millen, 2019; Leto et al., 2016). Starting around e13.5, the distribution of neurogenesis switches from Purkinje cell dominant production towards the generation of local interneuron progenitors. Excepting the earliest born Purkinje cells, VZ-derived cells migrate towards the cerebellar anlage along radial glia, the antecedents of Bergmann glia (**Figure 1-2A**).

Rhombic lip derived neurogenesis is a hotbed of tumorigenic potential. For example, the lower rhombic lip gives rise to dorsal brainstem progenitors, the cell-of-origin for WNT-MB (Gibson et al., 2010). The upper rhombic lip is characterized by expression of Math1 (mouse atonal homolog 1, ATOH-1 in humans), an essential transcription factor for these lineages (Leto et al., 2016). *Math1*-null mice have smaller rhombic lips and fail to produce glutamatergic neurons (**Figure 1-2A-B**) (Ben-Arie et al., 1997; Englund et al., 2006; Wang et al., 2005); whereas, *Math1* misexpression in the ventricular zone can induce ectopic expression of

glutamatergic neurons (Yamada et al., 2014). Unlike the VZ, where neuronal subtypes are generated from a common pool of progenitors, distinct progenitor populations drive specification in the rhombic lip (Leto et al., 2006; Machold and Fishell, 2005). First born are the deep cerebellar nuclei neurons (e10.5-e13.5) that sequentially express transcription factors Pax6 (Paired box 6), Tbr2 (T-box brain 2), and then Tbr1, which persists into adulthood (Fink et al., 2006; Wang et al., 2005). The next cells generated are GCPs (e13.5-postnatal), which express Pax6 but not Tbr1/2 (Hovestadt et al., 2019b; Machold and Fishell, 2005; Yamasaki et al., 2001). They are followed by unipolar brush cells (UBCs, e14.5-birth) that express Pax6 transiently and Tbr2 permanently but do not express Tbr1 (**Figure 1-2A**) (Englund et al., 2006; Hovestadt et al., 2019b).

While a plethora of data exists in support of GCPs as a cell-of-origin for SHH-MB, tumors may also emerge from cochlear nucleus progenitors that derive from the lower rhombic lip (Grammel et al., 2012; Schüller et al., 2008; Yang et al., 2008). For G4-MB, recent single cell RNA sequencing studies of human MB and normal mouse cerebella suggested that this subgroup may arise from progenitors of cerebellar nuclei neurons and UBCs, a finding that corroborates earlier evidence showing higher levels of *TBR1* and *TBR2* (aka *EOMES*) in G3 and G4 tumors (Hovestadt et al., 2019b; Jones et al., 2012; Vladoiu et al., 2019).

Following specification, the deep cerebella nuclei neurons migrate tangentially on the surface of the cerebellar anlage and aggregate to form the nuclear transitory zone prior to establishing individual nuclei (**Figure 1-2A**) (Fink et al., 2006; Haldipur and Millen, 2019; Machold and Fishell, 2005; Wang et al., 2005). Although GCPs follow a similar migratory route, they remain on the cerebellar surface where they form a secondary germinal zone known as the external granule layer (EGL) starting around e14.5. UBC migration occurs through the

prospective white matter (PWM) into the internal granule layer (IGL) without coalescing in a secondary tissue region (Englund et al., 2006; Haldipur and Millen, 2019).

1.3.2 GCP expansion and differentiation

Around birth, cerebellar cell production shifts to the PWM and the EGL, secondary germinal zones (**Figure 1-2B** left) (Leto et al., 2016; Wojcinski et al., 2017). The PWM gives rise to late born interneurons and glial cell populations, and it is comprised of pools of progenitors including NSCs that are distinguished by Prominin1 expression, neural progenitors expressing Nestin and Sox2 (SRY-box 2)[1] among other markers, and lineage restricted interneuron and astroglial progenitors (Lee et al., 2005; Leto et al., 2016; Wojcinski et al., 2017). The EGL solely drives production of cerebellar granule neurons, which are the most numerous neuron type making up more than 50% of the brain's total neuron population. In addition to the rhombic lip-derived GCPs, the EGL contains a small, transient population of less differentiated progenitors that express *hGFAP*-driven DsRed, Nestin, and/or Sox2, markers also present in a subset of cells in the Purkinje layer (Li et al., 2013; Selvadurai et al., 2020; Silbereis et al., 2010). These progenitors support the massive amplification of GCPs that occurs during the first two postnatal weeks in mice and that is associated with foliation of the cerebellar cortex.

Shh, which is released by Purkinje cells starting around e17.5, stimulates the proliferation of GCPs through its canonical signaling cascade (**Figure 1-3**) (Dahmane and Ruiz-i-Altaba, 1999; Izzi et al., 2011; Wallace, 1999; Wechsler-Reya and Scott, 1999). In the absence of ligand, the 12-pass transmembrane protein Ptch1 inhibits the activity of the 7-pass transmembrane

[1] Defining multipotent NSCs and more restricted progenitors with single markers is near impossible; for example, a subset of cells co-express Prominin1 and Sox2 (Tao et al., 2019). I tried to apply consistent naming throughout the thesis, but I acknowledge that cell states fall on a spectrum rather than a binary scale.

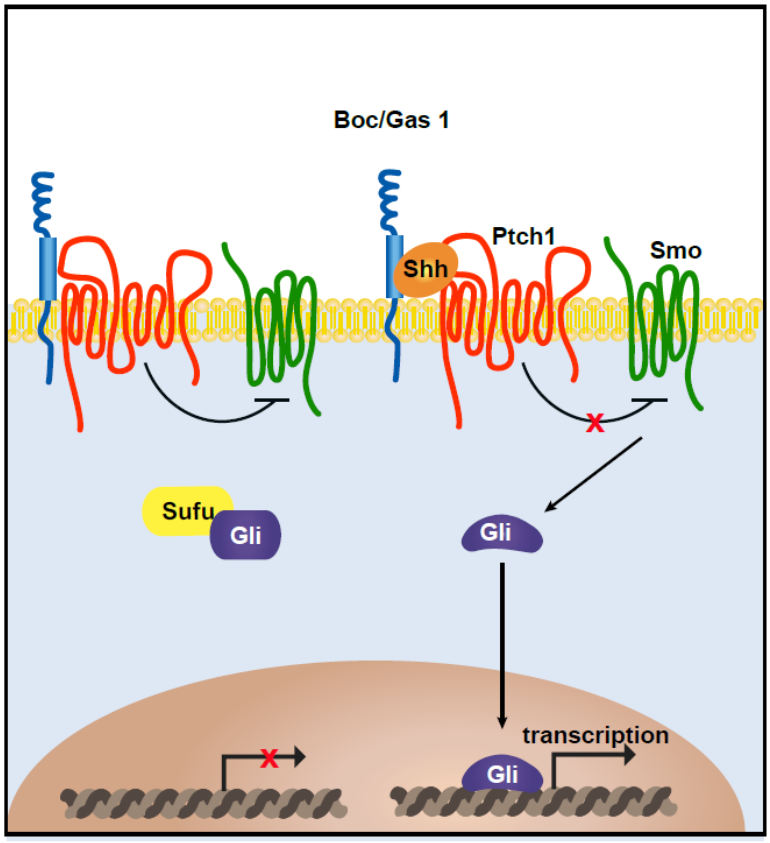

Figure 1-3. GCPs activate canonical Shh signaling during proliferation

Model of canonical Shh signaling. In the absence of ligand depicted on the left-hand side, Ptch1 inhibits Smo and Sufu binds Gli preventing its nuclear translocation. In the presence of Shh, Shh binds a receptor complex of Ptch1 and either Boc or Gas1, which relieves Smo inhibition resulting in activation of Gli-mediated transcription. Figure adapted from (Yam and Charron, 2013).

protein Smo while the transcription factor Gli is bound by Sufu, thereby sequestering Gli in the cytoplasm (Briscoe and Thérond, 2013). Shh binds to a receptor complex of both Ptch1 and one of the two co-receptors expressed by GCPs[2]: Brother-of-Cdo (Boc), a single-pass transmembrane protein, or Growth-arrest specific 1 (Gas1), a GPI-anchored protein (Izzi et al., 2011). While deletion of either *Boc* or *Gas1* leads to decreased proliferation in the EGL, loss of both receptors completely abolishes the ability of GCPs to respond to Shh stimulation (Izzi et al., 2011; Liu et al., 2001). Ligand-binding impedes Ptch1-dependent Smo inhibition resulting in Gli-mediated transcription of genes, such as *N-myc*, which is necessary for proliferation, *Cdk6* (*cyclin dependent kinase 6*), which is central for cell cycle progression, and even *Boc* itself (Lee et al., 2010; Oliver et al., 2003).

Along with Shh signaling, GCPs rely on Phosphatidylinositol 3-kinase (PI3K) and its effectors for proliferation (**Figure 1-4**). In this cascade, insulin-like growth factor 1 or 2 (IGF1/2) binds to the IGF1 receptor (IGF1R), a member of the receptor tyrosine kinase family, initiating autophosphorylation and interaction with PI3K (Weinberg, 2007). This interaction occurs via the PI3K regulatory subunit p85α (encoded by *Pik3R1*) and leads to allosteric activation of its catalytic subunit p110α (encoded by *Pik3ca*). PI3K catalyzes the conversion of phosphatidylinositol (4,5)-bisphosphate (PIP_2) to phosphatidylinositol (3,4,5)-triphosphate (PIP_3), an action that is opposed by the phosphatase Pten. PIP_3 production triggers the activation of the serine/threonine kinase Akt (originally named protein kinase B). Akt subsequently phosphorylates numerous downstream targets including mouse target of rapamycin (mTOR), an important regulator of protein translation; $p27^{Kip1}$, a Cdk inhibitor involved in the differentiation of GCPs; and glycogen synthase kinase 3β (GSK-3β), which phosphorylates many substrates

[2] CAM-related/downregulated by oncogenes (Cdo), a third Shh co-receptor is not expressed in GCPs.

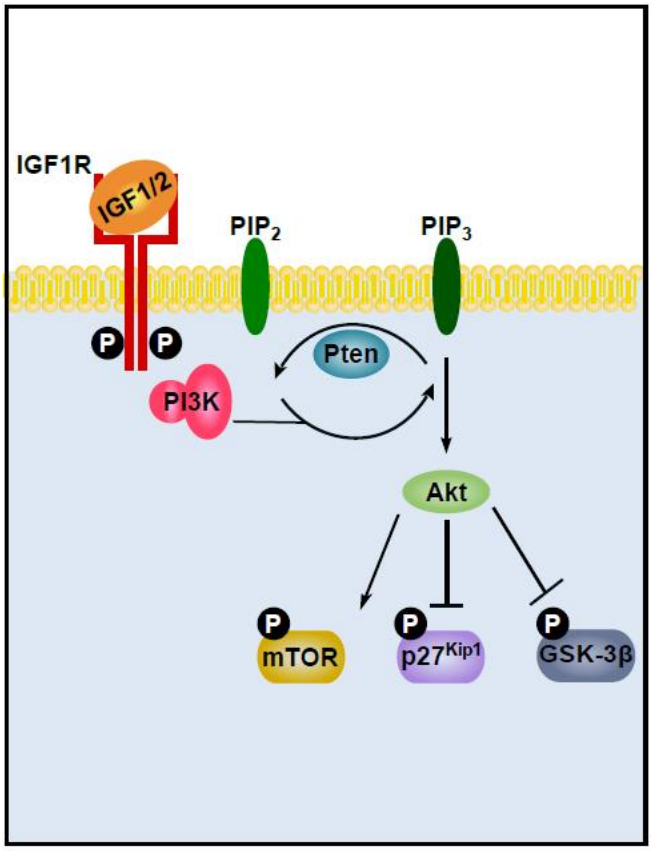

Figure 1-4. IGF also acts as a mitogen for GCPs

Model of the IGF/PI3K/Akt signaling cascade. IGF1 or IGF2 can bind IGF1R, which autophosphorylates and interacts with PI3K. Active PI3K converts PIP_2 to PIP_3 by phosphorylation while Pten catalyzes the reverse reaction. PIP_3 production triggers Akt activation which subsequently phosphorylates many downstream targets including mTOR, $p27^{Kip1}$, and GSK-3β. Figure adapted from (Yam and Charron, 2013).

including N-myc (Fresno Vara et al., 2004; Kenney et al., 2004; Miyazawa et al., 2000; Weinberg, 2007). Because phosphorylation of GSK-3β inhibits its activity, PI3K signaling results in stabilization of N-myc by preventing it from being phosphorylated by GSK-3β and thus targeted for degradation (Kenney et al., 2004).

Both Shh and PI3K pathways require the activity of N-myc, and to further highlight its importance in proliferation, overexpression of N-myc is sufficient to drive GCP proliferation *in vitro* independent of either mitogen (Kenney et al., 2003). In addition, conditional deletion of *N-myc* in neural progenitors leads to a smaller cerebellar anlage at e17.5 that includes a thinner EGL and obliterates the postnatal expansion of GCPs, producing a cerebellum that is 6 times smaller than wildtype by postnatal day 20 (P20) (Knoepfler et al., 2002). This convergence on N-myc may partially account for the synergistic effect of combined Shh and IGF1/2 administration compared to each mitogen individually (Fernandez et al., 2010). Intriguingly, administration of an IGF1R blocking antibody impedes IGF1- or Shh-mediated proliferation while inhibition of Shh signaling with cyclopamine had no effect when IGF1/2 is administered alone.

GCP proliferation, which continues until P14, peaks between P5 and P7, correlating with loss of the less differentiated progenitors (Li et al., 2013; Selvadurai et al., 2020). At P7, the outer region of the EGL contains actively proliferating GCPs, which move into the inner layer as they exit the cell cycle and begin to differentiate (**Figure 1-2B** right) (Haldipur and Millen, 2019). These inner EGL GCPs express $p27^{Kip1}$ and NeuroD1, a transcription key for GCP differentiation (Miyata et al., 1999; Miyazawa et al., 2000; Pan et al., 2009). Differentiated GCPs then migrate past the Purkinje cell layer to the IGL – a process that is completed by P21 (Haldipur and Millen, 2019). The mature granule neurons will then synapse with and stimulate Purkinje cells.

Less is known about cerebellar development in humans, whose cerebella are more foliated than those of mice. GCP expansion occurs over a prolonged period extending from the tenth gestational week until the end of the second postnatal year when no EGL remains (Haldipur and Millen, 2019). As a result, humans have more than 10 times as many granule neurons per Purkinje cell compared to mice. Uncovering the similarities and discrepancies between mouse and human development will facilitate critical analyses of animal MB models.

1.4 Oncogenic drivers derail normal development

Much of our knowledge about the functional consequences underlying genetic alterations of oncogenes and tumor suppressors has come from pre-clinical studies in model systems. Cancer cell lines are a cheap, easy, and rapid way to screen potential chemotherapies for efficacy, but they lack the complexity of an *in vivo* model, and long-term passaging fuels genetic and epigenetic changes that diverge from the initial sample (Neumann et al., 2017). Patient-derived xenograft (PDX) models are more expensive and slower than cell lines, but they offer a rare opportunity at 'personalized medicine' because a patient's treatment strategies can be selected based on the responsiveness of the model tumor.

Because cell lines and PDX models originate from advanced tumors and the focus of this thesis is the neoplastic transformation of GCPs in Shh-MB, a detailed though not exhaustive account of MB mouse models follows. Specifically, these are tumors that formed *in vivo* following 1) the manipulation of naïve cells – achieved by initiating tumorigenesis in mouse or human cells *in vitro* – followed by orthotopic transplantation of those cells into mice, 2) the direct transfection or viral-mediated transduction of cerebella in embryonic or postnatal mice, or 3) the use of transgenic mouse lines. These models are often technically arduous, can require the

use of immune-compromised mice, and may not fully recapitulate the identity and complexity of human tumors, but they provide means to study mechanisms of tumorigenesis in a controlled manner (Neumann et al., 2017; Pöschl et al., 2014).

1.4.1 Classical driver genes in MB

Juxtaposition of MB molecular profiling with paradigms of normal development were critical for the establishment of a Wnt-MB mouse model. The gene expression profiles of WNT tumors match that of the lower rhombic lip and the embryonic dorsal brainstem explaining why conditional activation of *Ctnnb1*[3], the most common significantly mutated gene in WNT-MB, in *Math1*-derived progenitors failed to induce tumors (Gibson et al., 2010; Gilbertson and Ellison, 2008). Instead, expression of a *Ctnnb1*-activating mutation in the developing hindbrain (*Blbp*-Cre) in combination with either partial or complete loss of *p53*, an essential tumor suppressor in many tissues, produces tumors at low penetrance (Gibson et al., 2010). Rather than effecting proliferation or survival, brainstem progenitors with mutant *Ctnnb1* displayed deficient migration leading to cell accumulation independent of p53. Tumor incidence increased to 100% with the addition of hyperactivated PI3K signaling by knocking-in an allele containing the E545K mutation of the PI3K catalytic subunit (*Pik3ca*^{E545K}), a mutation identified in human WNT-MB (Robinson et al., 2012). The same group has demonstrated that complete loss of *Ddx3x* in combination with mutant *Ctnnb1* and *p53*$^{+/-}$ had a variable effect on penetrance but led to cerebellar rather than brainstem tumors – indicative of a different tumor-initiating-cell (Patmore et al., 2020).

[3] Conditional transgenic models utilize restricted expression of the Cre-recombinase to excise DNA flanked by loxP sites. These models can also be inducible by fusing Cre to an estrogen receptor mutant (Cre^{ER}) (Reviewed in Feil et al., 2009).

By and large, there are more Shh-MB models compared to the other subgroups, and most of these involve genetically altering mediators of Shh signaling to increase GCP proliferation (Neumann et al., 2017; Roussel and Stripay, 2020). Shortly after the identification of *PTCH1* as the causative gene in Gorlin's syndrome, two separate groups created *Ptch1*$^{+/-}$ transgenic lines that develop medulloblastoma tumors at a low frequency[4] but will induce tumors in 100% of *p53*-null mice (Goodrich et al., 1997; Hahn et al., 1996; Hahn et al., 1998; Johnson et al., 1996; Wetmore et al., 2001). Specifically, *Ptch1*$^{+/-}$ tumors are most alike the Shhα subtype according to recently published data from our lab (Tamayo-Orrego et al., 2020). Targeted overexpression of Shh in neural progenitors can also induce tumors at a low rate (Rao et al., 2004); however, fully activating the pathway in the germline, such as *Ptch1*$^{-/-}$, is embryonic lethal, thereby mandating selective strategies for most models (Goodrich et al., 1997). Strong activation of Shh signaling specifically in GCPs, which retain their tumorigenic potential until P10, will produce tumors with high penetrance and can be achieved by homozygous deletion of *Ptch1*, activation of *Smo* by either a W539L (*SmoA1/M2*) or S537N (*SmoA2*) point mutation, or overexpression of Gli1 (Ayrault et al., 2010; Dey et al., 2012; Hallahan et al., 2004; Schüller et al., 2008; Yang et al., 2008). While those manipulations are sufficient to drive tumors, neither conditional *Sufu* deletion nor germline heterozygosity can produce tumors without additional genetic alterations such as *p53* deletion, possibly due to the newly recognized dual function of Sufu in promoting and inhibiting Gli activity (Lee et al., 2007; Yin et al., 2019).

Ptch1 loss or *Smo* activation in ventricular zone and/or rhombic lip progenitors that express *hGFAP*, *Olig2*, *Nestin* or *Sox2* will also fuel formation of MB, whose cellular and transcriptional composition is similar to those generated from unipotent GCPs, but it will not

[4] MB incidence in *Ptch1*$^{+/-}$ mice is only slightly increased when the homologue *Ptch2* is also deleted (Lee et al., 2006).

produce other types of brain tumors (Li et al., 2013; Schüller et al., 2008; Selvadurai et al., 2020; Yang et al., 2008). Although *p53*$^{-/-}$ mice are not predisposed to medulloblastoma, knocking out *p53* specifically in *Nestin*-expressing cells will trigger brain tumors, half of which are MBs (Wetmore et al., 2001; Zhu et al., 2017). Similarly, Shh-MBs can be induced with variable penetrance in mice by transplanting neuroepithelial stem cells derived from human induced pluripotent stem cells (iPSCs) that were either transduced with *MYCN* or that originated from a Gorlin's syndrome patient's keratinocytes (Huang et al., 2019). Overexpression of a stable N-myc mutant (N-myc^{T58A}) in GFAP^{+} NSCs from the e16 cerebellum also induced tumors that expressed markers associated with Shh-MB when transplanted into nude mice (Swartling et al., 2012); on the other hand, the same manipulation of P0 cerebellar NSCs, which do not generate GCPs *in vivo*, triggered G3-MBs (Pöschl et al., 2014; Swartling et al., 2012). Collectively, these data signify that GCP specification is necessary in Shh-MB tumorigenesis.

PI3K signaling is important for neoplastic transformation in Shh-MB, but it is not sufficient to induce tumorigenesis alone. A study of human MBs showed that 10 of 17 tumors were positive for phosphorylated IGF1R (p-IGF1R), a proxy for pathway activation, and that tumors displayed higher levels of IGF1R and p-Akt, another marker of PI3K signaling, compared to the normal fetal cerebellum but expression of the p85 PI3K subunit was unchanged (Del Valle et al., 2002). Moreover, desmoplastic human MBs – a histology type that is overrepresented in the SHH subgroup – express higher IGF2 levels compared to classic MBs (Hartmann et al., 2005; Pomeroy et al., 2002), and loss of *Ptch1* increases *Igf2* expression in the early murine embryo in a dose dependent manner (Hahn et al., 2000). Shh-MBs cannot form in the absence of PI3K signaling components. For examples, deletion of *Igf2* prevents tumor formation in *Ptch1*$^{+/-}$ mice without affecting the incidence of preneoplastic lesions (Corcoran et

al., 2008; Hahn et al., 2000), and conditional knockout of *IGF1R* in *Ptch1*$^{+/-}$, *p53*-null GCPs increased tumor latency and drastically reduced their size (Yao et al., 2020). Conversely, targeted retroviral expression of IGF2 or activated Akt in combination with Shh increased the frequency of tumors compared to Shh alone (Rao et al., 2004), and *Ptch1*$^{+/-}$ mice that overexpressed IGF1 had a higher incidence of advanced tumors without affecting the rate of preneoplastic lesions at P21 (Tanori et al., 2010). Likewise, loss of either one or both alleles of *Pten* or constitutive activation of PI3K via an H1047R mutation of the p110α subunit promote tumor formation in multiple Shh-MB models (Castellino et al., 2010; Metcalfe et al., 2013; Niesen et al., 2020; Zhu et al., 2017). Of note, *Pten* deficient tumors display increased neuronal differentiation and can even present an MBEN histology, features associated with SHH-MB in infants where *PTEN* deletions most often occur (**Figure 1-1)** (Castellino et al., 2010; Cavalli et al., 2017; Metcalfe et al., 2013; Zhu et al., 2017).

Many mouse models have exploited dysregulation of cell cycle exit and GCP differentiation in boosting Shh-MB tumorigenesis. For instance, combined deletion of *p53* and the cell cycle regulator Retinoblastoma (*Rb*) using a *GFAP*-Cre instigated MB formation in 100% of mice (Marino et al., 2000). Furthermore, overexpression of *Math1*, normally expressed in proliferating GCPs, increased the incidence and decreased the latency of Gli1-driven tumors, and these Math1+Gli1 tumors expressed lower levels of genes associated with cell cycle exit and neuronal differentiation (Ayrault et al., 2010). Loss of either *p27*^{Kip1}, which inhibits Cdk2 and is expressed in postmitotic granule neurons throughout adulthood, or *p18*^{Ink4c}, which targets Cdk4/6 and is transiently expressed by GCPs as they exit the cell cycle, will collaborate with either *Ptch1*$^{+/-}$ or *p53*$^{-/-}$ to produce MBs (Ayrault et al., 2009; Lee et al., 2003; Uziel et al., 2005; Zindy

et al., 2003). Conversely, conditionally knocking out *Cdk6* in a *Math1*-driven Shh-MB model extends the lifespan of mice compared to wildtype controls (Raleigh et al., 2018).

Nearly all mouse models of G3-MB involve Myc overexpression. Though Myc increases proliferation of NSCs, it is a strong inducer of apoptosis, so two groups utilized orthotopic transplantation of retroviral-mediated Myc (wildtype or the T58A stable mutant) overexpression and p53 loss-of-function (transgenic knock-out or expression of a dominant-negative mutant) as a work around to generate tumors (Kawauchi et al., 2012; Pei et al., 2012). Similarly, combined overexpression of Myc and Bcl-2, which is an anti-apoptotic protein, can also lead to tumor formation (Jenkins et al., 2016). Since 2012, the Myc-p53 model has expanded to include an assortment of techniques to upregulate Myc, such as CRISPR-directed endogenous expression (Vo et al., 2018). More importantly, selective overexpression of Myc can induce G3-MB tumors, with variable efficacy, from a number of different embryonic and postnatal cell types[5] – early hindbrain (*Blbp*-Cre), cerebellar ventricular zone progenitors (*Ptf1a*-Cre), neural progenitors (*Nestin*-Cre), inhibitory interneurons (*Pax2*-Cre), postnatal NSCs (*Prominin1*-Cre^{ER}), and even GCPs (*Math1*-Cre^{ER}, *Math1*-Cre) (Jenkins et al., 2016; Kawauchi et al., 2017). The downregulation of Math1 expression in *Math1*-derived Myc-p53 models and the NSC-like gene expression profiles of G3-MBs suggest that Myc not only blocks NSC differentiation but can also activate de-differentiation during tumorigenesis (Kawauchi et al., 2017; Pei et al., 2012).

One criticism of the Myc-p53 model is that it does not reflect the reality of human G3-MBs which lack *TP53* mutations in primary tumors. Although Myc alone is insufficient to drive tumors in most cell types, lentiviral-mediated gene transfer of Myc in postnatal Sox2^{+} astroglial progenitors produced tumors that have transcriptomes similar to subtype II G3-MBs (Tao et al.,

[5] *Blbp*-Cre and *Math1*-Cre are also expressed in the developing choroid plexus where Myc-p53 can also drive choroid plexus carcinomas.

2019). Additionally, the overexpression of *Myc* and *Gfi1/1b* can generate tumors from multiple types of cells, such as NSCs or GCPs, via either orthotopic transplantation or *in vivo* transfection (Ballabio et al., 2020; Northcott et al., 2014; Vo et al., 2017). This year, one group utilized cerebellar organoids derived from human iPSCs to drive tumors in mice using either Myc-Gfi1 or Myc-Otx2, another gene that is amplified in a subset of G3-MBs, and they showed that Myc-Gfi1 tumors are similar to subtype II tumors while Myc-Otx2 tumors are more like subtype IV, although neither *MYC* nor *OTX2* are amplified in subtype IV tumors (Ballabio et al., 2020).

Generating a G4-MB mouse model has proved the most challenging, such that the first and only G4-MB model was created in 2018 (Forget et al.). Proteomic analysis of primary MBs identified an enrichment of ERRB4 signaling in G4 (Forget et al., 2018), and high ERBB4 expression is associated with poor outcomes in G4-MB though the effect is less strong when all subgroups are merged, harkening back to older studies (Aldaregia et al., 2020; Gilbertson et al., 1997). Downstream of ERRB4 in G4-MB lies multiple effectors including MAPK, PI3K and SRC, and the expression of a constitutively active truncated SRC along with a dominant-negative p53 in both VZ and rhombic lip progenitors by *in utero* electroporation at e13.5 engendered tumors transcriptionally similar to G4-MB in 100% of mice (Forget et al., 2018).

1.4.2 The epigenetic component of MB, a sampling

An observation made early in the genomics era was that the mutational burden of pediatric cancers was significantly lower than adult malignancies (Parsons et al., 2011), and since then it has been repeatedly noted that epigenetic regulators are the most common group of significantly mutated genes among pediatric cancer types (Gröbner et al., 2018; Huether et al., 2014). Together, this hints that deregulation of the epigenome may strongly induce neoplastic

transformation by broadly changing gene expression programs and cellular activity, and work in model systems have since opened avenues to investigate these possibilities. A few examples are detailed in this section.

In MB, *KMT2D* mutations are one of the most frequent events, and these mutants likely encode truncated proteins (Parsons et al., 2011). Indeed, *KMT2D* was altered in 7% of samples across all subgroups from a recent analysis of nearly 400 MBs (Northcott et al., 2017). All six KMT2 family members are part of a complex comprised of the core subunits (WDR5, DPY30, ASH2L, RBBP5) and act to promote transcription via methylation of lysine 4 of histone 3 (H3K4) (Rao and Dou, 2015). KMT2D along with its paralogue KMT2C, also recurrently mutated in MB, interact with Lysine-specific demethylase 6a (KDM6A) – another MB relevant gene that removes methyl groups from tri-methylated H3K27 ($H3K27me^3$). KMT2D predominantly catalyzes H3K4 mono-methylation, a mark enriched at enhancers, but it is also important for broad, rather than sharp, $H3K4me^3$ peaks at the transcription start sites of genes associated with cell identity and tumor suppression (Dhar et al., 2018; Rao and Dou, 2015).

Specific deletion of *Kmt2d* with *Nestin*-cre impairs expression of NeuN, a marker of neuronal differentiation, in the cerebellum and is sufficient to cause MBs that express Group 3 associated genes (Dhar et al., 2018). *Kmt2d*-deficient tumors and neurospheres display reduced activation of super-enhancers and less broad $H3K4me^3$ peaks, and this correlates with decreased expression both of key granule neuron genes like *Neurod2* and *Pax6* and known tumor suppressors such as the transcriptional repressor *Bcl6*. This same group recently reported in a published abstract that loss of one *Kmt2d* allele, which does not generates tumors alone, increases MB incidence in $Ptch1^{+/-}$ mice (Dhar et al., 2018; Dhar et al., 2020). This probably acts via the same mechanism because mice with GCP-specific deletion of *Bcl6* and *p53* can also

develop MBs (Tiberi et al., 2014). Interestingly, *KMT2D* and *BCOR*, an obligate BCL6 co-repressor, are both recurrently mutated in infants with SHH-MB, though in different subtypes (β and γ, respectively), which suggests that these tumors potentially share therapeutic targets (**Figure 1-1**).

Studies of human MB genomics have implicated a tumor suppressive role for SMARCA4, an ATPase of the SWI/SNF complex that is frequently but not exclusively mutated in WNT-MB (Hovestadt et al., 2019a). The SWI/SNF complex acts to both activate and repress transcription by utilizing the energy released upon ATP hydrolysis to remodel nucleosomes, which are the smallest unit of chromatin defined by 147 base pairs of DNA wrapped around a histone octamer that is composed of four distinct core histones H2A, H2B, H3, and H4 (Armstrong, 2013; Wilson and Roberts, 2011). In MB, *SMARCA4* missense mutations, including T910M, cluster in either the ATP binding pocket or the downstream helicase superfamily carboxy-terminal domain (Dykhuizen et al., 2013). SMARCA4^{T910M} can still integrate into the SWI/SNF complex but has diminished enzymatic activity. *In vivo* overexpression of SMARCA4 prevented tumorigenesis in a Myc-Otx2 model, and in cerebellar organoids SMARCA4 blocked proliferation induced by Myc-Otx2, an effect that could be rescued by co-expression of the dominant-negative SMARCA4^{T910M} (Ballabio et al., 2020). Intriguingly, Myc-Gfi1 tumors expressed higher levels of SMARCA4 than Myc-Otx2 tumors because *MYC* amplifications, *GFI1* activation, and *SMARCA4* mutations all occur in subtype II G3-MBs (**Figure 1-1**), which points to the potential necessity of impeding SWI/SNF activity specifically in these tumors and which emphasizes the need to elucidate the molecular consequences of expressing mutant SMARCA4 in this model.

A crucial factor in designing animal models is knowing how mutations of a gene in human tumors affect the expression and/or function of the protein. For example, loss of *SMARCA4* in a *SmoM2* Shh-MB model robustly reduced tumor incidence to near 25% compared to 100%, but as detailed above, evidence indicates that *SMARCA4* mutations do not alter SMARCA4 expression (Shi et al., 2016). Notably, expression of a catalytically dead SMARCA4 mutant can rescue Shh signaling defects caused by *SMARCA4* deletion hinting that SMARCA4 plays a non-enzymatic role in Shh-MB tumorigenesis (Zhan et al., 2011). Moreover, fewer SHH-MBs contain *SMARCA4* mutations compared to other subgroups suggesting that it might at least partially play a tumor supportive role in this context (Northcott et al., 2017).

Exploration of chromosome 7(q) amplifications in a subset of G3- and G4-MBs demonstrated a corresponding elevation in *EZH2* (Enhancer-of-Zeste 2) expression (Robinson et al., 2012). EZH2 is the enzymatic subunit of the Polycomb Repressive Complex 2 (PRC2), a methyltransferase that catalyzes H3K27me^2 and H3K27me^3 – the latter of which is a mark of transcriptional repression at both promoters and enhancers (Kim and Roberts, 2016). Chromosome 7 amplifications are associated with strong H3K27me^3 staining in human MBs (Robinson et al., 2012). As stated earlier, the H3K27me^3 demethylase *KDM6A* is also recurrently mutated or deleted in MB, most often in Group 4 (Northcott et al., 2017), and a subset of tumors display deletions of *KDM6B*, which resides on chromosome 17p. Together these genetic alterations define what Dubuc *et al.* deemed an "H3K27-methylator phenotype" within G3/G4-MBs, suggesting that this mark and by extension EZH2 activity are oncogenic (2013).

G3-MB animal models have provided contradictory evidence for the function of Ezh2 in tumor development. Xenograft transplantation of an immortalized NSC cell line overexpressing Ezh2 and Myc was pro-tumorigenic (Sola, 2019), and inhibition of Ezh2 activity fueled

apoptosis in Myc-Otx2 expressing human cerebellar organoids (Ballabio et al., 2020). On the other hand, tumors developed more rapidly in a Myc-p53 transplantation model where *Ezh2* was knocked out (Vo et al., 2017). The consequences of Ezh2 function are also unclear in Shh-MBs. Replacing lysine 27 with a methionine (H3K27M) blocks methylation, thus mimicking at least in part Ezh2 loss-of-function, and expression of H3K27M in *p53*-null neural progenitors strongly favored the development of Shh-MBs over gliomas (Larson et al., 2019). However, orthotopic transplantation of H3K27M-transduced, $p53^{-/-}$ NSCs did not yield tumors (Mohammad et al., 2017). Ezh2 inhibition in $Ptch1^{+/-}$ tumors concurrently reduced proliferation and increased differentiation of tumor cells *in vitro* and *in vivo* (Cheng et al., 2020). One potential explanation for the differences observed may be the cell-of-origin such that Ezh2 may be a tumor suppressor in more differentiated progenitors (*Nestin*-expressing cells or GCPs) and an oncogene in NSCs, but direct evidence is necessary to support this idea.

Because PRC2 acts to antagonize the activity of both SWI/SNF and the KMT2D complex, which itself can recruit SWI/SNF via KDM6A, the genetic changes to KMT2D complex components, SWI/SNF subunits, or EZH2 observed in MB may result in shared functional consequences (Brand et al., 2019). In stem cells, balancing the activity of these chromatin modifiers is important for modulating self-renewal capabilities, lineage specification, and differentiation in a coordinated manner, so it will be critical to uncover how alterations to these complexes exploit the various tumor-initiating-cells of MB. It has already been established in multiple *SMARCB1*-deficient cancer models that disrupting Ezh2 can counteract tumor growth, which could be a feasible therapeutic option for *SMARCA4* mutant MBs and maybe others (Kim and Roberts, 2016; Knutson et al., 2013; Wilson et al., 2010).

1.4.3 Genomic instability fuels neoplastic transformation

As put forth by Hanahan and Weinberg and supported by the many animal models described above, alterations in key regulatory genes endow cells with certain features fundamental to tumor formation (2000). To acquire these necessary mutations during transformation, cells must overcome their intrinsic surveillance system that maintains genomic stability. The complex network of intracellular signaling that composes the DNA damage response (DDR) pathway represents a bridge between the detection of DNA lesions and mechanisms of DNA repair and changes to cell status, such as cell cycle arrest, senescence, or apoptosis, and it thus acts as an essential blockade of pro-tumor mutagenesis.

Because the complexity of the DDR and repair network is beyond the scope of this project, a simplified outline of the process is presented here (**Figure 1-5**). DNA double-stranded breaks (DSBs) resulting from agents like ionizing radiation are sensed by Mre11-Rad50-Nbs1, which recruit key protein complexes involved in the activation of the apical kinase *Ataxia telangiectasia* mutated (ATM) (Sulli et al., 2012). Among its many substrates, ATM phosphorylates the downstream mediator H2AX (a variant of histone 2A) and checkpoint kinase 2 (Chk2), which can then phosphorylate and activate p53. In the absence of DNA repair, p53 activation leads to either apoptosis or arrest and possibly senescence. Genotoxic agents that do not directly generate DSBs will disrupt DNA replication producing long stretches of replication protein A (RPA)-coated single-stranded DNA. This leads to the recruitment of *Ataxia telangiectasia* and Rad3-related (ATR) via ATR-interacting protein (ATRIP) and the 9-1-1 (Rad9-Rad1-Hus1) protein complex. ATR, like ATM, phosphorylates H2AX and its own effector kinase Chk1. To illustrate how the DDR is more complicated than the picture painted in **Figure 1-5**, work from multiple research groups has demonstrated that ATM can also

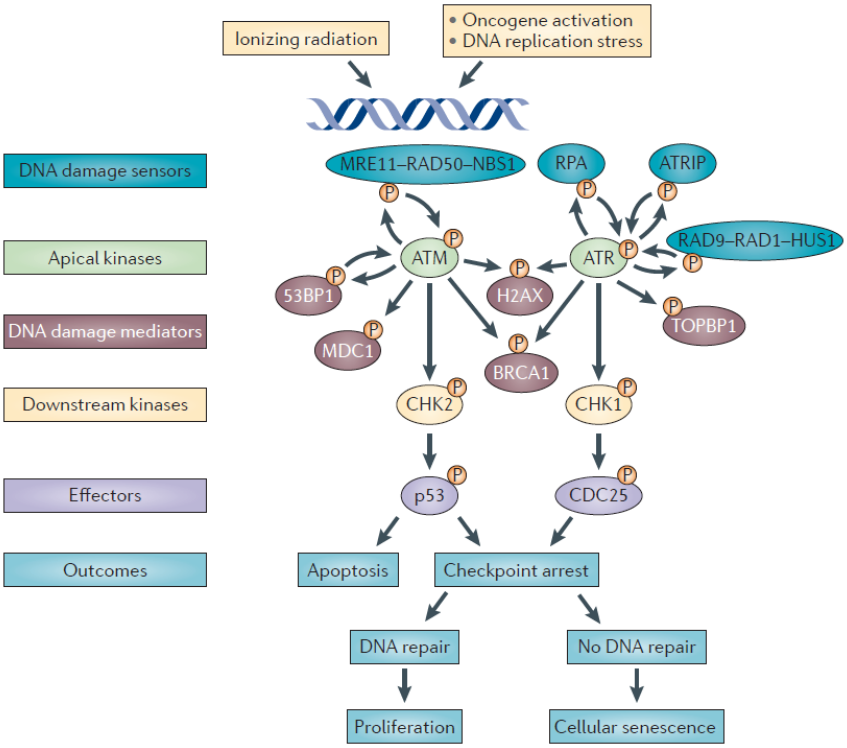

Figure 1-5. The DNA damage response pathway DNA lesions from sources such as ionizing radiation and replication stress are detected by protein complexes like Mre11-Rad50-Nbs1 or Rad9-Rad1-Hus1 that then recruit apical kinases, ATM and ATR. ATM and ATR phosphorylate many downstream mediators including the kinases Chk2 and Chk1, respectively, and they will phosphorylate effector proteins p53 and cdc25 which can trigger cell cycle arrest, apoptosis, or senescence. Figure from (Sulli et al., 2012).

phosphorylate Chk1, ATR can phosphorylate Chk2, and they both phosphorylate p53 (Smith et al., 2010; Weinberg, 2007).

Bartek Jr. *et al.* showed that DDR activation in MB is widespread using an immunohistochemical screen of 25 human samples (2017). One probable reason for this is that oncogenes and tumor suppressors can themselves trigger DNA damage (Halazonetis et al., 2008). Expression of SMARCA4 mutants, like the T910M, in MEFs leads to an increase in a specific mitotic defect known as anaphase bridges at levels reminiscent of *BRCA1*-deficient cells, and a similar phenotype was observed in human MB samples containing *SMARCA4* mutations, suggesting that the chromatin remodeler is involved in maintaining genomic stability (Dykhuizen et al., 2013).

In G3-MB, high CHK1 expression seems to be associated with poor outcomes (Prince et al., 2016). CHK1 and its upstream kinase ATR are essential factors for normal replication such that conditional deletion of *Atr* in neural progenitors leads to cerebellar hypoplasia and blocks tumor formation in *SmoM2* mice (Lang et al., 2016). Consequently, CHK1 is currently being considered as a therapeutic target in MB. In fact, promising results from Chk1/2 inhibition in MB cell lines, where high Myc expression was associated with increased drug sensitivity, and in a G3-MB mouse model, where *in vivo* administration of a pharmacological inhibitor penetrated the CNS and activated DNA damage, have prompted St. Jude's to organize a Phase 1 clinical trial with the dual inhibitor prexasertib (LY2606368) (Campagne et al., 2020; Krüger et al., 2018; NCT04023669, 2019).

The importance of DDR and repair genes in genomic stability makes them vulnerable targets for neoplastic transformation in many cancers including MB, and though rare, somatic and germline mutations of certain components, such as *TP53*, *ATM*, *BRCA1/2*, *PALB2*, and

others, have been identified in human MB samples (Northcott et al., 2017; Waszak et al., 2018). In mice, deletion of genes related to DNA repair are not sufficient to cause MBs, yet in conjunction with loss of *p53*, they will instigate tumor development. For instance, conditional deletion (*Nestin*-cre) of *Brca2* or *Xrrc2*, two effectors of homologous recombination, in a $p53^{-/-}$ background will lead to tumors that resembles Shh-MBs, yet *Brca2* deletion did not collaborate with $Ptch1^{+/-}$ to generate tumors (Frappart et al., 2007; Frappart et al., 2009). Like *Brca2*, mice lacking *Parp1*, a gene important for base excision repair among other functions, will develop Shh-MBs when combined with loss of *p53* but not $Ptch1^{+/-}$ (Tanori et al., 2008; Tong et al., 2003). Moreover, *p53* deletion and loss of *DNA ligase IV*, *Xrrc4*, *Ku70*, or *Ku80*, which are mediators of Non-homologous end joining (NHEJ), also lead to medulloblastomas and/or lymphomas in mice (Frappart et al., 2009; Holcomb et al., 2006; Lee and McKinnon, 2002; Li et al., 2009; Yan et al., 2006). Of the NHEJ models, only *DNA ligase IV* and *Xrrc4* were assessed for molecular changes, and they demonstrated enhanced Shh pathway activation (Frappart et al., 2009; Yan et al., 2006)

1.5 DNA damage and tumorigenesis in $Ptch1^{+/-}$ mice

The link between loss of genes involved in homologous recombination or NHEJ and Shh-MB suggests that GCPs, the cell-of-origin, are exquisitely sensitive to DNA repair regulation. This is likely due to the elevated baseline levels of DNA damage that proliferating GCPs display *in vivo* even when compared to robustly proliferative tissues like the intestinal epithelia and that is a direct consequence of Shh signaling, which triggers a specific form of replication stress caused by a high density of active replication origins (Tamayo-Orrego et al., 2020). Moreover, the replication-induced DNA damage instigated by Shh leads to an increase in recombination

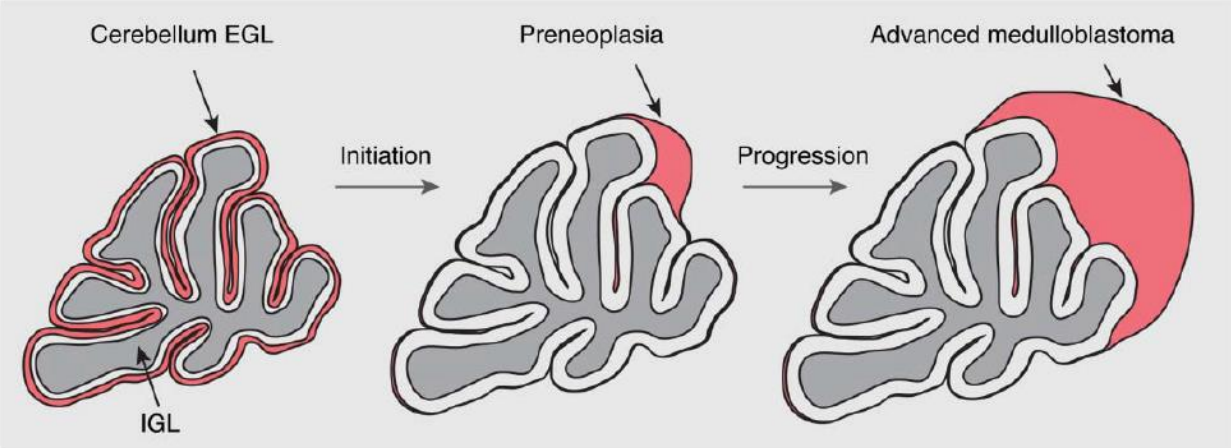

Figure 1-6. Shh-MB tumorigenesis is a multistep process

Schematic illustrating the three stages of tumor development in *Ptch1*$^{+/-}$ mice. In GCPs (pink) of the early postnatal EGL, Shh signaling increases proliferation and invokes genomic instability through replication stress resulting in loss of the wildtype *Ptch1* allele and preneoplasia formation. The transition to advanced tumor requires additional genetic alterations to overcome tumor preventing barriers such as senescence. Figure from (Tamayo-Orrego et al., 2016a).

events, and in the context of *Ptch1*$^{+/-}$, recombination events drive loss of the wildtype *Ptch1* allele, known as loss-of-heterozygosity (LOH), thus initiating preneoplasia formation (**Figure 1-6**).

While the incidence of these lesions (and of tumors also) fluctuates among mouse strains, some preneoplasia will never transition to fully advanced tumors, suggestive of additional impediments to tumorigenesis (Mille et al., 2014; Oliver et al., 2005). Indeed, preneoplasia display an elevated number of senescent cells, a known cancer barrier. According to Halsonetis, Gourgoulis, and Bartek, this senescence observed in preneoplasia can be explained by "the oncogene-induced DNA damage model" where activation of the oncogene (or loss of the tumor suppressor) leads to DSBs in the DNA – a result of replicative stress – thus triggering the ATM-mediated arm of the DDR pathway, which in turn instigates senescence via activation of p53 (2008). Earlier publications established the ability of ATM inhibition to interfere with oncogene-induced senescence both *in vitro* using cell lines and *in vivo* using animal models of cancer (Bartkova et al., 2006). The authors contend that such a model would explain the frequency of both chromosomal instability and *p53* mutations in various human cancers, both of which are features of Shh-MB. In fact, SHH-MBs with *TP53* mutations often display a specific form of genomic instability known as chromothripsis, which is defined as catastrophic levels of chromosomal rearrangement (Rausch et al., 2012). Work from *Ptch1*$^{+/-}$ mice shows that progression to advanced tumor requires senescence evasion achieved via mutations in *p53* or related proteins, disruption of the p53 signaling cascade, and/or reduced expression of *p16*^{ink4a} (a cyclin-dependent kinase inhibitor) through increased promoter methylation (Tamayo-Orrego et al., 2016b).

In summary, Shh-MBs occur in a stepwise manner that requires multiple genetic alterations where ligand-independent Shh signaling is an early event (**Figure 1-6**); as a result, our lab is now expanding our inquiries into both Shh pathway dependent and independent mechanisms of tumorigenesis.

1.6 Rationale and overall objectives

The identification of recurrent mutations in human patients and the refinement of the stepwise progression of tumor development in *Ptch1*$^{+/-}$ mice have laid the foundation for unearthing the molecular mechanics of tumorigenesis. Our lab has previously established a role for Boc in the progression of MB where they demonstrated that Boc is highly expressed in murine and human tumors, which can occur through gains of the *BOC* gene (Mille et al., 2014). *Boc* inactivation in *Ptch1*$^{+/-}$ mice not only led to smaller preneoplasia but also to a reduction in tumor incidence that correlated with a decreased incidence in *Ptch1* LOH.

While *Boc* deletion only has a partial effect on proliferation, it quells the DNA damage caused by either *Ptch1*$^{+/-}$ or Shh stimulation (Izzi et al., 2011; Mille et al., 2014). Therefore, we hypothesized that high expression of Boc contributes to MB tumorigenesis by promoting genomic instability through induction of DNA damage. Using an *in vitro* experimental paradigm, I sought to determine if Boc is sufficient to induce DNA damage using H2AX phosphorylation as an outcome measure. I then attempted to elucidate downstream effectors of Boc-mediated H2AX phosphorylation by screening small molecule inhibitors of potential signaling cascades, and I tried to characterize the downstream activation of the DNA damage response by immunostaining for members of the DDR network. Unfortunately, my ability to further test the role of Boc in tumor formation was limited by technical challenges associated with my

unsuccessful attempt to establish an *in vivo* model of Boc overexpression. Moreover, repeated failure to disrupt phosphorylation of H2AX following BocGFP electroporation prompted me to test if the construct was both being expressed and triggering DNA damage in GCPs, the cells-of-interest, by generating primary cultures from a reporter mouse line.

More recently, our lab has established that medulloblastoma formation is a multi-step process in which the transition from preneoplasia to advanced tumor requires the acquisition of Shh-signaling independent genomic alterations (Tamayo-Orrego et al., 2016b). This finding has incited an interest in the lab to identify and characterize other co-driver mutations of Shh-MB. Serendipitously, while investigating the role of *Boc* deletion on MB incidence in $Ptch1^{+/-}$ mice, we discovered a tumor containing a spontaneous, oncogenic *Pik3ca* mutation (H1047R), and this tumor displayed higher expression of genes associated with muscle identity and function (**Figure 1-7A, B**). The presence of myogenic differentiation in human MB tumors, also known as MMB, is a rare but well-documented phenomenon (Helton et al., 2004). Therefore, we postulated that combination of germline $Ptch1^{+/-}$ and conditional $Pik3ca^{H1047R}$ would create mouse tumors resembling human MMB.

In Chapter 4 of the thesis, I will document our efforts to characterize this putative mouse model and assess its similarities to human MMB. Additionally, we have identified other potential mediators of the muscular phenotype, which inspired us to assess whether loss of *Ezh2* can also generate myogenic marker expression in mouse tumors. Finally, we have utilized these model systems to better understand the molecular events that instruct the appearance of myogenic cells in the central nervous system.

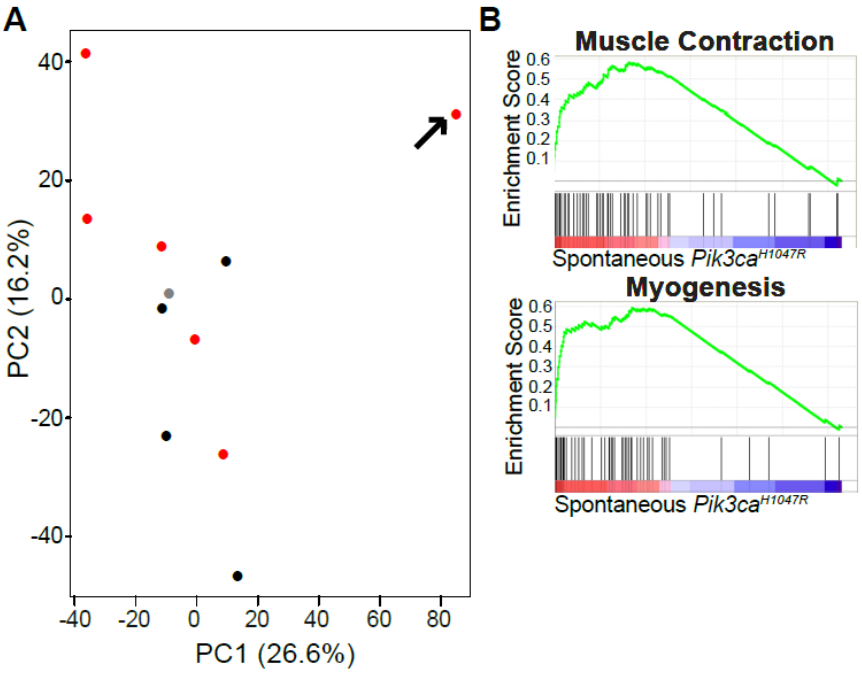

Figure 1-7. Mouse tumor with spontaneous PI3K mutation displays elevated expression of muscle genes

A) Identification of H1047R *Pik3ca* mutation in a mouse *Ptch1*$^{+/-}$ tumor. Principal component analysis (PCA) of all expressed genes from *Ptch1*$^{+/-}$ advanced tumors that were also *Boc*$^{+/+}$ (black dots), *Boc*$^{+/-}$ (grey dot), or *Boc*$^{-/-}$ (red dots). Sample with spontaneous H1047R mutation indicated by arrow.

B) Enrichment of genes associated with muscle contraction (top plot) and myogenesis (bottom) by Gene set enrichment analysis (GSEA) in spontaneous PI3K mutant tumor (n=1) compared to the others (n=10). q, false discovery rate adjusted p. NES, normalized enrichment score.

Chapter 2: Experimental Procedures

2.1 Mouse lines

All experiments involving mice were carried out in accordance with the Canadian Council on Animal Care Guidelines. Wildtype C57BL/6 mice were obtained from Jackson Labs, and all mice were maintained on C56BL/6 background unless otherwise specified. Also obtained from Jackson laboratories were the *Ptch1*$^{+/-}$ (officially *Ptch1*-LacZ or *Ptch1*^{tm1Mps}/J) mice; *Math1*-Cre [Tg(*Atoh1*-cre)1Bfri] mice; and *Pik3ca*^{H1047R} [FVB.129S6-Gt(ROSA)26Sor$^{tm1(Pik3ca*H1047R)Egan}$/J] mice, which was the only line maintained on a FVB/129S6 background (Adams et al., 2011; Goodrich et al., 1997; Matei et al., 2005). Boc$^{-/-}$ (*Boc*$^{tm1Aok/tm1Aok}$) mice were obtained from A. Okada and S. K. McConnell; *Boc*$^{AP2/AP2}$ mice were obtained from B. Allen; and TdTomato [B6.Cg-Gt(ROSA)26Sor$^{tm14(CAG-tdTomato)Hze}$/J] mice were obtained from Y. Zhang (Madisen et al., 2010; Okada et al., 2006; Zhang et al., 2011b).

2.2 Cerebellar dissociation and purification of GCPs

The isolation of GCPs described here is a modified protocol previously described (Izzi et al., 2011). The cerebella of P5-P7 mice were collected and digested with 0.25% Trypsin in HBSS for 20 minutes at 37^{o}C. The tissue was titrated with fire-polished glass pipettes into a homogenous suspension and GCPs were isolated by centrifuging the cell suspension (3200 RPM for 22 minutes at RT with the break removed) on a 30%/65% sucrose gradient. The cells at the interface of the two sucrose concentrations were transferred to HBSS, centrifuged at 950 RPM for 5 min at RT, and resuspended in Neurobasal supplemented with B27, sodium pyruvate, glutamax, and penicillin/streptomycin. Unless cells were further manipulated, 0.5 x 10^6 cells in 500 µL of media were plated on PDL-coated coverslips. For Ezh2 inhibitor experiments, 1 µM EPZ6438 (Selleckchem) or an equivalent dilution of DMSO and 10 nM Shh (R&D) or an equal

volume of media was added at plating while only EPZ6438 or DMSO was added at DIV 2 when the media was changed.

2.3 Electroporation of GCP cultures

The mBocGFP construct in a pEGFP-N1 vector was a gift from A. Okada. The pEGFP was generated by Steves Morin from a SmoGFP construct in a pEGFP-N3 vector, and mBocGFPΔcytotail was generated from the pEGFP vector by Steves Morin. Regardless of Amaxa electroporation kit, cells suspensions were centrifuged for 5 minutes at 3000 RPM, media was discarded, and cells were resuspended in nucleofector solution. For P3 primary kit electroporation, each 96-well cuvette contained $1x10^6$ dissociated GCPs in 10 µL P3 primary nucleofector solution plus 0.3 µg of plasmid, and the cuvettes were electroporated in the Nucleofector II (Lonza) using the DC-100 program (Mille et al., 2014). For the NSC kit electroporation, each 100 µL cuvette contained $6x10^6$ dissociated GCPs suspended in 100 µL NSC nucleofector solution plus 1.0 µg of plasmid, and the cuvettes were electroporated in the Nucleofector I (Lonza) using the A-33 program. Electroporated cells were diluted in completed neurobasal media to a concentration of $1x10^6$ cells per 500 µL of media (except **Figure 3-1** in which the concentration was $0.5x10^6$ cells per 500 µL) and cultured in 24-well plates on PDL-coated glass coverslips at 37ºC. For drug experiments, all small molecules: 134 nM SANT1 (Calbiochem), 5 µM GANT58 (EMD), 0.2 µM PP2 (Millipore), 0.2 µM PP3 (Millipore), 15 µM LY294002 (gift from M. Tessier-Lavigne) or 10 µM SB203580 (Cell Signaling), were added at the time of plating, and except for the overnight SANT1 and PP2 experiments, equivalent dilutions of DMSO were added to control conditions. Shh (10 nM, R&D) was added 30 minutes after SANT1.

2.4 *In utero* electroporation

All gRNAs were cloned into the all-in-one CRISPR vector, PX458**.** The *Asxl3*, control, and *Ptch1* gRNAs were custom made through GeneScript; the latter two gRNAs were previously described (Zuckermann et al., 2015). The Ezh2-E18 and Ezh2-E10 gRNAs, previously validated in a G3-MB mouse model, were originally gifted from Martine Roussell (Addgene) and were combined at a 1:1 ratio prior to mixing with the *Ptch1* plasmid (Vo et al., 2017). *Ptch1*+ target gene or control plasmid were mixed 1:1 for *in utero* electroporation. Using a foot-pedal operated picospritzer (Parker), 1 ug in 1 uL of plasmid mixture was injected into the rhombic lip of e14.5-15.5 embryos followed by 5 pulses of 45mV at 950 ms intervals that were applied by an ECM-830 electroporator (Harvard Apparatus) through platinum electrode tweezers (Protech) placed over the embryo's ears. Embryos were then placed back into the pregnant female, who was anesthetized by isofluorane throughout the surgery, allowed to be born, to be weaned, and to survive until symptomatic for brain tumors. Animals showing no symptoms by 240 days were euthanized.

2.5 Lentivirus preparation and GCP transduction

Lentivirus production was adapted from a previously described protocol (Tamayo-Orrego et al., 2016b). HEK293T/17 cells in 15 cm dishes were switched to DMEM supplemented with 0.5% FBS, 1% Penicillin/Streptomyocin, and 2 mM caffeine and were transfected using Lipofectamine 2000 with 15 µg pLP1, 7 µg pLP2, and 10 µg pVSVG packing plasmids along with 15ug of one lentiviral vector: pPrime-CMV_GFP (gift from M. Tremblay), pLv-CMV-mMyod (originally from Jeffrey Chamberlain through Addgene), pLV-GG-hUBC-dsRed (originally from Charles Gersbach through Addgene), or pLV-hMyoD-IRES-dsRed (originally

from Charles Gersbach through Addgene). 72 hours after transfection, viral media was collected then centrifuged, and gravity filtered (0.45 µM) to remove debris. 40 mL of filtered viral media and 10 mL of 40% PEG6000-2.4M NaCl were rocked overnight at 4°C; the mixture was then centrifuged at 3750 RPM for 1 hour at 4°C to precipitate virus, and the supernatant was discarded. The virus was resuspended in 1 mL of neurobasal media and the concentrated virus was centrifuged at 12000 RPM for 5 min. $5x10^6$ purified GCPs were spin-inoculated with 250 µL concentrated virus at 800 g for 30 min at RT, resuspended in supplemented Neurobasal media and plated ($0.5x10^6$ cells in 500 µL media) on 1 mM glass coverslips coated with PDL in 24-well plates. Cells were treated 1 µM EPZ6438 or an equivalent dilution of DMSO at plating. On DIV 2, media was changed and fresh drug/DMSO was added.

2.6 Immunostainings:

2.6.1 Dissociated GCP immunofluorescence:

Cells were fixed by adding an equal volume of 8% PFA in PBS to the cell culture media and then incubating plates at 4°C for 15 min (Ch. 4) or 20 minutes (Ch. 3). Coverslips were washed in PBS. When necessary (p-Chk1, Chk1, p-Chk2, Chk2, and p-p53), antigen retrieval was performed by incubating the coverslips in sodium citrate buffer (10mM sodium citrate, 0.05% tween 20 in water, pH 6.0) for 13 minutes at 95°C before washing in PBS. Cells were permeabilized in 0.3% triton for 15 minutes, washed in PBS, and blocked in 10% serum (goat/donkey), 0.1% triton in PBS for 1 hour at RT. Cells were incubated overnight at 4°C in primary antibody(s) diluted in 1% serum, 0.1% triton (**Table 2-1**). Coverslips were washed in 1% serum, 0.1% triton before they were incubated in diluted fluorophore-conjugated secondary

Table 2-1. Antibodies

Antibody	Source (Catalog #)	Dilution
Mouse monoclonal anti-GFP	ThermoFisher (A11120/A11121)	1:1000
Rabbit polyclonal anti-γH2AX	Cell Signaling (9718S)	1:2000
Chicken polyclonal anti-GFP	Abcam (ab13970)	1:1000
Rabbit anti-p-Chk1 (S345)	Cell Signaling (2348)	1:150
Mouse monoclonal anti-Chk1	Santa Cruz (sc-8408)	1:100
Rabbit anti-p-Chk2 (T68)	Cell Signaling (26613)	1:150
Mouse monoclonal anti-Chk2	Santa Cruz (sc-5278)	1:100
Rabbit polyclonal anti-p-p53 (S15)	Cell Signaling (9284S)	1:150
Rabbit polyclonal anti-p53	Santa Cruz (sc-6243)	1:100
Mouse monoclonal anti-Ki67	BD Pharmingen (550609)	1:200
Rabbit monoclonal anti-myoglobin	Abcam (ab77232)	1:1000
Goat polyclonal anti-troponin I FS	Santa Cruz (sc-8120) obtained from J. Drouin	1:100
Mouse monoclonal anti-troponin T FS	DSHB (JLT12)	1:5 (Tissue), 1:10 (cells)
Mouse monoclonal anti-SERCA1	ThermoFisher (MA3-912)	1:100 (Tissue IF), 1:2000 (IHC), 1:1000 (cells)
Rabbit polyclonal anti-H3K27me3	Active Motif (39155)	1:500
Mouse monoclonal anti-TPM2	DHSB (CG1)	1:10
Mouse monoclonal anti-MyoD	BD Pharmigen (554130)	1:100
Mouse monoclonal anti-myogenin	DHSB (F5D) obtained from JF Coté	1:50
Rabbit polyclonal anti-Pax6	Biolegend (901310)	1:1000
Goat anti-mouse IgG Alexafluor488	Jackson Immunoresearch (115-545-166)	1:1000
Goat anti-mouse IgG Cy3	Jackson Immunoresearch (115-165-146)	1:1000
Goat anti-mouse IgG biotinylated	Vector (BA-9200)	1:200
Goat anti-rabbit IgG Alexafluor488	Jackson Immunoresearch (111-545-144)	1:1000
Goat anti-rabbit IgG Cy3	Jackson Immunoresearch (111-165-144)	1:1000, 1:2000 (γ-H2AX)
Goat anti-rabbit IgG biotinylated	Vector (BA-1000)	1:200
Goat anti-chicken IgG Alexafluor488	Molecular Probes (A11039)	1:1000
Donkey anti-mouse IgG Alexafluor488	Jackson Immunoresearch (715-545-151)	1:1000
Donkey anti-mouse IgG Cy3	Jackson Immunoresearch (715-165-151)	1:1000, 1:500 (Chk1, Chk2)
Donkey anti-mouse IgG Alexafluor 647	Jackson Immunoresearch (715-605-151)	1:1000
Donkey anti-rabbit IgG Cy3	Jackson Immunoresearch (711-165-152)	1:1000, 1:2000 (γ-H2AX), 1:500 (p-Chk1, p-Chk2, p-p53)
Donkey anti-rabbit IgG AlexaFluor647	Jackson Immunoresearch (711-605-152)	1:2000 (γ-H2AX)
Donkey anti-goat Cy3	Jackson Immunoresearch (705-165-147)	1:1000

antibody(s) for 1 hour at RT and then washed again in 1% serum, 0.1% triton. For sequential staining (MyoD then Tnnt3), secondary antibody (goat anti-mouse IgG Cy3) was diluted 1:100 to achieve saturated binding, and coverslips were washed 1% serum, 0.1% triton before they were incubated in Tnnt3 antibody dilution for 1 hour at RT. Coverslips were washed in 1% serum, 0.1% triton before a 1-hour incubation in secondary antibody (goat anti-mouse IgG Alexfluor488) at RT. Cells were counterstained with DAPI and coverslips were mounted onto slides with mowiol.

2.6.2 Cerebellar section immunofluorescence:

Mice were euthanized by transcardial perfusion with 0.9% saline followed by 4% PFA in PB – except for animals with advanced tumors who were perfused with saline only. Whole brains were post-fixed overnight at 4^{o}C in 4% PFA, washed, and cryoprotected in 30% sucrose in PBS at least 48 hours at 4^{o}C. Cerebella hemispheres were frozen in OCT and sliced using a cryostat into 12 µM sagittal sections. Cryosections were subjected to antigen retrieval in sodium citrate buffer (10mM sodium citrate, 0.05% tween 20 in water, pH 6.0) at 98^{o}C for 1 hour except for SERCA1 staining which was only for 12 minutes. Slides were then washed in PBS before tissue was permeabilized in 0.3% triton for 15 minutes at RT. After washing slides in PBS, slides were washed with 0.3M glycine to reduce autofluorescence. The tissue was again washed in PBS and then blocked in 10% serum (goat/donkey), 0.1% triton in PBS for 1 hour at RT and then incubated in diluted antibody (1% goat/donkey serum, 0.1% triton in PBS) overnight at 4^{o}C (**Table 2-1**). Tissue was washed in PBS, incubated in diluted alexafluor-conjugated secondary antibody for 1 hour at RT, washed again, and counterstained in DAPI. Coverslips were attached to slides with mowiol. 20X epifluorescence images were acquired on the DM6 (Leica) except for

the myoglobin and Tnni2 labeling in **Figure 4-1E** where the myoglobin images are confocal images at 40X from the LSM700 (Zeiss) and the Tnni2 images were acquired on the DM6 at 63X.

2.6.3 Immunohistochemistry of mouse cerebella or human MMB:

Slides containing paraffin-embedded sections of tumor were kindly provided by Dr. C. Hawkins and were dewaxed with xylene followed by decreasing concentrations of ethanol. Slides of mouse sections were acquired as related above. Tissue was washed in PBS before antigen retrieval in sodium citrate buffer (10mM sodium citrate, 0.05% tween 20 in water, pH 6.0) for 1 hour at 98^{o}C. Tissue was washed with PBS before and after endogenous peroxidase inhibition in 2% H_20_2 (diluted in PBS) for 30 minutes at RT. The tissue was blocked in 10% serum (goat/donkey), 0.1% triton in PBS for 1 hour at RT and then incubated in diluted antibody (1% goat/donkey serum, 0.1% triton in PBS) overnight at 4^{o}C (**Table 2-1**). Slides were washed in 1% serum, 0.1% triton before a 1-hour incubation in 1:200 dilution of biotinylated secondary antibody (1% serum, 0.1% triton) at RT. The tissue was washed before and after a 1-hour incubation in ABC-peroxidase kit (Vectastain) at RT. Antibody binding was visualized by DAB substrate reaction, which was quenched with water. Mouse tissue was counterstained with Nissl while human MMB was counterstained with hematoxylin before tissue was dehydrated, and then coverslips were attached with permount. Brightfield images acquired at 20X or 63X on the DM4000B (Leica) and were processed in ImageJ for figures.

2.7 Image quantification

For fluorescence intensity measurements in dissociated cells, confocal images were acquired at 63X on either the Zeiss LSM700 (Ch. 3) or Leica SP8 (Ch. 3 and Ch. 4). Analysis of nuclear fluorescence mean intensity was conducted in FIJI (ImageJ software), which was also used to process images for figures. Following background subtraction, individual nuclei were traced in the DAPI channel before measuring mean intensity in the channel of interest. Averages and data normalization were calculated in Excel.

For cell counts in a defined population (either electroporated or myogenic cells), 63X images acquired with the SP8 (Leica) were used to define Ki67/TdTomato/MyoD/Pax6 status by hand. For muscle marker cell counts (TPM2, SERCA1, Tnnt3), all positive cells on the coverslip were counted by hand at 20X on the DM6 (Leica). The total cell number was extrapolated based on the number of DAPI cells, counted using an ImageJ macro, from 20X images (DM6). For MyoD percentages in dissociated cells, the MyoD-positive cells were counted from 20X images (DM6) using the ImageJ counter feature and DAPI cell counts were made using an ImageJ macro. For MyoD counts in P7 sagittal sections, MyoD-positive cells were counted from 63X images using the counter feature on ImageJ and divided by the area of the EGL.

2.8 Statistical analysis

Both graph production and statistical analyses were performed in Prism 8 (GraphPad Software). Reported n are recorded in the figure legends. Statistical tests are indicated in figure legends and include Mann-Whitney U test, two- or three-way ANOVA with Tukey's multiple comparisons, Kruskal-Wallis test with Dunn's multiple comparisons, Fisher's exact test, and an unpaired t-test. Significance is defined by p-value, where n.s. stands for not significant, and is represented by asterisks: *, $p<0.05$; **, $p<0.01$; ***, $p<0.001$; ****, $p<0.0001$. All error bars

represent 95% confidence interval. Kaplan-Meier Curves were used to assess survival in Chapter 4 and were analyzed by log-rank test.

2.9 RNA sequencing and analysis

mRNA was extracted from dissociated P7 GCPs from *Ptch1*^{Wt}*;Boc*$^{+/+}$, *Ptch1*^{WT}*;Boc*$^{-/-}$, *Ptch*$^{+/-}$*;Boc*$^{+/+}$, or *Ptch*$^{+/-}$*;Boc*$^{-/-}$ mice, tumors from *Ptch1*$^{+/-}$*;Boc*$^{+/+,+/-,or-/-}$ mice, and tumors from *Ptch1*$^{+/-}$*;Pik3ca*^{WTorH1047R} mice. cDNA libraries from *Ptch1;Boc* samples, tumor or GCPs, were prepared using the unstranded polyA RNA Illumina Prep Kit while libraries from *Ptch1;Pik3ca* samples were prepared with the TruSeq Stranded mRNA (polyA) LT Sample Kit. The libraries were subsequently sequenced on the Illumina HiSeq2000 using 50bp paired-end reads, and quality control of read sequences was implemented with the FastQC algorithm (Andrews, 2010). First, adaptor sequences and low-quality score bases (Phred score<30) were trimmed by Trimmomatic v.022, and reads fewer than 32-bp long were discarded (Lohse et al., 2012).

Gene quantification was only performed on concordant mapped reads. Using HTSeq 0.6.1p1, gene mapping read counts were obtained based on Ensembl (release 86) gene annotation (UCSC genome browser) (Anders et al., 2015; Dreszer et al., 2012). A total of 48526 genes resulted from merging single gene transcript isoforms using cufflink (Trapnell et al., 2010). From this list, genes containing more than 10 mapping reads in at least a single sample were defined as being expressed above background. Gene expression levels were then normalized before measuring differential gene expression, all using the R Bioconductor package DESeq2 (Love et al., 2014). Exploratory analysis was first performed between the *Ptch1*$^{+/-}$*;Boc*$^{-/-}$ sample containing the spontaneous *Pik3ca*^{H1047R} mutations compared to other *Ptch1*$^{+/-}$ MBs, and repeated using the genetically engineered *Ptch1*$^{+/-}$*;Pik3ca*^{H1047R} tumors versus the *Ptch1*$^{+/-}$

;Pik3ca^{WT}. A gene was considered significantly different if the q-value was less than 0.05 and the absolute value of the expression fold-change was at least 2. In total, 1678 genes were differential expressed in our exploratory analysis, and 118 genes were differential expression in *Ptch1*$^{+/-}$ *;Pik3ca*^{H1047R} tumors compared to *Pik3ca*^{WT}. Gene set enrichment analysis (GSEA) with the pre-ranked option was applied to identify enriched gene sets among the differentially expressed genes.

2.10 Public mouse data collection, processing, and clustering

From the Gene Expression Omnibus, data generated using Affymetrix Mouse Genome 430 2.0 Array was extracted from 19 murine samples that included NSCs, Myc-driven tumors, and Ptch1$^{+/-}$ MBs (GSE34126) (Pei et al., 2012). The data (CEL files) was processed using the R Bioconductor package affy (Gautier et al., 2004), and the robust multichip analysis (RMA) algorithm was applied to the processed data, which include background correction, quantile normalization, and median polish through summarization of probes in genes. The final dataset contained 17599 genes expressed as a log2 scale. Combining the mouse datasets yielded a total of 12422 genes, from which we performed clustering analysis, after applying the empirical Bayes' method ComBat in the sva R package to reduce variability generated by batch and platform effects (Leek et al., 2017).

2.11 Public human MB data collection and processing

In total, the gene expression data of 901 human MB samples from 4 published datasets were downloaded from the Gene Expression Ominibus: data from 138 samples originating from three of the studies (GSE12992, GSE67850, GSE37418) were produced using Affymetrix

Human Genome U133 Plus 2.0 Array while the 763 sample from Cavalli *et al.* (GSE85217) were profiled using Affymetrix Human Gene 1.1 ST Array (Cavalli et al., 2017; Fattet et al., 2009; Ho et al., 2015; Robinson et al., 2012). Microarray data was processed the same as the public mouse dataset described above.

2.12 Identification of MMB gene signature and mouse sample clustering

Because the 4 MMBs (GSM324062, GSM918644, GSM918618, GSM1657171) came from only 3 of the data sets (GSE37418, GSE12992, and GSE67850), the gene expression information from these were merged using the empirical Bayes' method Combat in the sva R package, which would adjust for batch effects. To determine differential expression (q-value<0.01, |log2(fold change)|≥1) of the 19425 identified genes between the 4 MMBs and other MBs with defined subgroups in the original publications (12 WNT, 10 SHH, 16 G3, 39 G4), the Bioconductor R package Limma was used (Ritchie et al., 2015). The 219 genes deemed differentially expressed were adopted as an MMB gene signature. GSEA with the pre-ranked option was applied to identify enriched gene sets among the differentially expressed genes. Mouse orthologs were identified for all 219 MMB signature genes and were downloaded from Ensembl using the BioMart online tool, and at least one mouse sample contained 10 reads or more of 181 of these genes (Zhang et al., 2011a).

Chapter 3

Probing the link between high expression of the Shh receptor Boc and DNA damage in GCPs

3.1 Summary

Dysregulated Shh signaling in cerebellar granule cell precursors (GCPs) can generate medulloblastoma (MB), the most common brain malignancy of childhood. Although our lab has previously shown that loss of *Boc*, a Shh co-receptor highly expressed in MB, greatly reduces tumor incidence in *Ptch1*$^{+/-}$ mice, we still do not understand how upregulation of Boc contributes to tumor formation. The work in this chapter reflects my intention to show that Boc overexpression induces DNA damage in GCPs, to elucidate downstream effectors involved in this damage, and to characterize the subsequent activation of the DNA damage response network. While electroporation of the BocGFP construct mostly targets non-GCPs, I do find that overexpression of Boc in GCPs can – at least transiently – trigger phosphorylation of H2AX, an event associated with DNA damage. My attempts to identify mediators both upstream and downstream of this effect did not account for the paucity of Boc-expressing GCPs and thus do not address the function of Boc in GCPs. Consequently, the role that Boc upregulation plays in DNA damage induction is largely an open question. The current results suggest that high levels of Boc are associated with DNA damage although future work is needed to provide corroborating evidence of this effect using an alternative method to express Boc in GCPs.

3.2 Results

3.2.1 Boc triggers phosphorylation of H2AX *in vitro*

Having previously established that Boc is not only required for Shh-dependent DNA damage but is also highly expressed in human and mouse MB, we wanted to understand how elevated levels of Boc may enhance tumorigenesis (Mille et al., 2014). To model Boc upregulation *in vitro* and test whether Boc itself induces DNA damage, I dissociated GCPs from

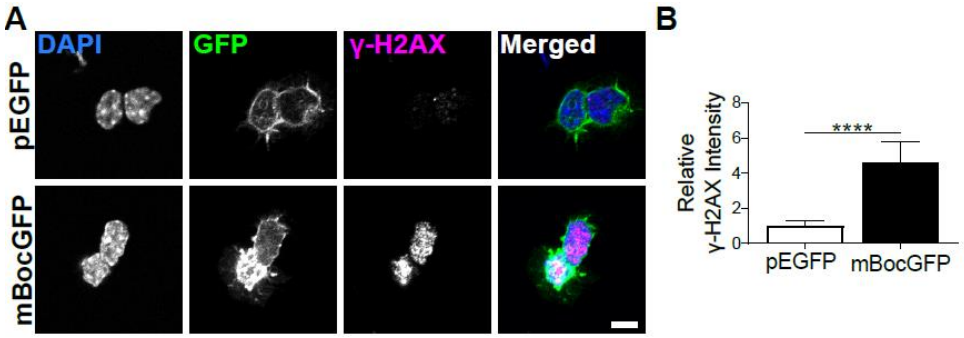

Figure 3-1. Boc triggers phosphorylation of H2AX *in vitro*

A) Representative images of electroporated cells labeled with DAPI and with antibodies against GFP and γ-H2AX. Images cropped and adjusted for brightness/contrast. Scale bar: 5 μM.

B) Significantly higher levels of γ-H2AX in Boc-expressing cells (n=85). Graph of mean intensities after normalization to the pEGFP average for each experiment (pEGFP n=146 cells from four independent experiments). Data represented as mean + 95% confidence interval and analyzed using a Mann-Whitney U test (****, $p<0.0001$).

P7 c57/B6 mice and electroporated them with either a mouse BocGFP (mBocGFP) fusion construct or a GFP (pEGFP) control. After culturing the cells overnight, they were immunostained with antibodies against GFP, to label transfected cells, and phosphorylated H2AX (γ-H2AX) – the phosphorylation of H2AX at serine 139 is a common marker of DNA damage (**Figure 3-1A**) (Rogakou et al., 1999; Rogakou et al., 1998; Ward and Chen, 2001). Although γ-H2AX triggered by double strand breaks (DSBs) creates a pattern of nuclear foci that can be counted, many of the Boc-positive cells displayed pan-nuclear staining, a pattern more commonly associated with genotoxic agents like ultraviolet (UV) radiation (de Feraudy et al., 2010; Marti et al., 2006; Rogakou et al., 1999; Ward and Chen, 2001). Therefore, I chose to measure the mean intensity of γ-H2AX within the nuclei of electroporated cells (**Figure 3-1B**). Compared to control cells, those expressing Boc displayed roughly four times the level of γ-H2AX.

3.2.2 Blockade of canonical or non-canonical Shh signaling does not inhibit Boc-mediated γ-H2AX

During cerebellar development, Boc, which is expressed by GCPs, serves in a receptor complex with Ptch1 for the mitogen Shh (Izzi et al., 2011). Ligand-binding prevents inhibition of Smo by Ptch1 and triggers proliferation via activation of Gli-dependent transcription (Briscoe and Thérond, 2013). Importantly, this signaling cascade also leads to DNA breaks, and the consequent elevation of γ-H2AX can be blunted by inhibition of either Smo or Gli (Mille et al., 2014; Tamayo-Orrego unpublished data). Thus, we initially hypothesized that Boc drives DNA damage through this canonical Shh pathway.

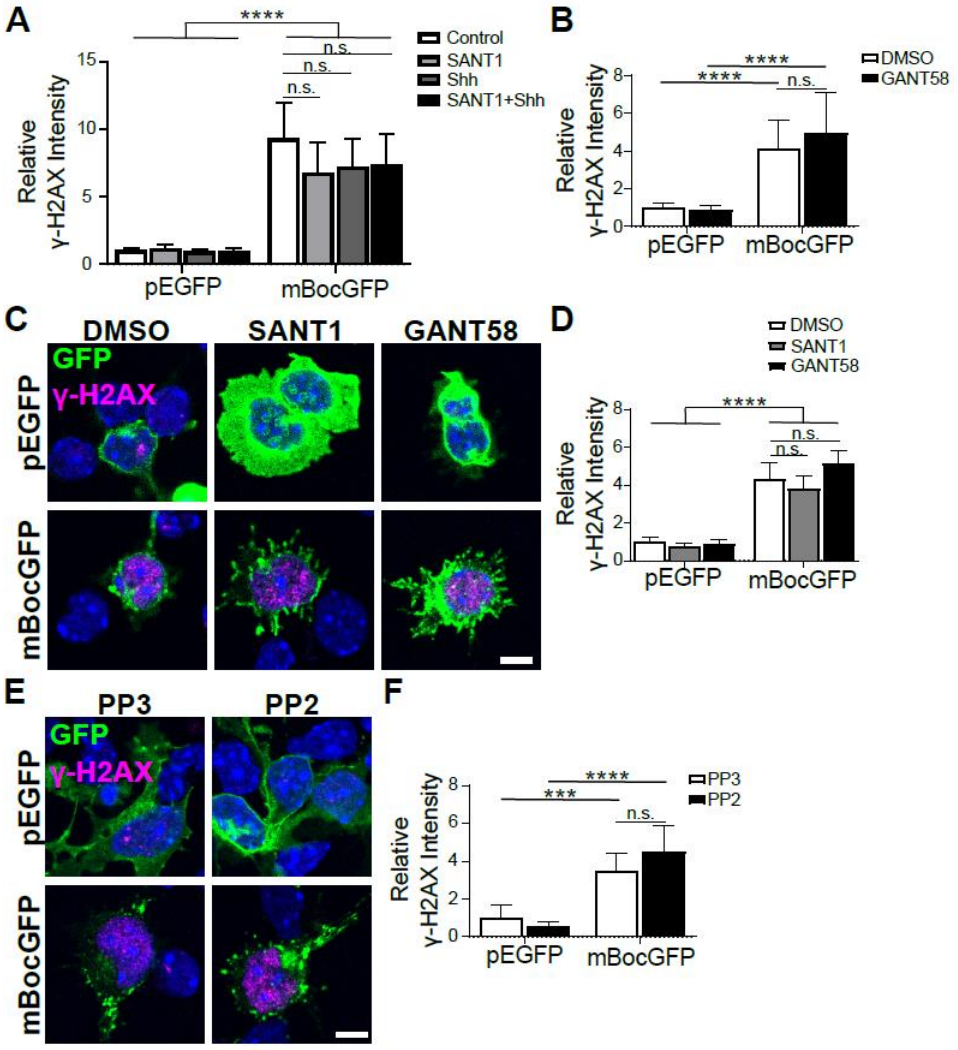

Figure 3-2. Inhibition of Smo, Gli, or SFKs does not reduce Boc-mediated γ-H2AX

A) 18 hours of 134 nm SANT1, 10 nM Shh, or both unable to significantly alter γ-H2AX. Graphs displaying γ-H2AX mean intensities normalized to pEGFP, DMSO ($n \geq 123$ cells per condition from three independent experiments). Error bars: 95% confidence interval. Data analyzed using three-way ANOVA with Tukey's multiple comparisons (****, $p<0.0001$; n.s., not significant).

B) No significant change to γ-H2AX after 18 hours of exposure to 5 μM GANT58. Bar graphs of γ-H2AX mean intensities normalized to pEGFP, DMSO ($n \geq 81$ cells per condition from two independent experiments). Error bars: 95% confidence interval. Data analyzed using two-way ANOVA with Tukey's multiple comparisons (****, $p<0.0001$; n.s., not significant).

C) Representative images of GFP and γ-H2AX immunostaining of transfected cells cultured for 6 hours in the presence of DMSO, 134nM SANT1, or 5 μM GANT58. Counterstained with DAPI. Images cropped and adjusted for brightness/contrast. Scale bar: 5 μM.

D) No significant change in γ-H2AX intensity following 6 hours of 134 nM SANT1 or 5 μM GANT58. Quantification of average γ-H2AX mean intensities normalized to pEGFP, DMSO ($n \geq 121$ cells per condition from three independent experiments). Error bars: 95% confidence

interval. Data analyzed using two-way ANOVA with Tukey's multiple comparisons (****, $p<0.0001$; n.s., not significant).
E) Representative images depicting electroporated cells treated with 0.2 μM of either PP3 or PP2 for 18 hours prior to GFP and γ-H2AX co-labeling. Counterstained with DAPI. Images cropped and adjusted for brightness/contrast. Scale bar: 5 μM.
F) PP2 does not blunt Boc-triggered γ-H2AX. Quantification of γ-H2AX mean intensities normalized to pEGFP, PP3 ($n \geq 91$ cells per condition from two independent experiments). Error bars: 95% confidence interval. Data analyzed using two-way ANOVA with Tukey's multiple comparisons (***, $p<0.001$; ****, $p<0.0001$; n.s., not significant).

First, I chose to block Smo activity with the antagonist SANT1, which acts by binding Smo at high affinity (Chen et al., 2002). Overnight exposure of electroporated cells to a concentration of SANT1 (134nM) sufficient to block Shh-dependent γ-H2AX did not significantly reduce γ-H2AX levels either alone or in combination with 10 nM Shh (**Figure 3-2A**) (Mille et al., 2014; Tamayo-Orrego unpublished data). As Shh stimulation did not significantly augment the levels of Boc-triggered γ-H2AX, I opted to perform future experiments without Shh for simplicity's sake. Next, I treated cells with 5 μM of GANT58, a drug that interferes with Gli-dependent transcription and at a dose that inhibits Boc-mediated proliferation in GCPs (Lauth et al., 2007; Mille et al., 2014). At 18 hours following electroporation, I observed no significant difference in the relative γ-H2AX intensity of BocGFP-expressing cells compared to the DMSO control (**Figure 3-2B**). Given the robust elevation of γ-H2AX observed 18 hours following Boc transfection, I speculated that any influence resulting from the small molecule inhibitors may be overwhelmed at this timepoint. Therefore, I also measured γ-H2AX in cells cultured for 6 hours after electroporation in the presence of either DMSO, SANT1, or GANT58 (**Figure3-2C, D**). Even at this shorter timepoint, overexpression of Boc was associated with a large increase in γ-H2AX; however, neither SANT1 nor GANT58 significantly diminished the effect of Boc (**Figure 3-2D**).

Second, I wondered if Boc-induced DNA damage may be mediated via a non-canonical cascade. Indeed, Boc, in addition to its role in GCPs, is also a co-receptor in a non-canonical Shh pathway, where Smo-activation leads to phosphorylation of Src-family kinases (SFKs) (Yam et al., 2009). This cascade is critical for the axon guidance of spinal commissural neurons. To test if SFK activity is necessary for Boc-triggered γ-H2AX, we utilized the inhibitor PP2, which our lab has previously employed to prevent axon turning in response to Shh. Compared to PP3, an

analogue of PP2 that does not affect SFK activity, administration of 0.2 μM PP2 did not significantly alter γ-H2AX levels in Boc-expressing cells after 18 hours in culture (**Figure 3-2E, F**). Hence, I have showed that H2AX phosphorylation in cells overexpressing Boc is unchanged by blockade of either canonical or non-canonical Shh signaling.

3.2.3 Boc-induced γ-H2AX does not require its cytoplasmic tail and is independent of PI3K or p38 MAPK signaling

Boc is a single-pass transmembrane protein of the Immunoglobin (Ig) superfamily, and its 1113 amino acids (1110 in mice) yield four IgG domains, three Fibronectin III (FNIIIa-c) repeats, a transmembrane region, and a relatively short cytoplasmic tail of 238 amino acids (Kang et al., 2002). The FNIII repeats are critical for Shh signaling through their interaction with Shh (FNIIIc) and Ptch1 (FNIIIa-b) (Izzi et al., 2011; Okada et al., 2006; Tenzen et al., 2006). On the other hand, the cytoplasmic tail is dispensable for canonical pathway activation, although it is likely involved in non-canonical signaling via its interaction with the guanine nucleotide exchange factor (GEF) Dock and its binding partner ELMO (Makihara et al., 2018; Song et al., 2015; Tenzen et al., 2006). If Boc directly regulates DNA damage in GCPs, then the interaction of the cytoplasmic tail with downstream effectors should be necessary for phosphorylation of H2AX.

To dissect the role of the intracellular domain, we employed a Boc mutant construct in which the cytoplasmic tail has been deleted (mBocGFPΔcytotail) and electroporated cells dissociated from *Boc*-null ($Boc^{AP2/AP2}$) cerebella to eliminate signal generated from dimerization of the mutant protein with endogenous Boc (Zhang et al., 2011b). At 6 hours post-transfection, there was no significant change in γ-H2AX between full-length and cytoplasmic tail-deleted Boc

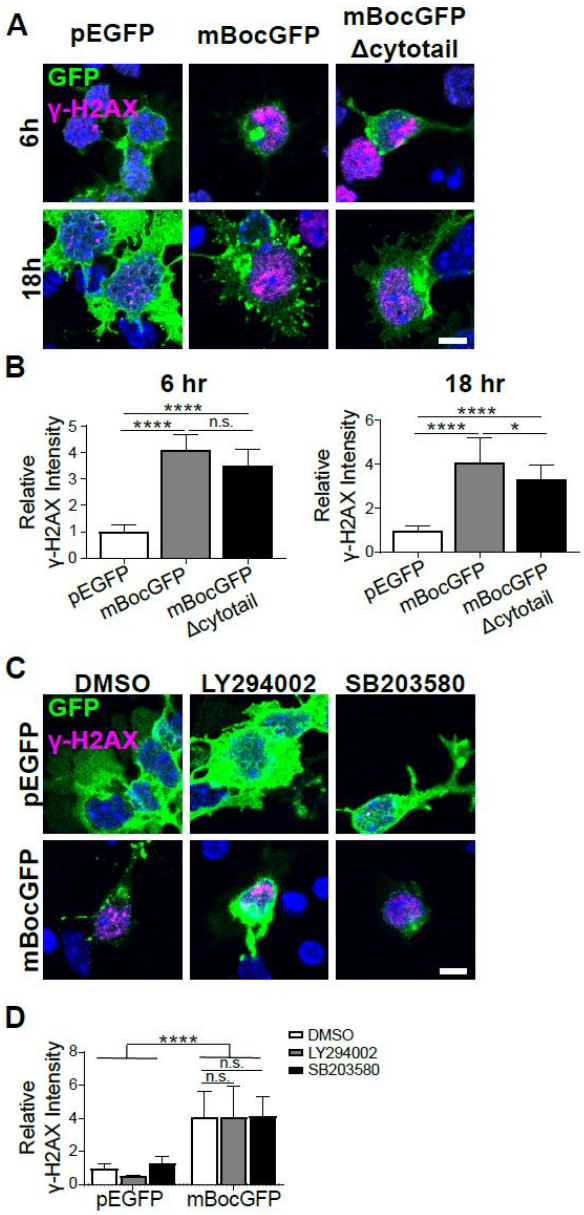

Figure 3-3. Boc-induced γ-H2AX does not require its cytoplasmic tail and is independent of PI3K and p38 MAPK signaling

A) Representative images of transfected *Boc*$^{AP2/AP2}$ cells cultured for 6 or 18 hours and labeled with antibodies against GFP and γ-H2AX. Counterstained with DAPI. Images cropped and adjusted for brightness/contrast. Scale bar: 5 μM.

B) Boc lacking the cytoplasmic tail (Δcytotail) induces high levels of γ-H2AX at both 6 (left graph) and 18 (right graph) hours post-electroporation. Quantification of γ-H2AX mean intensities normalized to pEGFP ($n \geq 160$ cells per condition from three independent experiments). Error bars: 95% confidence interval. Data analyzed using Kruskal-Wallis test with Dunn's multiple comparisons (*, $p<0.05$; ****, $p<0.0001$; n.s., not significant).

C) Representative images of GFP and γ-H2AX immunostaining on electroporated cells cultured for 18 hours in the presence of DMSO, 15 μM LY294002, or 10 μM SB203580. Counterstained with DAPI. Images cropped and adjusted for brightness/contrast. Scale bar: 5 μM.

D) No significant changes to γ-H2AX after treatment with either 15 μM LY294002 or 10 μM SB203580. Graph of γ-H2AX mean intensities normalized to pEGFP, DMSO ($n \geq 80$ cells per condition from two independent experiments). DMSO conditions (pEGFP and mBocGFP) are the same as **Figure 3-2B**. Error bars: 95% confidence interval. Data analyzed using two-way ANOVA with Tukey's multiple comparisons (****, $p<0.0001$; n.s., not significant).

(**Figure 3-3 A**[top]**, B**[left]). By 18 hours, however, there is a slight reduction of γ-H2AX in cells expressing the mutant construct although the levels are still much higher than the control, suggesting that the cytoplasmic tail, though not required, modulates Boc-induced γ-H2AX (**Figure 3-3 A**[bottom]**, B**[right]).

Along with functioning as a Shh co-receptor, Boc plays a ligand-independent role in the differentiation of myotubes (Kang et al., 2002). In this process, its cytoplasmic tail is expendable, and Boc acts upstream of p38 MAPK and Akt activation (Bae et al., 2010; Kang et al., 2002). Notably, both p38 MAPK and PI3K-Akt signaling have been linked to GCP proliferation. For instance, p38 MAPK expression is elevated in GCPs following Shh stimulation *in vitro*, and it is also strongly expressed in the EGL (Guldal et al., 2012). Either knock-down of p38 MAPK or inhibition of its activity with SB203580 blocked transcription of Shh signaling targets and attenuated GCP proliferation. Similarly, PI3K-Akt signaling is important for GCP proliferation and survival via upstream activators IGF1 and IGF2 (Dudek et al., 1997; Fernandez et al., 2010; Wechsler-Reya and Scott, 1999). In GCPs, impeding PI3K activity with the inhibitor LY294002 in the presence of Shh could reduce levels of N-Myc, a Gli transcriptional target important for proliferation (Kenney et al., 2004). Nevertheless, culturing electroporated cells overnight in the presence of 15 μM LY294002 or 10 μM SB203580 did not significantly abrogate the amount of γ-H2AX associated with Boc overexpression (**Figure 3-3C, D**). Here, the DMSO controls are the same as **Figure 3-2B**. These results suggest that high levels of Boc lead to H2AX phosphorylation independent of either PI3K or p38 MAPK inhibition.

3.2.4 Boc overexpression leads to activation of the DNA damage response network and cell cycle exit

The phosphorylation of H2AX occurs rapidly following DNA damage and represents an early step in the DDR cascade (Fernandez-Capetillo et al., 2004; Rogakou et al., 1998). The DDR is a complex signaling network which functions to sense DNA damage, to coordinate cell cycle arrest with DNA repair processes, and to modify, when necessary, mediators of cell senescence and apoptosis. The serine/threonine kinases Chk1 and Chk2 are key effectors of the DDR, and their activation is initiated when they are phosphorylated by ATR or ATM, respectively (Bartek and Lukas, 2003; Brown et al., 1999; Chaturvedi et al., 1999; Matsuoka et al., 1998; Smith et al., 2010). According to the textbook model, the introduction of DSBs instigates ATM-dependent phosphorylation of Chk2 at threonine 68 (T68) (Ahn et al., 2000; Matsuoka et al., 2000); whereas, replication stress triggers Chk1 phosphorylation by ATR at multiple sites, notably at serines 345 (S345) and 317 (S317) (Capasso et al., 2002; Liu et al., 2000; Niida et al., 2007; Smith et al., 2010; Wilsker et al., 2008). However, the molecular reality seems to be more complicated than this as there is evidence of crosstalk (Gatei et al., 2003; Hirao et al., 2002; Smith et al., 2010; Tominaga et al., 1999).

To assess the state of the DDR in cells overexpressing Boc, we cultured electroporated cells overnight and labeled them with antibodies against phosphorylated Chk1 (p-Chk1, S345), total Chk1, phosphorylated Chk2 (p-Chk2, T68), and total Chk2 (**Figure 3-4A, B, E, F**). Compared to control, cells transfected with Boc exhibited a slight increase in p-Chk1 (**Figure 3-4C**), but the difference in Chk1 expression, though significant, is negligible (**Figure 3-4D**). On the other hand, high levels of Boc correlate with a heartier elevation of both p-Chk2 and total Chk2 hinting at a more active ATM-Chk2 arm of the DDR (**Figure 3-4G, H**).

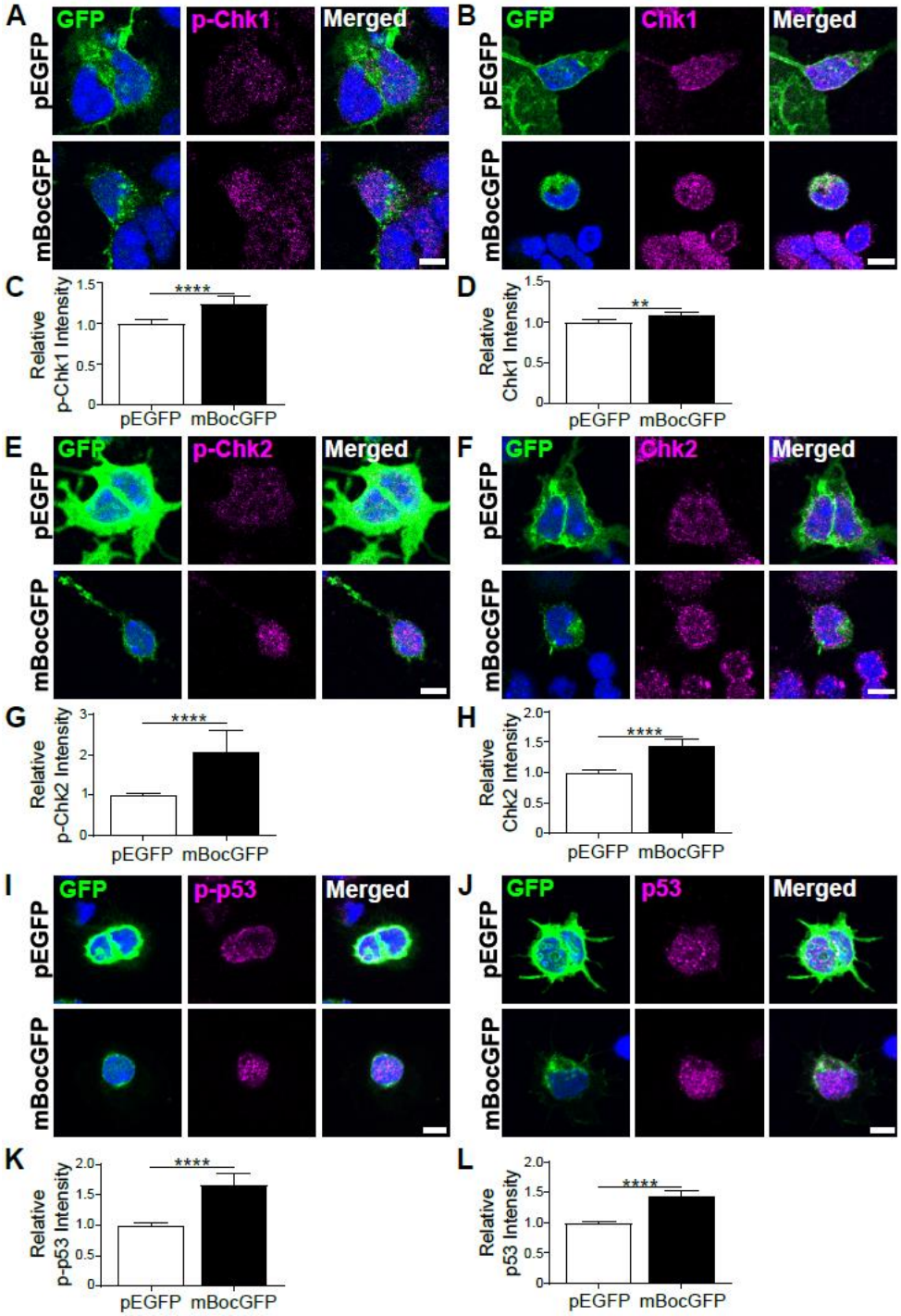

Figure 3-4. Boc overexpression is associated with activation of the DNA damage response network

A) Representative images of p-Chk1 (S345) and GFP immunofluorescence from electroporated cells. Counterstained with DAPI. Images cropped and adjusted for brightness/contrast. Scale bar: 5 µM.

B) Representative images of transfected cells co-labeled with antibodies against GFP and Chk1. Counterstained with DAPI. Images cropped and adjusted for brightness/contrast. Scale bar: 5 µM.
C) Increased p-Chk1(S345) levels in Boc-expressing cells (n=84) compared to pEGFP (n=121). Graph of relative p-Chk1 intensities normalized to pEGFP (two independent experiments). Error bars: 95% confidence interval. Data analyzed using Mann-Whitney U test (****, $p<0.0001$).
D) Negligible effect on Chk1 expression following mBocGFP electroporation. Graph of relative Chk1 intensities from mBocGFP cells (n=132) normalized to pEGFP (n=234 cells from three independent experiments). Data analyzed using Mann-Whitney U test (**, $p<0.01$).
E) Representative images of p-Chk2 (T68) co-labeling with GFP following electroporation. Counterstained with DAPI. Images cropped and adjusted for brightness/contrast. Scale bar: 5 µM.
F) Representative images of electroporated cells immunostained with antibodies against GFP and Chk2. Counterstained with DAPI. Images cropped and adjusted for brightness/contrast. Scale bar: 5 µM.
G) Elevated expression of p-Chk2 (T68) in Boc-expressing cells (n=69). Graph of relative p-Chk2 intensities normalized to pEGFP (n=170 cells from two independent experiments). Error bars: 95% confidence interval. Data analyzed using Mann-Whitney U test (****, $p<0.0001$)
H) Total Chk2 levels increased in mBocGFP-positive cells (n=73). Graphs of relative Chk2 intensity normalized to pEGFP (n=169 cells from two independent experiments). Error bars: 95% confidence interval. Data analyzed using Mann-Whitney U test (****, $p<0.0001$).
I) Representative images of p-p53 (S15) and GFP immunostaining following transfection. Counterstained with DAPI. Images cropped and adjusted for brightness/contrast. Scale bar: 5 µM.
J) Representative images of electroporated cells co-labeled with antibodies against GFP and p53. Counterstained with DAPI. Images cropped and adjusted for brightness/contrast. Scale bar: 5 µM.
K) Higher p-p53 (S15) in Boc-expressing cells (n=93). Graphs of relative p-p53 intensities normalized to pEGFP (n=204 cells from two independent experiments). Error bars: 95% confidence interval. Data analyzed using Mann-Whitney U test (****, $p<0.0001$).
L) Upregulation of p53 following mBocGFP electroporation (n=143 cells). Graphs of relative p53 intensities normalized to pEGFP (n=329 cells from three independent experiments). Error bars: 95% confidence interval. Data analyzed using Mann-Whitney U test (****, $p<0.0001$).

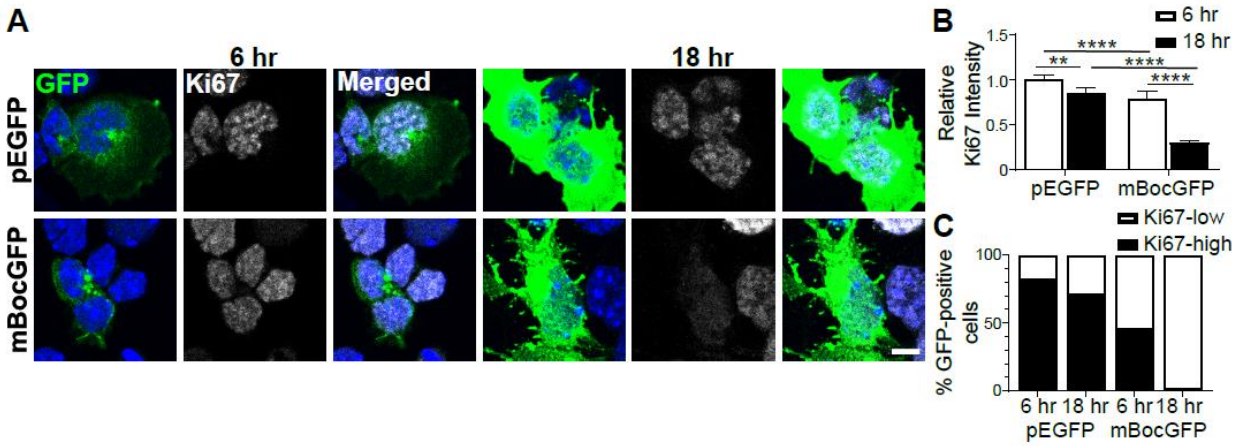

Figure 3-5. Loss of Ki67 expression in BocGFP-positive cells by 18 hours post-electroporation

A) Representative images of Ki67 and GFP co-labeling at 6 and 18 hours after electroporation of *Boc*$^{AP2/AP2}$ cells. Counterstained with DAPI. Images cropped and adjusted for brightness/contrast. Scale bar: 5 µM.

B) Ki67 levels highly diminished 18 hours after mBocGFP transfection. Graphs of relative Ki67 intensities normalized to 6h pEGFP (n≥160 cells from three independent experiments). Error bars: 95% confidence interval. Data analyzed using two-way ANOVA with Tukey's multiple comparisons (**, $p<0.01$; ****, $p<0.0001$).

C) Fewer Ki67-positive cells 18 hours after mBocGFP transfection. Graph depicting that 82.6% (190/230) and 72.2% (151/209) of pEGFP-positive cells express high levels of Ki67 (black bars) at 6 and 18 hours post-electroporation, respectively. On the other hand, mBocGFP-positive cells that express high levels of Ki67 (black bars) drops to 1.9% (3/160) at 18 hours from 46.2% (103/223) at 6 hours. Data combined from three independent experiments.

Activation of cell cycle checkpoints following DNA damage is vital for maintenance of genomic stability and thus represents an essential anti-cancer barrier. Likewise, senescence and apoptosis provide more permanent impediments to the propagation of DNA damage. The stabilization and activation of p53 is central to regulating these choice points; hence, ATM/ATR also phosphorylate p53 at serine 15 (S15), thus disrupting the interaction of p53 with its negative regulator MDM2 and leading to protein accumulation (Banin et al., 1998; Canman et al., 1998; Khanna et al., 1998; Lakin et al., 1999; Tibbetts et al., 1999; Weinberg, 2007). As a result, loss of *Atm* blocks phosphorylation and accumulation of p53 in murine GCPs following *in vivo* irradiation and renders them insensitive to irradiation-induced apoptosis (Herzog et al., 1998; Lee et al., 2001). BocGFP-positive cells express higher levels of both phosphorylated p53 (p-p53, S15) and total p53 (**Figure 3-4I-L**).

The intense staining of γ-H2AX in Boc-overexpressing cells implies extensive DNA damage that is unlikely to be tolerated by the cell; therefore, we aimed to measure the cell cycle consequence of Boc upregulation by immunostaining cells for Ki67 at both 6 and 18 hours after electroporation. Although there is a modest reduction of Ki67 in GFP-positive cells 6 hours after mBocGFP electroporation compared to control, Ki67 levels are drastically lower in Boc-expressing cells by 18 hours (**Figure 3-5A, B**). A similar trend is observed when we compare the percent of electroporated cells that highly express Ki67 (**Figure 3-5C**). Together, these results suggest that overexpression of Boc is associated with activation of the DDR network which leads to cell cycle exit.

3.2.5 Electroporation of mBocGFP targets relatively few GCPs in culture but still triggers a transient increase in γ-H2AX

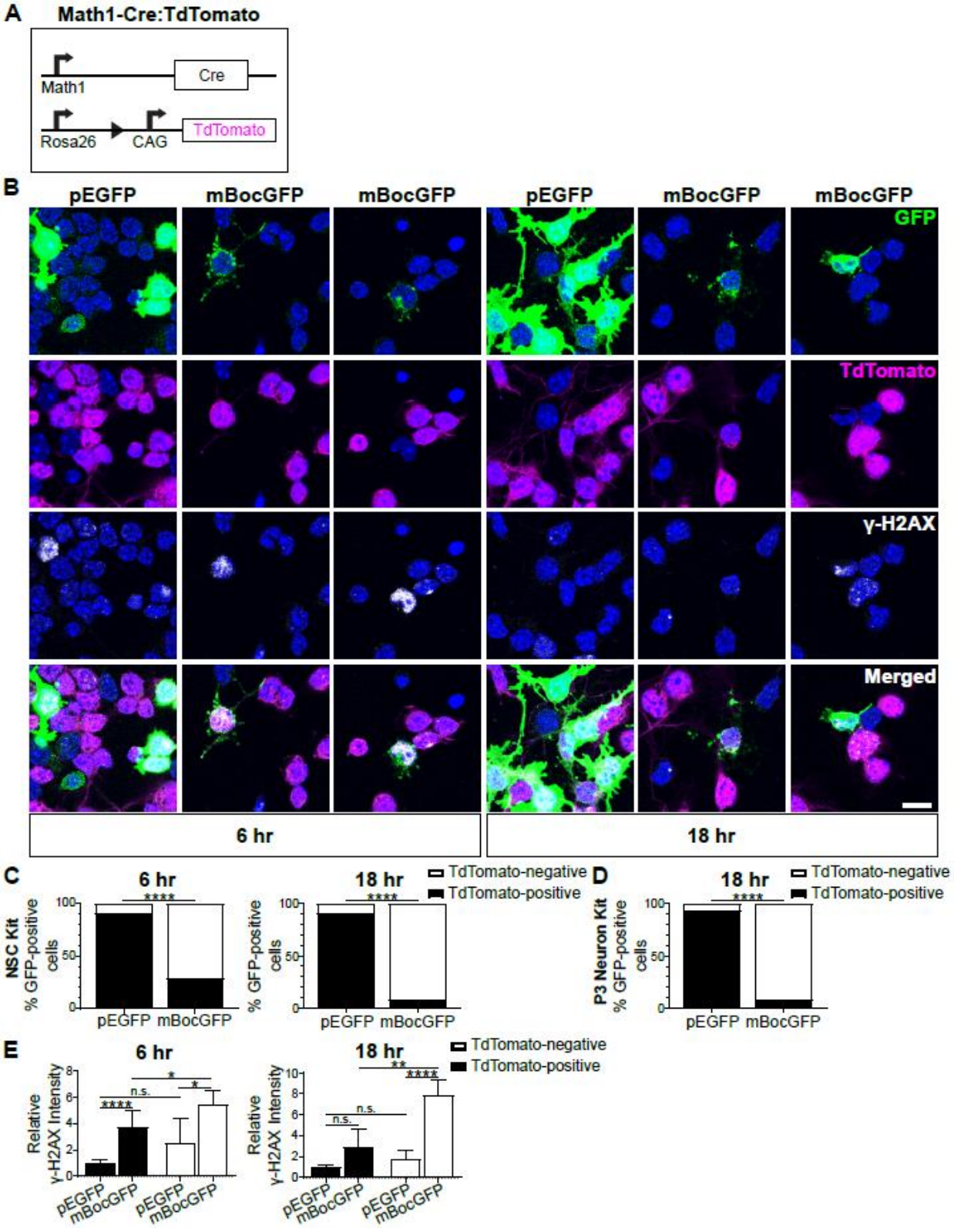

Figure 3-6. Electroporation of BocGFP mostly targets *Math1*-Cre;TdTomato-negative cells *in vitro* but still triggers a transient increase of γ-H2AX in TdTomato-positive cells

A) Schematic illustrating transgenes of *Math1*-Cre;TdTomato mice.
B) Representative images of *Math1*-Cre;TdTomato dissociated GCPs labeled with antibodies against GFP and γ-H2AX 6 or 18 hours after transfection with either pEGFP or mBocGFP. Counterstained with DAPI. Images cropped and adjusted for brightness/contrast. Scale bar: 10 μM.
C) Few cells transfected with mBocGFP express TdTomato at either 6 or 18 hours. Assessment of TdTomato expression 6 hours (left graph) or 18 hours (right graph) after electroporation with neural stem cell (NSC) kit shows that 90.8% (237/261) and 90.7% (284/313) of pEGFP-positive cells express TdTomato. Only 28.6% (60/210) of mBocGFP-expressing cells are TdTomato-positve at 6 hours, which decreases to 7.7% (13/169) by 18 hours. Data analyzed using Fisher's exact test (n=261 and 210 at 6hr; n=313 and 169 at 18 hr from three independent experiments; ****, $p<0.0001$).
D) The percent of TdTomato-positive cells expressing mBocGFP unchanged by primary neuron electroporation solutions. Graph depicting that 93.4% of pEGFP-positive cells (226/242) but only 8.3% of mBocGFP-positive cells (10/120) are also TdTomato-positive. Data analyzed with Fisher's exact test (n=242 and 120 from two independent experiments; ****, $p<0.0001$)
E) Regardless of TdTomato expression, Boc significantly increases γ-H2AX 6 hours post-electroporation, whereas only TdTomato-negative cells show significant upregulation at 18 hours. Quantification of γ-H2AX mean intensities normalized to pEGFP, TdTomato-positive. 6 hours after electroporation (left graph), γ-H2AX is significantly higher in both TdTomato-positive cells (black bars) and TdTomato-negative cells (white bars) expressing mBocGFP (n=60 and 150, respectively) compared to pEGFP (n=237 and 24 from three independent experiments). 18 hours after electroporation (right graph) γ-H2AX is significantly higher in TdTomato-negative cells (white bars) but not TdTomato-positive cells (black bars) expressing mBocGFP (n=266 and 23, respectively) compared to pEGFP (n=45 and 510 from five independent experiments). Data analyzed using two-way ANOVA with Tukey's multiple comparisons (****, $p<0.0001$, **, $p<0.01$, *, $p<0.05$, n.s., not significant).

Though the change to y-H2AX after Boc electroporation *in vitro* has been consistent, I have been unable to robustly interfere with this effect using small molecules. Furthermore, my struggle to model Boc overexpression by *in vivo* electroporation has been too technically challenging to make conclusions regarding H2AX phosphorylation (data not shown). These concerns combined with the fact that the overall efficiency of BocGFP expression is drastically lower than that of the pEGFP control prompted me to test whether the experimental paradigm is actually targeting GCPs.

Dissociation of dissected cerebella and purification using sucrose gradients yields cultures that are mostly GCPs with rare interneurons, astrocytes, and oligodendrocytes (Wechsler-Reya and Scott, 1999). To distinguish GCPs from the others, we took advantage of reporter mice where strong expression of TdTomato via the CAG promoter is restricted by Cre expression – controlled by the *Math1*-promoter – that drives recombination of loxP sites flanking the stop codon inserted upstream of *TdTomato* in the *Rosa26* locus (**Figure 3-6A**) (Madisen et al., 2010; Matei et al., 2005). In the postnatal cerebellum, the Math1-lineage, and thus TdTomato expression, is dominated by GCPs and granule neurons (Yang et al., 2008). As expected, about 90% of the GFP-positive cells in the control are also TdTomato-positive regardless of time in culture (**Figure 3-6B, C**). Contrariwise, 28.6% of the GFP-positive cells express TdTomato 6 hours after mBocGFP electroporation, and even fewer of the mBocGFP-expressing cells are TdTomato-positive at 18 hours (7.7%) (**Figure 3-6B, C**). These experiments were conducted using the Amaxa kit designed for NSCs. Because many of my previous experiments were performed using the kit designed for primary neurons (P3 neuron kit), I also electroporated *Math1*-Cre;TdTomato cells with the P3 neuron kit, and as shown in **Figure 3-6D**, the results are

nearly identical at 18 hours post-electroporation compared to the NSC kit indicating that the difference observed was not due to the specific reagents (**Figure3-6C** [right graph]).

Because the relative number of GCPs that express mBocGFP compared to pEGFP are so different, it is possible that this difference is what drives the effect on γ-H2AX. Therefore, I also labeled these *Math1*Cre;TdTomato cells with an antibody against γ-H2AX (**Figure 3-6B**). At 6 hours, both TdTomato-positive (black bars) and TdTomato-negative (white bars) cells that expressed mBocGFP displayed significantly higher levels of γ-H2AX compared to pEGFP (**Figure 3-6E** [left]). Because of the paucity of mBocGFP-positive cells that express TdTomato at 18 hours, I combined the NSC and P3 neuron kit experiments to increase the number of cells for quantification and found that Boc expression was only significantly associated with elevated γ-H2AX in TdTomato-negative cells at 18 hours (**Figure 3-6E** [right]). These results indicate that while only a few GCPs express mBocGFP, it still – at least transiently – leads to an increase in H2AX phosphorylation, a marker of DNA damage.

3.3 Discussion

For all these experiments, I employed electroporation to highly express Boc with the aim to simulate the upregulation that occurs during the neoplastic transformation of GCPs. The intense γ-H2AX levels observed was reminiscent of the expression pattern following UV radiation and seemed at the time to indicate that Boc can induce DNA damage in GCPs – a result that was supported by immunolabeling cells with other DDR effectors. To identify mediators of H2AX phosphorylation, I screened a total of 11 small molecule inhibitors including those presented above, none of which significantly altered the intensity of γ-H2AX in Boc-expressing cells compared to the control-treated condition (**Table 3-1**). In what was intended to be a final

Table 3-1. Screen targeting Boc-triggered γ-H2AX with small molecule inhibitors

Drug ([Final])	Target	Result relative to mBocGFP control (# of experiments)
SANT1 (134 nM)	Smo	No effect (3 at 18h, 3 at 6h)
GANT58 (5 μM)	Gli	No effect (2 at 18h, 3 at 6h)
PP2 (0.2 μM)	SFKs	No effect (2)
LY294002 (15 μM)	PI3K	No effect (2)
SB203580 (10 μM)	p38 MAPK	No effect (2)
Rapamycin (0.1 μM)	mTOR	No effect (2)
U0126 (10 μM)	MKK 1/5	No effect (1)
H89 (10 μM)	PKA	No effect (1)
IWR1 (10 μM)	TNKS/Axin	No effect (1)
GSK2606414 (100 nM, 500nM)	PERK	No effect (2)
NAC (2.5 mM)	Glutathione reductase	No effect (1)
LY294002 (15 μM) + GSK2606414 (100nM)	PI3K + PERK	No effect (2)

control experiment to confirm that electroporated cells are in fact GCPs, I capitalized on a reporter mouse line readily available in the lab to label GCPs. Shockingly, the data indicate that GCPs are a minority of mBocGFP-positive cells, especially at 18 hours; a finding that hinders the interpretation of the previously presented results. Nevertheless, Boc overexpression by transient transfection can trigger γ-H2AX acutely.

Granule neurons and their precursors are overwhelmingly the major cell type of the developing cerebellum, representing more than 80% of all cells at P7 (Carter et al., 2018), and data generated from whole cerebellum extracts – even without purification using a sucrose gradient – reflect mostly this lineage (Frank et al., 2015). Thus, our assumption that the cell-type composition targeted by electroporation would mirror the overall distribution was not inherently inappropriate. In fact, the GFP expression profile did match expectations (**Figure 3-6B-D**). In retrospect, the results align with multiple instances where transfection of Boc thwarted our expectations: (1) the paucity of BocGFP-positive cells following transfection, (2) the presence of pan-nuclear rather than foci of γ-H2AX immunolabeling, and (3) the lack of γ-H2AX modulation in response to chemical inhibition of canonical Shh signaling. None of these points are proof that Boc-expressing cells are not GCPs, but they do indicate that Boc electroporation does not mimic our observations about the function of endogenous Boc.

While GCPs are a small subset of BocGFP-positive cells, γ-H2AX is higher in these cells compared to control at 6 hours (**Figure 3-6E**). By 18 hours, this effect is diminished and is no longer statistically significant. When we compare the distribution of Ki67 staining (**Figure 3-5C**) with the expression of TdTomato (**Figure 3-6C**), it becomes apparent that the proportion of GCPs at each time point is probably the major contributor to the levels of Ki67. Ironically, the general conclusion may still be correct because this reduction in TdTomato-positive cells is

likely due to a loss of GCPs; I consistently notice fewer Boc-positive cells at 18 hours than at 6 hours as suggested by the 'n' for the above experiments (**Figure 3-5C**, n=223 at 6h and 160 at 18h; **Figure 3-6C**, n=210 at 6h and 169 at 18h). From this data, I think it is probable that Boc-expressing GCPs with high levels of y-H2AX die between 6- and 18-hours following transfection. Although electroporation in cerebellar granule neurons has been successfully implemented to study neurite outgrowth and is highly efficient at expressing pEGFP in my own experiments, instances of transfection-related toxicity both in the literature and my own experience inform my insistence that future experiments need to be done with a second method of overexpressing Boc (Hutson et al., 2011; Kim et al., 2002; Rodriguez and Flemington, 1999).

As it stands, Boc-expressing cells are almost entirely non-GCPs at 18 hours. Based on the elevation of y-H2AX, p-Chk1, p-Chk2, and p-p53, it is tempting to speculate that Boc activates the DDR in non-GCPs and that this phenotype is resistant to the small molecule inhibitors we tested, which did not attenuate γ-H2AX compared to the mBocGFP control (without considering pEGFP). However, there are multiple non-GCP cell types in these cultures (Wechsler-Reya and Scott, 1999). For instance, it has been previously reported that a sub-population of Nestin-positive cerebellar progenitors in the EGL will proliferate following Shh stimulation *in vitro*, though they are mostly quiescent *in vivo* (Li et al., 2013). Furthermore, these cells exhibit low expression of certain DNA repair genes and more DNA breaks than GCPs following *Ptch1* deletion. Future work will be necessary to determine if there is a link between Boc expression and DDR activation in other cerebellar cell types. As non-GCPs are such a small portion of these cultures, it would be more efficient to apply different purification methods for testing this question, and fortunately, specific protocols currently exist for the isolation of NSCs or astrocytes (Lee et al., 2005; McCarthy and de Vellis, 1980).

Boc is also expressed embryonically in the ventricular zone, the source of cerebellar inhibitory neurons and glia, where it has been demonstrated that Shh is involved in the proliferation of radial glia (Huang et al., 2010; Izzi et al., 2011; Leto et al., 2016). Moreover, Shh signaling has also been implicated in the differentiation of Bergmann glia at early postnatal stages *in vitro* and in the regulation of astrocyte diversity in the adult cerebellum (Dahmane and Ruiz-i-Altaba, 1999; Farmer et al., 2016). It would be interesting both to determine if Boc is an obligate receptor for these Shh-related functions and to test if glial progenitors also display Shh-dependent DNA damage.

Chapter 4

Manipulation of PI3K or Ezh2 signaling in the developing mouse cerebellum induces a myogenic phenotype: Insights into a rare medulloblastoma variant

4.1 Summary

The era of molecular profiling has not only enhanced the search for targeted cancer therapies but has also highlighted the heterogeneity within various tumor-types, such as the pediatric brain malignancy MB. Moving forward, the creation of more preclinical models to better reflect the diversity of human tumors will improve the design and testing of novel treatments. Here, we describe a mouse model of medullomyoblastoma (MMB), a rare MB variant. *Ptch1*$^{+/-}$ mice that conditionally express *Pik3ca*^{H1047R} in the early cerebellum develop brain tumors whose transcriptome resembled that of human MMBs. In addition, mutant PI3K produced a myogenic phenotype in the postnatal cerebellum independent of Ptch1. Interestingly, tumors caused by targeted deletion of both *Ptch1* and *Ezh2* also displayed myogenic marker expression, and *in vitro* blockade of Ezh2 enzymatic activity in the presence of Shh triggered myogenic marker expression in GCPs, an MB cell-of-origin. A subset of wildtype GCPs endogenously express the muscle-specific transcription factor Myogenic differentiation (MyoD), and though there are more MyoD-positive GCPs in the EGL of Pik3ca^{H1047R} mice, Ezh2 inhibition did not change the number of MyoD-expressing cells. In both experimental paradigms, MyoD colocalized with muscle markers while the GCP transcription factor Pax6 did not. Collectively, our results indicate that manipulation of either PI3K or Ezh2 signaling can trigger a fate change in GCPs, likely through the activation of MyoD-dependent transcription, to produce the myoblast-like cells found in MMB.

4.2 Results

4.2.1 PI3K H1047R in *Ptch1*$^{+/-}$ mice induces muscle-related gene expression in advanced tumors

As documented in Chapter 1, our lab uncovered a murine *Ptch1*$^{+/-}$ tumor that contained a spontaneous H1047R mutation in p110α, the catalytic subunit of PI3K (*Pik3ca*^{H1047R}), and this tumor exhibited elevated expression of muscle-related genes (**Figure 1-7A-B**). The H1047R mutation has been reported to induce fate plasticity in a mouse model of breast cancer when it is expressed in a lineage-restricted manner, leading us to suspect that aberrant activation of PI3K signaling caused the observed changes in the *Ptch1*$^{+/-}$ tumor transcriptome (Koren et al., 2015; Van Keymeulen et al., 2015).

To test if *Pik3ca*^{H1047R} in combination with *Ptch1*$^{+/-}$ is sufficient to trigger expression of muscle genes, we took advantage of a three readily available mouse lines: the previously described conditional *Pik3ca*^{H1047R} knock-in mouse, a *Math1*-Cre mouse, and the *Ptch1*$^{+/-}$ mouse (Adams et al., 2011; Goodrich et al., 1997; Matei et al., 2005). Crossing the three lines generated transgenic mice that were germline heterozygous for *Ptch1* and that expressed constitutively active PI3K in Math1-expressing cells and their progeny (**Figure 4-1A**). For simplicity, we will henceforth use *Ptch1*$^{+/-}$*;Pik3ca*^{WT} and *Ptch1*$^{+/-}$*;Pik3ca*^{H1047R} to distinguish Cre-negative from Cre-positive animals.

In accordance with recently published results, we observed that the *Pik3ca* mutation alone did not drive tumor formation but did collaborate with loss of *Ptch1* to increase tumor incidence (**Figure 4-1B**) (Niesen et al., 2020). We collected tissue from *Ptch1*$^{+/-}$*;Pik3ca*^{WT} and *Ptch1*$^{+/-}$*;Pik3ca*^{H1047R} advanced tumors for RNA sequencing to compare the gene expression profiles between the two genotypes. To do this, we first utilized the t-Distributed Stochastic Neighbor Embedding (t-SNE) algorithm to visualize the transcriptional profiles of these tumors along with the previous cohort of *Ptch1*$^{+/-}$ tumors from our lab, P7 GCPs, and samples from a publicly available dataset (GSE34126) that included *Ptch1*$^{+/-}$ tumors, a G3-MB mouse model,

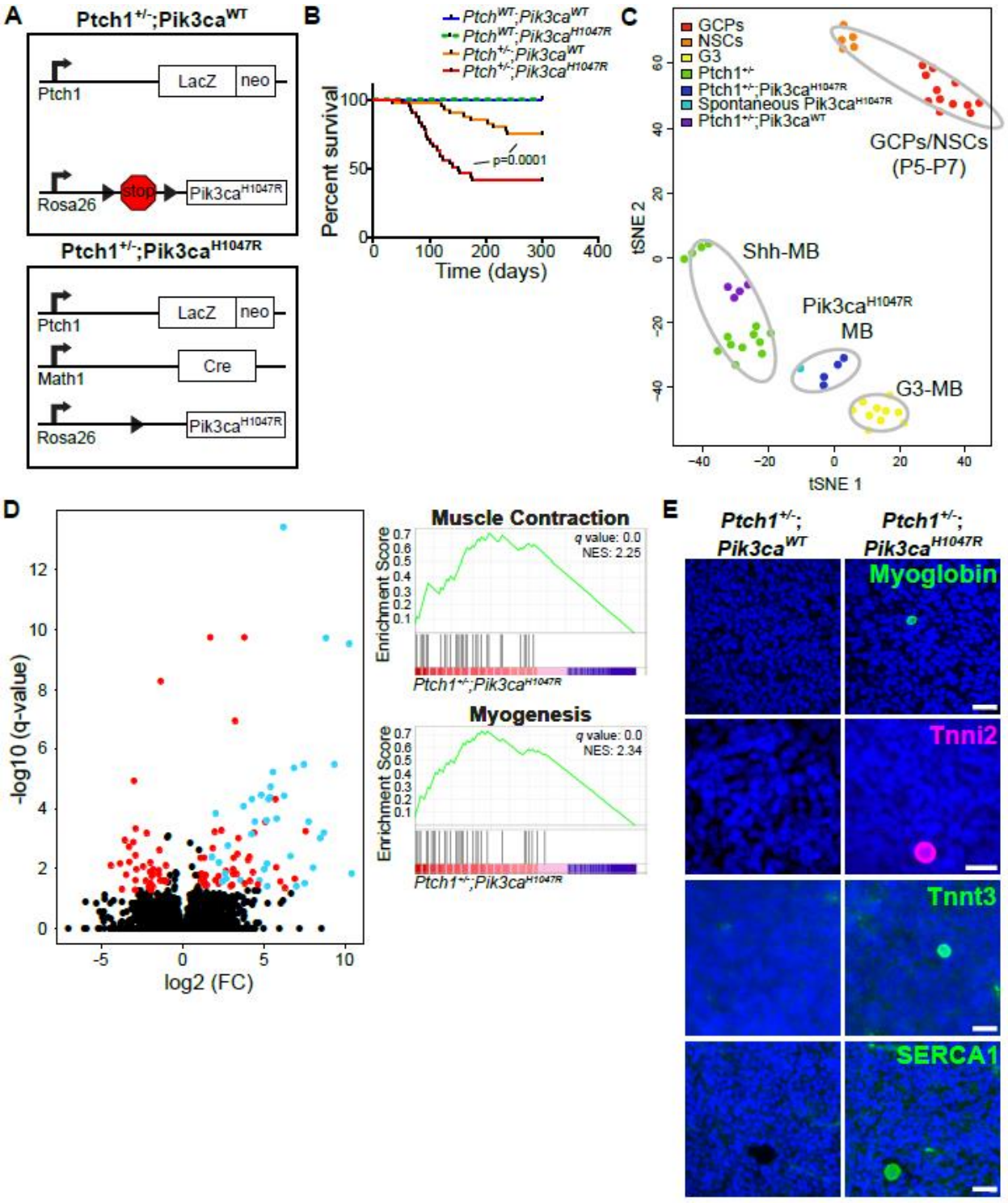

Figure 4-1. PI3K H1047R in *Ptch1*$^{+/-}$ mice induces muscle-related gene expression in advanced tumors

A) Schematic of transgenic mice genotypes. *Ptch1*$^{+/-}$*;Pik3ca*^{WT} (top) refers to mice with a mutant *Ptch1* allele and *Pik3ca*^{H1047R} transgene but lacking expression of Cre while *Ptch1*$^{+/-}$*;Pik3ca*^{H1047R} (bottom) refers to Cre-positive animals.

B) H1047R PI3K increases tumor incidence in *Ptch1*$^{+/-}$ background. Kaplan-Meier survival curve of *Ptch1*^{WT};*Pik3ca*^{WT} (blue line, n=0/42), *Ptch1*^{WT};*Pik3ca*^{H1047R} (green line, n=0/33), *Ptch1*$^{+/-}$;*Pik3ca*^{WT} (orange line, n=10/40), and *Ptch1*$^{+/-}$;*Pik3ca*^{H1047R} (red line, n=24/41). Data analyzed by log-rank test.
C) Spontaneous and genetically engineered *Pik3ca*^{H1047R} tumors cluster together. t-distributed stochastic neighbor embedding (t-SNE) graphical representation of expressed genes derived from either post-natal day 5-7 (P5-7) mouse cerebella: granule cell precursors (GCPs, red) or neural stem cells (NSCs, orange), or from mouse tumor samples: Group 3 model (G3, yellow), Sonic hedgehog (Shh) model (*Ptch1*$^{+/-}$, green; *Ptch1*$^{+/-}$;*Pik3ca*^{WT}, purple), and *Pik3ca*^{H1047R} (spontaneous, cyan; *Ptch1*$^{+/-}$;*Pik3ca*^{H1047R}, blue). GSE34126 provided data for NSCs, 4 *Ptch1*$^{+/-}$ MBs, and G3-MBs (Pei et al., 2012). 75% confidence ellipse drawn around each subgroup.
D) Increased muscle gene expression in *Ptch1*$^{+/-}$;*Pik3ca*^{H1047R} tumors. Volcano plot (left) illustrating differentially expressed genes between *Ptch1*$^{+/-}$;*Pik3ca*^{H1047R} (n=4) and *Ptch1*$^{+/-}$;*Pik3ca*^{WT} (n=4) tumor RNA sequencing Red dots indicate differentially expressed genes (|log2-fold change (FC)| ≥1 and *q* value <0.05) and cyan dots indicate upregulated muscle contraction and myogenesis genes. GSEA plots (right) depicting a significant muscle contraction (top plot) and myogenesis (bottom) gene enrichment. NES, normalized enrichment score.
E) Representative images of immunostainings on *Ptch1*$^{+/-}$;*Pik3ca*^{WT} and *Ptch1*$^{+/-}$;*Pik3ca*^{H1047R} tumor sections with antibodies against myoglobin (n=2/3 animals per genotype), Tnni2 (n=4 animals per genotype), Tnnt3 (n=5/4 animals per genotype), or SERCA1 (n=4 animals per genotype). Counterstained with DAPI. Images cropped and adjusted for brightness/contrast. Scale bars: 25 μM.

and NSCs (**Figure 4-1C**) (Pei et al., 2012). While the *Ptch1*$^{+/-}$*;Pik3ca*^{WT} tumors grouped with the other *Ptch1*$^{+/-}$ tumors, *Ptch1*$^{+/-}$*;Pik3ca*^{H1047R} tumors, whether spontaneous or genetically engineered, clustered closer to each other than to either *Ptch1*$^{+/-}$ or G3 tumors. Compared to *Ptch1*$^{+/-}$*;Pik3ca*^{WT} tumors, *Ptch1*$^{+/-}$*;Pik3ca*^{H1047R} tumors differentially expressed 118 genes (|log2-fold change| ≥1, FDR <0.05) (**Figure 4-1D** left). Of the 79 upregulated genes, 38 (48.1%) were related to the muscle contraction and myogenesis gene sets denoted by gene set enrichment analysis (GSEA) (**Figure 4-1D** right). We verified that these transcriptional changes were also reflected at the protein level by immunostaining tumor sections with antibodies against the following myogenic markers: myoglobin, troponin I2 (Tnni2), troponin T3 (Tnnt3), and sarcoplasmic/endoplasmic reticulum calcium ATPase 1 (SERCA1) (**Figure 4-1E**). For myoglobin, Tnni2, and Tnnt2, all of the Pt*ch1*$^{+/-}$*;Pik3ca*^{H1047R} tumors contained positive cells compared to zero control tumors. There was one *Ptch1*$^{+/-}$*;Pik3ca*^{WT} sample with a few SERCA1-positive cells, and again, all Pt*ch1*$^{+/-}$*;Pik3ca*^{H1047R} tumors analyzed contained positive cells. These results demonstrate that *Pik3ca*^{H1047R} triggers myogenic gene expression in a subpopulation of advanced tumor cells.

4.2.2 *Ptch1*$^{+/-}$*;Pik3ca*^{H1047R} tumors present a medullomyoblastoma-like phenotype

Although we were initially puzzled by this muscular phenotype, we were excited to find in the literature that the presence of myoblastic cells within medulloblastoma, often referred to as MMB, is an infrequent but well documented phenomenon (Helton et al., 2004). The gene expression profile of the *Ptch1*$^{+/-}$*;Pik3ca*^{H1047R} tumors made it plausible that these mice represented the first genetically engineered mouse model of MMB. Direct comparison of the

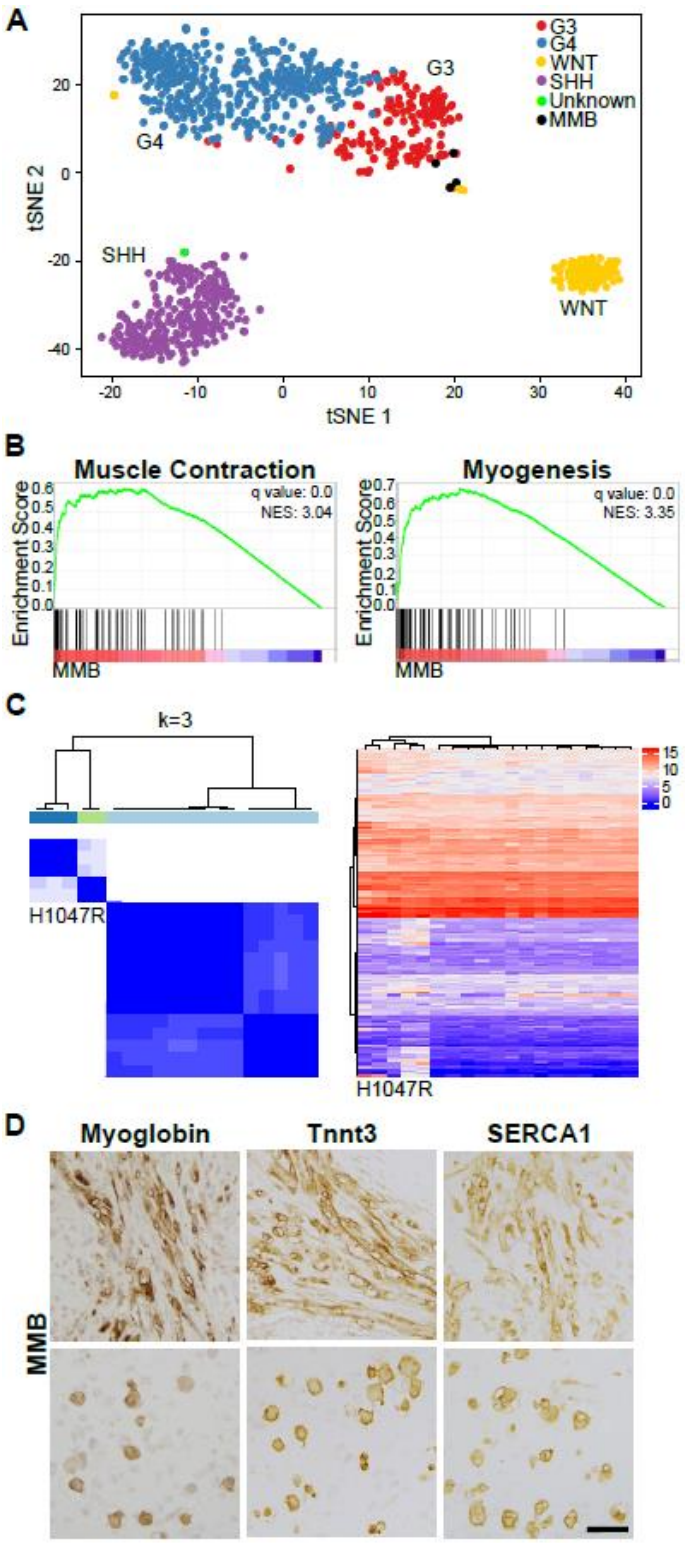

Figure 4-2. *Ptch1*$^{+/-}$;*Pik3ca*^{H1047R} tumors present a MMB-like phenotype

A) t-SNE representation of all expressed genes from human MBs obtained from 4 publicly available datasets (GSE37418, GSE67850, GSE12992, GSE85217) where all tumors except one unknown (green) are defined either by MMB histology (black) or by molecular subtype: G3 (red), G4 (blue), SHH (purple), WNT (yellow).

B) GSEA of genes upregulated in MMBs compared to MBs show a significant enrichment in muscle contraction (left plot) and myogenesis (right plot) gene sets. NES, normalized enrichment score.

C) Clustering with MMB gene signature distinguishes *Pik3ca*^{H1047R} from other *Ptch1*$^{+/-}$ tumors. Consensus clustering (left) of *Ptch1*$^{+/-}$ mouse tumors with (n=5) or without (n=14) the PI3K H1047R mutation using an MMB signature of 219 genes whose expression is visualized in the heatmap (right). In clustering, blue gradient is proportional to frequency of co-clustering.

D) Images illustrating the presence of either elongated strap-like or rounded myoblast-like cells in human MMB. Immunohistochemistry using antibodies against myoglobin, Tnnt3, and SERCA1. Counterstained with hematoxylin. Images cropped and adjusted for brightness/contrast. Scale bar: 50 µM.

mouse and human tumor transcriptomes was not a simple task as very little is known about the molecular signature of MMB; hence, we first set out to explore the gene expression profile of human MMB using four annotated samples (GSM324062, GSM918644, GSM918618, GSM1657171) from three publicly available datasets (GSE12992, GSE67850, GSE37418) plus a large, more recent dataset (GSE85217) (**Figure 4-2A**) (Cavalli et al., 2017; Fattet et al., 2009; Ho et al., 2015; Robinson et al., 2012). When subgroup classification was not assigned by the original publication, we adopted the subgroup provided by a recent re-analysis of human MBs (Weishaupt et al., 2019). Although our sample size is too small to determine whether MMB represents an independent molecular subgroup or whether it is a histology-type within one or more of the existing subgroups, it should be noted that the algorithms generated by Weishaupt *et al.* designated two of the MMBs (GSM324062, GSM1657171) as G3 tumors (2019).

GSEA analysis of differentially expressed genes ($|\log2\text{-fold change}| \geq 1$, FDR < 0.01) between MMB tumors and other MBs revealed an enrichment of genes associated with myogenesis and muscle contraction, the same pathways identified in the mouse tumor analysis (**Figure 4-2B**). Employing the 219 differentially expressed genes as an 'MMB gene signature,' we analyzed the mouse tumors by consensus clustering and found that *Pik3ca*^{H1047R} tumors clustered separately from the other *Ptch1*$^{+/-}$ tumors due to their elevated expression of many MMB signature genes as visualized by the heatmap (**Figure 4-2C**). Moreover, *Pik3ca*^{H1047R} tumors split into two clusters, suggesting that the gene expression profiles of these tumors are heterogeneous.

Along with the deep sequencing data, we also obtained formalin-fixed sections of a recently diagnosed MMB, which stained strongly with antibodies against myoglobin, Tnnt3, and SERCA1 – the same used on our mouse tumors (**Figure 4-2D**). In addition to an elongated

staining pattern associated with strap cells (top), there were many rounded myoblast-like cells that resembled those observed in the murine tumors (bottom). Together, these results indicate that *Ptch1*$^{+/-}$;*Pik3ca*^{H1047R} tumors model human MMB.

4.2.3 Muscle marker expression precedes and is independent of tumor formation

Having established a mouse model of MMB, we aimed to better dissect the role of *Pik3ca*^{H1047R} in driving the myogenic phenotype. Even though we spatially restricted the mutant p110α expression, we cannot exclude the possibility that these muscle-like cells arise from the stroma because tumors are complex, heterogeneous entities that include aberrant vascularization and infiltration of immune cells. Therefore, one important advantage of animal models, especially compared to human brain tumors, is the easy access to pre-neoplastic tissue. For instance, lineage-restricted expression of *Pik3ca*^{H1047R} drives cell fate changes in mammary tissue at early stages (Koren et al., 2015; Van Keymeulen et al., 2015), yet in this context unlike MB, it is also sufficient to induce tumors.

To test if myogenic marker expression occurs earlier than the advanced tumor stage in the mutant PI3K cerebellum, we immunolabeled preneoplastic lesions from P21 mice with myoglobin, Tnni3, Tnnt3, and SERCA1 antibodies (**Figure 4-3A**). Every *Ptch1*$^{+/-}$;*Pik3ca*^{H1047R} sample analyzed contained at least a few positive cells within the lesion; on the other hand, all but one of the *Ptch1*$^{+/-}$;*Pik3ca*^{WT} lesions were completely negative. At P7, a stage when GCPs are actively proliferating in the EGL of the cerebellum, the EGL of every *Ptch1*$^{+/-}$;*Pik3ca*^{H1047R} sample contained myoglobin-, Tnnt3-, and SERCA1-positive cells which were not found in any of the control cerebella (**Figure 4-3B**). Furthermore, the ability of mutant PI3K to induce myogenic marker expression does not require *Ptch1* heterozygosity because cells expressing

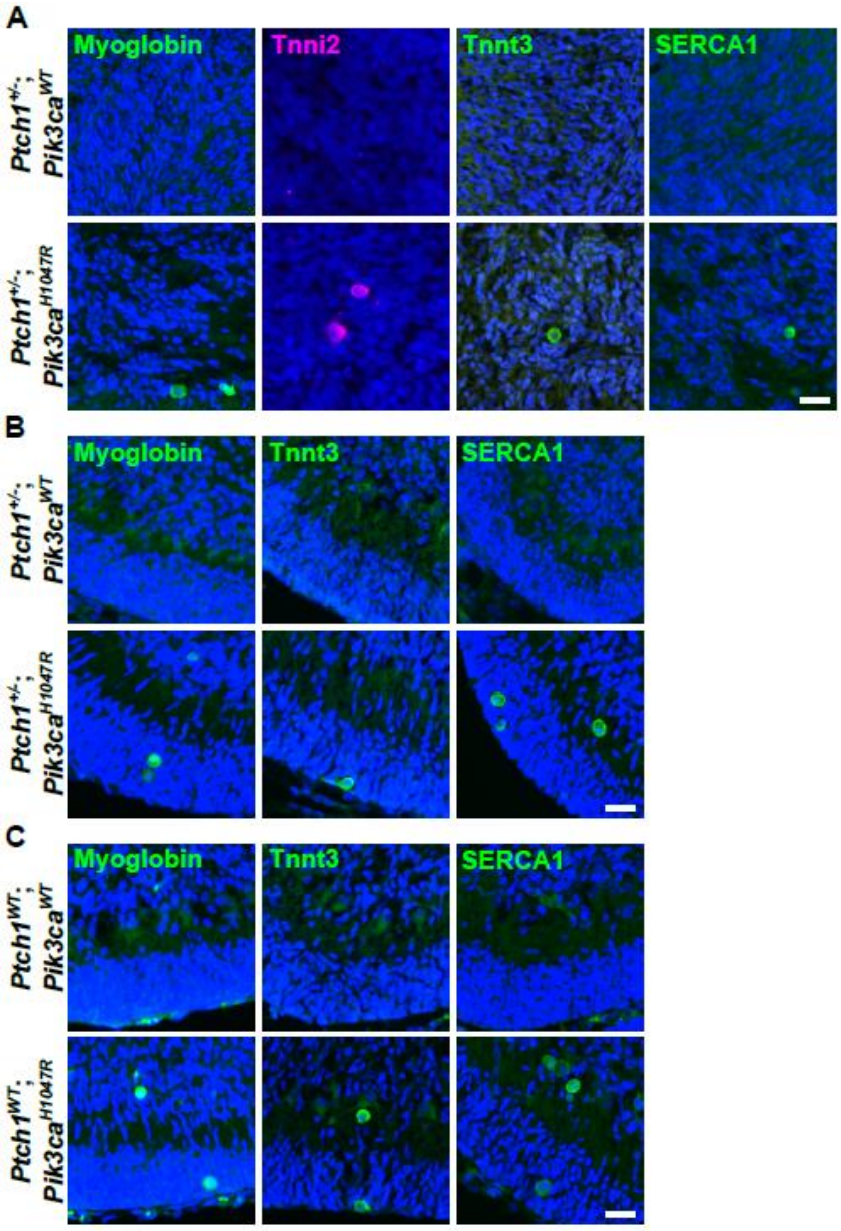

Figure 4-3. Myogenic cells in *Pik3ca^{H1047R}* cerebella appear prior to and independent of tumor formation

A) Example images of immunostainings on sections of *Ptch1$^{+/-}$;Pik3ca^{WT}* and *Ptch1$^{+/-}$;Pik3ca^{H1047R}* P21 preneoplasia with antibodies against myoglobin (n=5/4 animals per genotype), Tnni2 (n=2/4 animals per genotype), Tnnt3 (n=5 animals per genotype), or SERCA1 (n=5 animals per genotype). Counterstained with DAPI. Images cropped and adjusted for brightness/contrast. Scale bar: 25 µM.

B) Example images of immunostainings on sagittal sections of *Ptch1$^{+/-}$;Pik3ca^{WT}* and *Ptch1$^{+/}$;Pik3ca^{H1047R}* P7 cerebella with antibodies against myoglobin (n=4 animals per genotype), Tnnt3 (n=3 animals per genotype), or SERCA1 (n=3 animals per genotype). Counterstained with DAPI. Images cropped and adjusted for brightness/contrast. Scale bar: 25 µM.

C) Example images of Ptch1^{WT}*;Pik3ca^{WT}* and *Ptch1^{WT};Pik3ca^{H1047R}* P7 sagittal cerebella sections stained with antibodies against myoglobin (n=4/5 animals per genotype), Tnnt3 (n=3/4 animals per genotype), or SERCA1 (n=3/4 animals per genotype). Counterstained with DAPI. Images cropped and adjusted for brightness/contrast. Scale bar: 25 µM

myogenic markers were observed in the cerebellum of *Pik3ca*^{H1047R} mice that are wildtype for *Ptch1* (*Ptch1*^{WT}) (**Figure 4-3C**). This shows that constitutive activation of PI3K signaling can induce myocytic marker expression in a small population of Math1-derived GCPs of the EGL.

4.2.4 Ezh2 loss-of-function also produces a myogenic phenotype

Our data substantially support a model in which hyperactive PI3K signaling produces a myogenic phenotype; however, due to limited human data availability, we have not yet been able to identify a direct, statistically significant correlation between muscle gene expression and PIK3CA mutations in human MB (data not shown). Little is known about the mutational drivers of MMB, further constraining our ability to detect functionally similar alterations. Fortuitously, one of the human MMBs (GSM918618) was reported to contain a mutation in *ASXL3* (*Additional sex combs-like 3*) in an article about mutations of epigenetic regulators in pediatric cancer (Huether et al., 2014).

There are three ASXL proteins in mammals and, according to the epigenetic network generated by Huether *et al.*, ASXLs are transient components of PRC2, which acts as a transcriptional silencer through the deposition of di- and tri-methyl groups on H3K27 (Di Croce and Helin, 2013). However, the totality of ASXL molecular functions is controversial (Micol and Abdel-Wahab, 2016). In *Drosophila*, the orthologue Asx and its binding partner Calypso make up the polycomb repressive deubiquitinase (PR-DUB) complex, which hydrolyzes the mono-ubiquitin from H2AK118 (H2AK119 in mammals) to silence polycomb target genes (Scheuermann et al., 2010). Moreover, a screen for mutants with phenotypes referred to as 'polycomb syndrome' revealed both *Asx* and *Calypso* (Gaytán de Ayala Alonso et al., 2007). In humans, ASXL3 plays an important role in neurodevelopment as *ASXL3* mutations cause

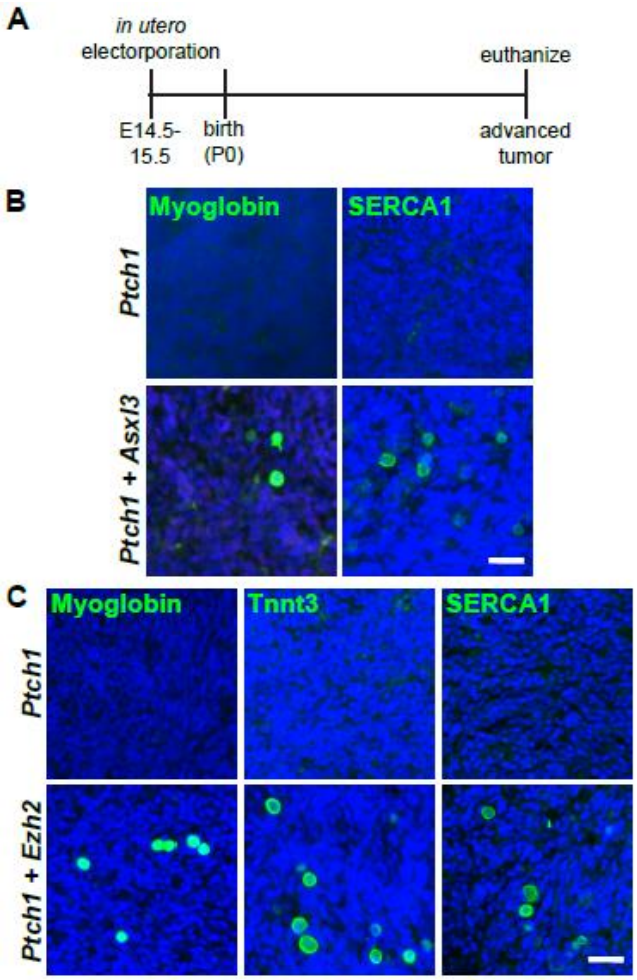

Figure 4-4. A subset of tumors express muscle markers following *in vivo* deletion of *Asxl3* or *Ezh2* with *Ptch1*

A) Schematic of the timeline for MB modeling via *in utero* electroporation of CRISPR constructs.

B) Example images showing myoglobin-positive or SERCA1-positive cells from 1 of the 5 *Ptch1+Asxl3* CRISPR tumors that were not found in *Ptch1* CRISPR tumors (n=5). Counterstained with DAPI. Images cropped and adjusted for brightness/contrast. Scale bar: 25 µM.

C) Example images of immunostaining with myoglobin, Tnnt3, or SERCA1 antibodies illustrates positive cells in *Ptch1+Ezh2* CRISPR tumors (n=2 of 6 animals) but not in the *Ptch1* CRISPR tumors (n=6). Counterstained with DAPI. Images cropped and adjusted for brightness/contrast. Scale bar: 25 µM.

Bainbridge Roper Syndrome (BRPS), which is characterized by microcephaly and/or cerebellar hypoplasia among other defects (Bainbridge et al., 2013; Srivastava et al., 2016), and deletion of *Asxl3* in *Xenopus* inhibits neuronal specification (Lichtig et al., 2020). Interestingly, loss of *Akt3* (the Akt isoform enriched in the brain) also causes a reduction in brain size in mice and humans (Easton et al., 2005; Gai et al., 2015; Tschopp et al., 2005).

The Q298H mutation identified in the human MMB sample is predicted to interfere with splicing, likely leading to truncation at exon 8 that is predicted to be deleterious to ASXL3 function (Huether et al., 2014). Given the high allelic frequency of the mutation and the paucity of copy number alterations in this tumor, we hypothesized that $ASXL3^{Q298H}$ could cause the muscle phenotype (Huether et al., 2014; Robinson et al., 2012). To assess the impact of Asxl3 loss-of-function, we performed *in utero* electroporation of the e14.5-e15.5 rhombic lip, a germinal center for the developing cerebellum, to achieve CRISPR-mediated deletion of *Ptch1* and *Asxl3* and mimic the effect of the human mutation although we targeted a different exon (**Figure 4-4A**). Of the five *Ptch1+Asxl3* tumors generated, one sample had myoglobin and SERCA1-positive cells while all five *Ptch1* control tumors were negative (**Figure 4-4B**).

Because of the functional connection between Asxl3 and PRC2 and because PI3K signaling has also been linked to post-translational modifications of H3K27 (both loss of tri-methylation and gain of acetylation), we were curious to know if depletion of $H3K27me^3$ in mouse MBs would affect myogenic gene expression (Badeaux and Shi, 2013; Cha et al., 2005; Huang and Chen, 2005). To do so, we chose to target Ezh2, the catalytic component of PRC2, by employing the same strategy outlined above (**Figure 4-4A**). Compared to zero of six *Ptch1* CRISPR control tumors, two of the six *Ptch1+Ezh2* CRISPR tumors exhibited labeling of muscle markers (**Figure 4-4C**).

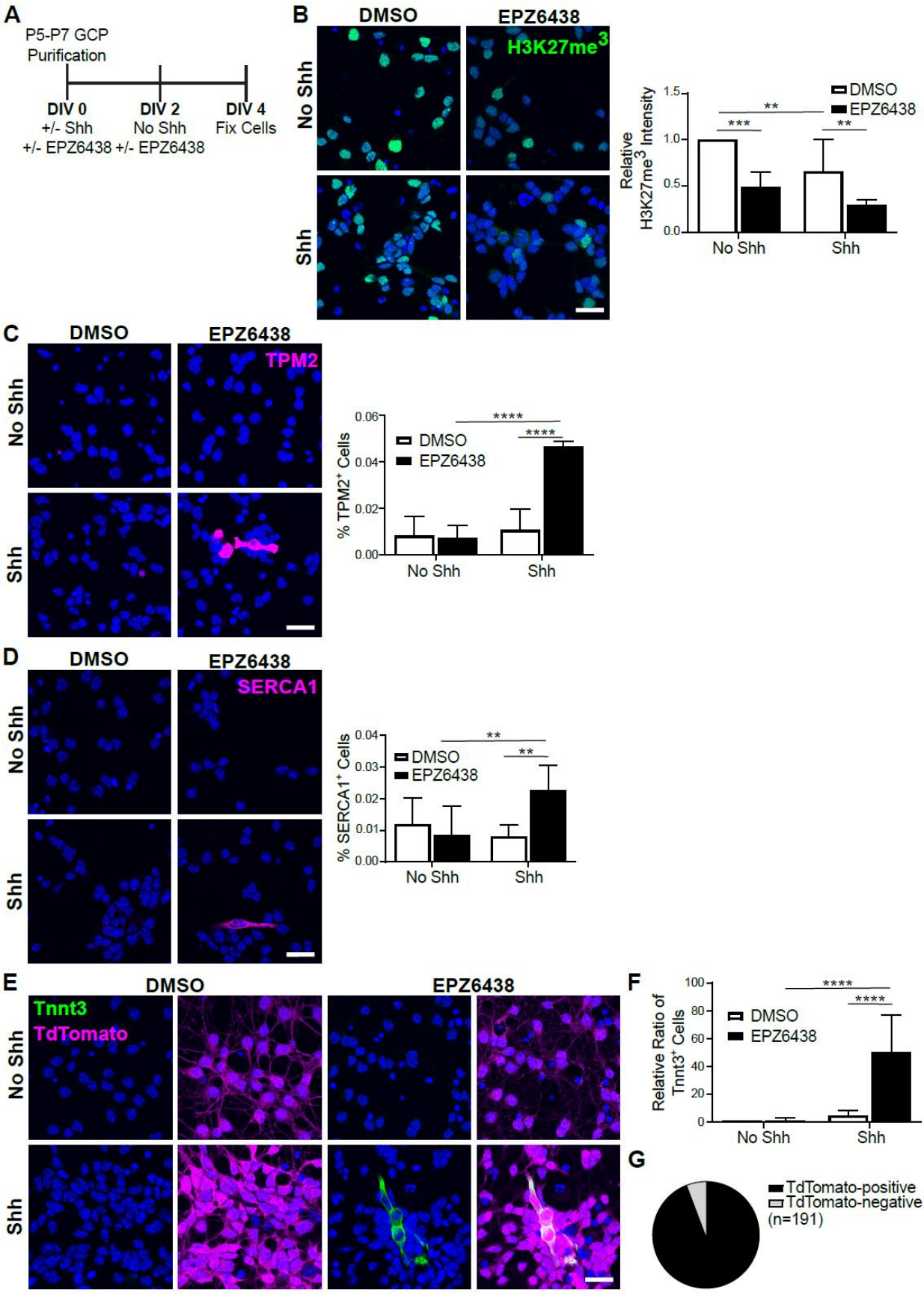
A
P5-P7 GCP Purification
DIV 0 +/- Shh +/- EPZ6438
DIV 2 No Shh +/- EPZ6438
DIV 4 Fix Cells
B
DMSO
EPZ6438
H3K27me3
No Shh
Shh
Relative H3K27me3 Intensity
DMSO
EPZ6438
C
TPM2
% TPM2+ Cells
D
SERCA1
% SERCA1+ Cells
E
Tnnt3
TdTomato
F
Relative Ratio of Tnnt3+ Cells
G
TdTomato-positive
TdTomato-negative
(n=191)

Figure 4-5. Ezh2 inhibition *in vitro* triggers expression of muscle markers in the presence of Shh and occurs in *Math1*-Cre;TdTomato-positive cells

A) Timeline outlining the treatment of purified GCPs with DMSO or 1 μM EPZ6438 +/- 10 nM Shh at DIV (Day *in vitro*) 0 and with either DMSO or 1 μM EPZ6438 at DIV2 before fixation in 4% PFA on DIV4.

B) Ezh2 inhibition reduces $H3K27me^3$ levels. Representative images of cells labeled with an $H3K27me^3$ antibody. Counterstained with DAPI. Images adjusted for brightness/contrast. Scale bar: 20 μM. Graph of relative $H3K27me^3$ mean intensity (normalized to DMSO, No Shh) from 3 independent experiments. Data presented as mean+95% confidence interval and analyzed using two-way ANOVA with Tukey's multiple comparisons (**, $p<0.005$; ***, $p<0.0005$).

C) TPM2 expression induced by co-administration of Ezh2 inhibitor and Shh. Example images illustrating the increase of TPM2-positive cells in GCP cultures treated with EPZ6438 and Shh. Counterstained with DAPI. Images adjusted for brightness/contrast. Scale bar: 20 μM. Graph of the percentage of TPM2-positive cells from 3 independent experiments. Data represented as mean+95% confidence interval and analyzed with two-way ANOVA and Tukey's multiple comparisons (**** $p<0.0001$).

D) SERCA1 expressed after Ezh2 inhibition in the presence of Shh. Example images illustrating the increase of SERCA1-positive cells in GCP cultures treated with EPZ6438 and Shh. Counterstained with DAPI. Images adjusted for brightness/contrast. Scale bar: 20 μM. Graph of the percentage of SERCA1-positive cells from 3 independent experiments. Data represented as mean+95% confidence interval and analyzed with two-way ANOVA and Tukey's multiple comparisons (** $p<0.005$).

E) Example images from *Math1*-Cre;TdTomato GCP cultures showing an increase of Tnnt3-positive cells that co-localize with TdTomato following treatment with 1 μM EPZ6438 and 10 nM Shh. Counterstained with DAPI. Images adjusted for brightness/contrast. Scale bar: 20 μM

F) Ezh2 blockade and Shh treatment trigger Tnnt3 expression. Graph of the relative ratio of Tnnt3-positive cells (normalized to DMSO, no Shh) from 3 independent experiments. Data presented as mean+95% confidence interval and analyzed with two-way ANOVA and Tukey's multiple comparisons (**** $p<0.0001$).

G) Tnnt3 expression occurs in GCPs. Pie chart showing the relative number of Tnnt3-positive cells from the Shh, EPZ6438 condition that are either positive or negative for TdTomato expression (n=191 cells from 3 independent experiments).

Given the stronger phenotype of those two *Ptch1+Ezh2* CRISPR tumors relative to the *Ptch1+Asxl3* sample, we wanted to extend our search into the role of Ezh2 in muscle-related gene expression by testing whether Ezh2 inhibition could generate myogenic cells in wildtype GCPs. Therefore, we treated purified GCPs for several days with either DMSO or 1 μM EPZ6438 – an efficient Ezh2 inhibitor that competitively interferes with the binding of the co-factor S-adenosylmethionine (SAM) – in the presence or absence of the potent mitogen Shh (10 nM) (**Figure 4-5A**) (Kim and Roberts, 2016). Not only was H3K27me^3 greatly reduced in EPZ6438-treated cells both with and without Shh, but Shh stimulation also significantly reduced H3K27me^3 levels on its own (**Figures 4-5B**). Nevertheless, only cultures exposed to both EPZ6438 and Shh significantly generated myogenic cells, as measured by tropomyosin 2 (TPM2), SERCA1, and Tnnt3 expression (**Figures 4-5C-F**).

While passing dissociated cerebellar cells through a sucrose gradient yields cultures that are mostly GCPs, rare interneurons, astrocytes, and oligodendrocytes are also present (Wechsler-Reya and Scott, 1999). Because the percentage of cells that express muscle markers is low, we wanted to confirm that GCPs, which express Math1, were the cells responsible for the observed phenotype. Accordingly, we performed Tnnt3 immunolabeling on cultures obtained from *Math1*-Cre;TdTomato mice and found that about 94% of Tnnt3-positive cells also expressed TdTomato (**Figure 4-5E**,**G**). Together, the *in vivo* and *in vitro* data indicate that Ezh2 loss-of-function can drive a myogenic phenotype in a small fraction of cells, and like constitutive activation of PI3K, Math1-expressing GCPs are the cell-of-origin.

4.2.5 MyoD transcriptional activation, not expression, likely underlies muscle gene expression in GCPs

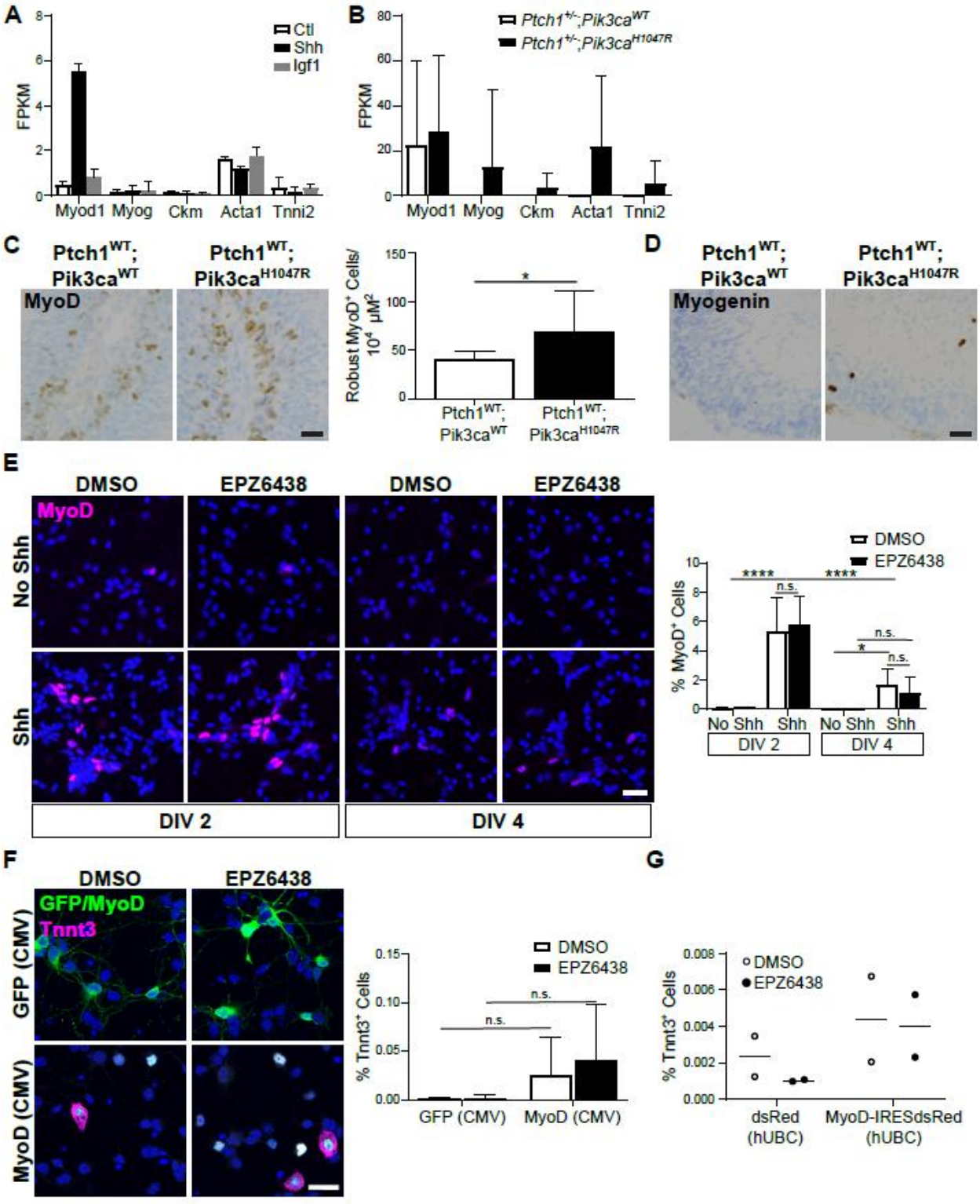

Figure 4-6. MyoD expression is not the rate-limiting step underlying the myogenic phenotype induced by either PI3K activation or Ezh2 inhibition

A) Enhanced *Myod1* expression after Shh stimulation without change to target expression. Graph of *Myod1*, *Myog*, *Ckm*, *Acta1*, and *Tnni2* expression (FPKM) from RNA sequencing of

dissociated GCP cultured in the absence or presence of either Shh or Igf1 for 24 hours. Data obtained from GSE147410 (Tamayo-Orrego et al., 2020).
B) Elevated expression of MyoD transcriptional targets but not *Myod1* in PI3K mutant tumors. Graph of *Myod1*, *Myog*, *Ckm*, *Acta1*, and *Tnni2* expression (FPKM) from RNA sequencing of *Ptch1*$^{+/-}$;*Pik3ca*^{WT} and *Ptch1*$^{+/-}$;*Pik3ca*^{H1047R} tumors. Data from **Figure 4-1D**.
C) Increase in highly expressing MyoD GCPs in PI3K mutant cerebella. Representative images of anti-MyoD immunohistochemistry on Ptch1^{WT};*Pik3ca*^{WT} and *Ptch1*^{WT};*Pik3ca*^{H1047R} P7 sagittal cerebella sections. Counterstained with Nissl. Scale bar: 50 µM. Graph of the number of robust MyoD-positive cells per 10,000 uM^2 (n=3 animals per genotype). Data represented as mean+95% confidence interval and analyzed with an unpaired t-test (*p<0.05).
D) Example images demonstrating the presence of myogenin-positve cells in *Ptch1*^{WT};*Pik3ca*^{H1047R} but not Ptch1^{WT};*Pik3ca*^{WT} P7 sagittal cerebella sections (n=3 animals per genotype). Counterstained with Nissl. Images cropped. Scale bar: 50 µM.
E) Shh but not Ezh2i stimulates MyoD expression in GCPs. Representative images from DIV2 and DIV4 GCP cultures treated with either DMSO or 1 µM EPZ6438 +/- 10 nM Shh and immunostained with a MyoD antibody (n=3 independent experiments). Counterstained with DAPI. Images cropped and adjusted for brightness/contrast. Scale bar: 25 µM. Graph of the percentage of MyoD-positive cells from 3 independent experiments. Data presented at mean+95% confidence interval and analyzed with two-way ANOVA and Tukey's multiple comparisons (* p<0.05, **** p<0.0001, n.s.- not significant).
F) No significant change to Tnnt3-positive cells induced by (CMV) MyoD with or without Ezh2i. Example images illustrating Tnnt3-positive cells from (CMV) MyoD-transduced GCP cultures treated with DMSO or 1 µM EPZ6438 but not control cultures. Cultures were immunostained with antibodies against either GFP or MyoD to label infected cells and Tnnt3. Counterstained with DAPI. Images adjusted for brightness/contrast. Scale bar: 20 µM. Graph of the percentage of Tnnt3-positive cells from 3 independent experiments. Data represented as mean+95% confidence interval and analyzed with two-way ANOVA and Tukey's multiple comparisons (n.s.- not significant).
G) (hUBC) MyoD-IRESdsRed has no effect on Tnnt3 expression. Graph of the percentage of Tnnt3-positive cells following (hUBC) dsRed or (hUBC) MyoD-IRESdsRed transduction of GCPs and treatment with DMSO or 1 µM EPZ6438. Dots represent an independent experiment and line indicates mean.

How does a neuronal progenitor express muscle-related genes? Normal myoblast specification and differentiation is controlled by the myogenic regulatory factors (MRF) MyoD, Myf5 (Myogenic factor 5), MRF4, and myogenin (Berkes and Tapscott, 2005). Tellingly, MyoD is expressed in a subset of GCPs within the outer EGL, a region of active proliferation, during normal cerebellar development (Dey et al., 2013). The location of the MyoD-positive GCPs pointed to a relationship with proliferation, which can be induced *in vitro* with either Shh or IGF1, so we probed the expression profile of GCPs stimulated with each mitogen (GSE147410) (Tamayo-Orrego et al., 2020). Shh but not IGF1 triggers transcription of *Myod1* (|log2-fold change| ≥ 1, FDR < 0.05) (**Figure 4-6A**). In line with this data, previous studies have shown that Gli2 can bind to and activate the *Myod1* promoter and also that MyoD, present in a population of Shh-MB tumor cells, is associated with Smo-inhibitor resistance (Ocasio et al., 2019; Voronova et al., 2013). Neither Shh nor IGF1 led to increased expression of the MyoD transcriptional targets *myogenin* (*Myog*), *creatine muscle kinase* (*Ckm*), *skeletal muscle α-actin* (*Acta1*), or *Tnni2* when compared to control cultures (**Figure 6-A**) (Bergstrom et al., 2002; Blais et al., 2005).

In contrast to the *in vitro* expression patterns, **Figure 4-6B** illustrates that $Ptch1^{+/-}$;$Pik3ca^{H1047R}$ tumors display elevated, though variable, expression (|log2-fold change| ≥ 1, FDR < 0.05) of MyoD targets but not *Myod1* itself, which is expressed in all tumors. Because neither IGF1-treated GCPs nor activated PI3K tumors showed enhanced *Myod1* levels, we were surprised to find that there were more MyoD-positive GCPs at P7 in the EGL of $Pik3ca^{H1047R}$ ($Ptch1^{WT}$) mice compared to $Pik3ca^{WT}$ (**Figure 4-6C**). Again, MyoD is present in both genotypes while Myogenin – a MyoD transcriptional target that is necessary for terminal myoblast

differentiation – is exclusively expressed in mutant cerebella (**Figure 4-6C, D**) (Berkes and Tapscott, 2005).

Because H3K27me^3 is found at the *Myod1* locus of both the embryonic and early postnatal cerebellum, we wanted to test whether EPZ6438 could further modulate MyoD expression in the presence of Shh (Feng et al., 2016; Pal et al., 2011). As expected, Shh greatly increased the number of MyoD-expressing cells at DIV2, an effect that was transient because removal of Shh from the media led to fewer MyoD-positive cells at DIV4 (**Figure 4-6E**). Ezh2 inhibition, however, did not change the percentage of MyoD-expressing cells either with or without Shh.

Administration of EPZ6438 only generates a myogenic phenotype in the presence of Shh, which made us wonder if the role of Shh was to provide a source of MyoD. If so, then ectopic expression of MyoD could replace Shh and induce muscle marker expression when Ezh2 is inhibited. Using two different MyoD lentiviral constructs, we transduced GCPs and cultured them in the presence of DMSO or EPZ648 for 4 days. In both sets of experiments, Ezh2 inhibition failed to significantly induce Tnnt3 expression compared to DMSO (**Figure 4-6F, G**). The CMV-MyoD construct alone had a variable though insignificant effect on Tnnt3 expression. Collectively, the above data show that Shh drives endogenous MyoD, which can be augmented by *Pik3ca*^{H1047R} but not EPZ6438. Moreover, physiological levels of MyoD do not trigger myogenesis in GCPs, implying that activation of MyoD-dependent transcription rather than protein overexpression underlies muscle gene expression when *Pik3ca* is mutated or Ezh2 activity is blocked.

4.2.6 Muscle marker positive cells maintain MyoD expression but lose Pax6

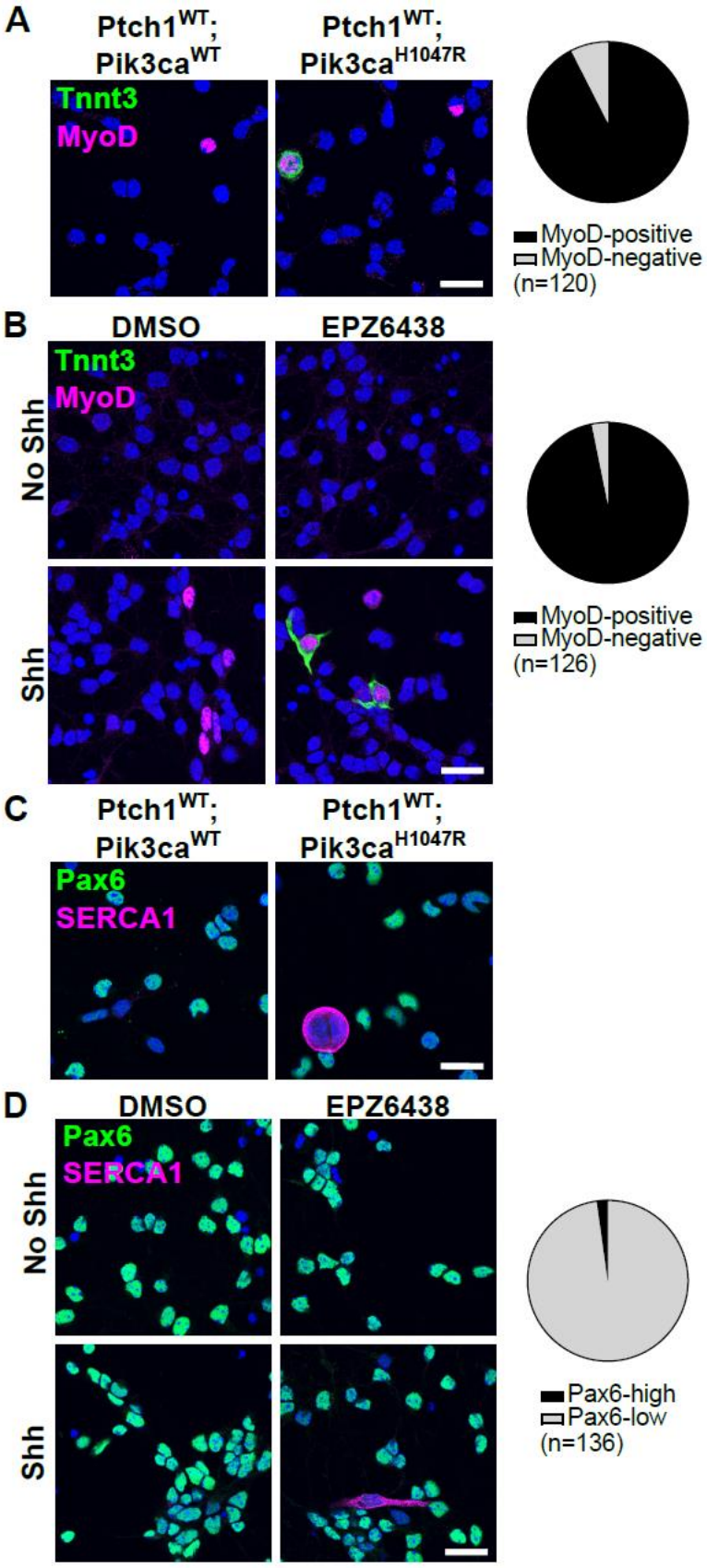

Figure 4-7. Myogenic cells express MyoD but not Pax6

A) *Pik3ca*^{H1047R} myogenic cells co-express Tnnt3 and MyoD. Example images of *Ptch1*^{WT}*;Pik3ca*^{WT} and *Ptch1*^{WT}*;Pik3ca*^{H1047R} purified P7 GCP cultures sequentially stained with antibodies against MyoD then Tnnt3. Counterstained with DAPI. Images adjusted for brightness/contrast. Scale bar: 20 µM. Pie chart showing the relative number of Tnnt3-positive cells from *Ptch1*^{WT}*;Pik3ca*^{H1047R} cultures that are either positive or negative for MyoD expression (n=120 cells from 3 independent experiments).

B) Tnnt3-expressing cells following Ezh2 inhibition and Shh administration co-label with MyoD. Example images of purified GCP cultures treated with DMSO or 1 µM EPZ6438 +/- 10 nM Shh and sequentially labeled with antibodies against MyoD then Tnnt3. Counterstained with DAPI. Images adjusted for brightness/contrast. Scale bar: 20µM. Pie chart showing the relative number of Tnnt3-positive cells from the Shh, EPZ6438 condition that are either positive or negative for MyoD expression (n=126 cells from 3 independent experiments).

C) SERCA1-positive cells from *Ptch1*^{WT}*;Pik3ca*^{H1047R} mice are negative for Pax6. Example images of *Ptch1*^{WT}*;Pik3ca*^{WT} and *Ptch1*^{WT}*;Pik3ca*^{H1047R} P7 purified GCP cultures co-stained with antibodies against Pax6 and SERCA1(n=4 independent experiments). Of 154 SERCA1-

positive cells imaged, 0 cells also expressed Pax6. Counterstained with DAPI. Images cropped and adjusted for brightness/contrast. Scale bar: 20 µM.
D) SERCA1 expression associated with loss of Pax6. Example images from **Figure 4-5D** with Pax6 labeling to illustrate that SERCA1-positive cells express low or no Pax6 after treatment with 1 µM EPZ6438 and 10 nM Shh. Counterstained with DAPI. Images adjusted for brightness/contrast. Scale bar: 20 µM. Pie chart showing the relative number of SERCA1-positive cells from the Shh, EPZ6438 condition that are either highly or lowly express Pax6 (n=136 cells from 3 independent experiments).

Thus far we have shown that both experimental strategies upregulate muscle markers in Math1-derived GCPs, a subset of which express MyoD as a consequence of Shh-dependent proliferation. To confirm that it is this MyoD-positive population that expresses muscle markers, we purified P7 *Ptch1*^{WT}*;Pik3ca*^{WT} and *Ptch1*^{WT}*;Pik3ca*^{H1047R} GCPs and sequentially labeled cells with antibodies against MyoD and then against Tnnt3 where we observed many double-positive cells in *Ptch1*^{WT}*;Pik3ca*^{H1047R} cultures (**Figure 4-7A**). In fact, 92.5% (111/120) of all Tnnt3-positive cells also expressed MyoD. Likewise, 96.8% (122/126) of Tnnt3-positive cells were also MyoD-positive following combined administration of Shh and EPZ6438, demonstrating that MyoD expression is sustained (**Figure 4-7B**).

This data, however, does not indicate whether upregulation of a myogenic transcriptional program in GCPs is accompanied by loss of neuronal identity or whether it is simply misexpression of muscle genes. To examine these possibilities, we co-labeled dissociated cells with antibodies against the myogenic marker SERCA1 and the transcription factor Pax6, which is expressed in proliferating GCPs, post-mitotic granule neurons, and Shh-MBs (Yamasaki et al., 2001; Zhang et al., 2019). Although most of the dissociated cells expressed Pax6 in all conditions, 100% of the 154 SERCA1-positive cells from *Pik3ca* mutant cerebella did not (**Figure 4-7C**). Similarly, 97.8% (133/136) of the SERCA1-positive cells – arising subsequent to EPZ6438 and Shh treatment in **Figure 4-5D** – expressed low levels of (if any) Pax6 (**Figure 4-7D**). These results provide further evidence that these myogenic cells originate from MyoD-expressing GCPs and suggest that induction of muscle genes signifies a change of cell fate.

4.3 Discussion

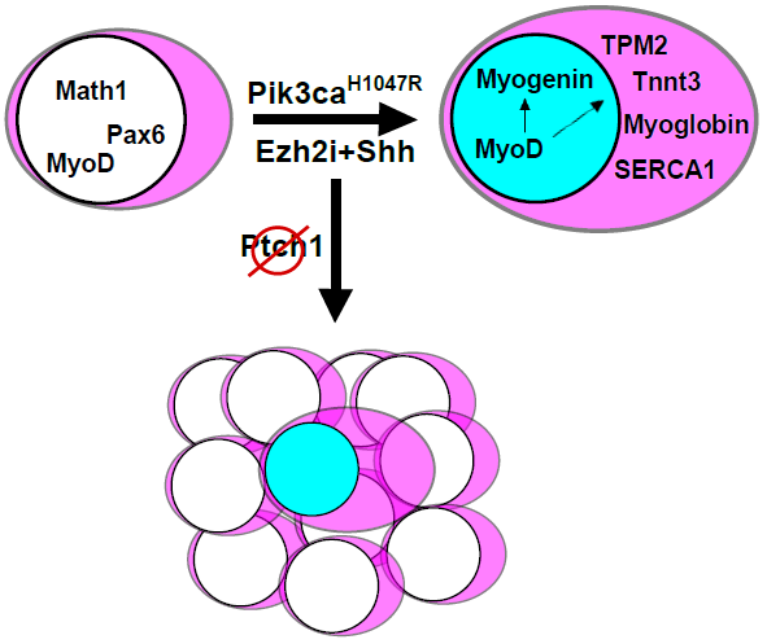

Figure 4-8. A myogenic conversion model
Schematic illustrating the fate switch activated by either *Pik3ca*^{H1047R} or Ezh2 inhibition (Ezh2i) plus Shh stimulation that is associated with loss of GCP factors like Math1 and Pax6, persistence of MyoD, and gain of muscle markers. This process can occur independently or in conjunction with tumor formation through loss of *Ptch1*.

Aberrant activation of PI3K signaling is known to be oncogenic in many cancers, and frequently occurs via *PIK3CA* mutations, the most common of which is the H1047R substitution. Though more rare compared to adult malignancies, recurrent *PIK3CA* mutations have been identified in medulloblastoma and are specifically enriched in the SHH subgroup (Gröbner et al., 2018; Kool et al., 2014; Niesen et al., 2020; Northcott et al., 2017); therefore, it was fitting to find the spontaneous Pik3ca^{H1047R} mutation in the *Ptch1*$^{+/-}$ tumor and to observe its pro-tumorigenic effect when combined with a Shh-MB model. On the other hand, the elevated expression of genes associated with muscle identity and function was entirely unexpected. Notably, these changes in mRNA and protein expression overlap with those displayed in human MMB. Constitutive activation of PI3K was sufficient to produce myogenic cells in the EGL of mice even when *Ptch1* was wildtype, and we could achieve a similar phenotype by *in vivo* deletion or *in vitro* inhibition of Ezh2 within murine tumors and wildtype GCPs, respectively. While MyoD is present in the normal EGL, its transcriptional targets are not, yet manipulation of either PI3K or Ezh2 activity results in expression of muscle markers that co-localize with MyoD but not Pax6 – a transcription factor expressed by the granule neuron lineage. Overall, we propose a model where GCPs that express Math1, Pax6, and MyoD switch their fates by concurrently activating a myogenic program and losing their neuronal identity as a consequence of either the p110α H1047R mutation or Ezh2 loss-of-function – an effect that occurs in either the normal or malignant cerebellum (**Figure 4-8**).

4.3.1 *Ptch1*$^{+/-}$;*Pik3ca*^{H1047R}, a genetically engineered mouse model of MMB

Nearly a century after it was first identified, MMB is still poorly understood. Not only have the scarcity of human MMBs hindered advances in knowledge, but animal models have

also been limiting. To date, two MMB-like tumors have been defined based on immunohistochemistry after transplacental injection of the mutagen N-ethyl-N-nitrosourea (ENU) in *cerebellar vermis defect* rats, whose cerebellar malformations are probably due to a truncating mutation in the netrin receptor *Unc5h3* (Kuramoto et al., 2004; Kuwamura et al., 2000). Another model was generated by xenograft implantation of *Otx2*-depleted D425 cells, a G3-MB cell line, into the forebrain of nude mice (Bai et al., 2012).

Here, we describe the first transgenic mouse model of MMB, which distinguishes itself because myogenic cells are present in every tumor that we tested without relying on a transformed cell line. Like the other examples described above, the number of myocytic cells are only a small subset of the total tumor population, yet we were able to very clearly detect transcriptional changes from bulk sequencing in both the spontaneous and genetically engineered PI3K mutant tumors, and this significantly altered the gene expression profiles of $Ptch1^{+/-}$;$Pik3ca^{H1047R}$ tumors. Multiple factors may account for this effect. For example, the transcript levels of muscle-related genes within a positive cell are probably high given how bright the staining is by immunofluorescence, and the signal-to-noise ratio is very high because these genes are not expressed at all in control tumors. Establishing the $Ptch1^{+/-}$;$Pik3ca^{H1047R}$ line as a novel mouse model of MMB is an important advancement not only for the work presented in this thesis but also for ongoing and future studies of the molecular mechanisms underlying the myogenic switch of neuronal progenitors.

PI3K signaling has been implicated in every MB subgroup. In addition to mutations and copy number alterations, PI3K pathway components have been identified by gene ontology assessment of both transcriptional profiles and DNA methylation patterns in human MBs (Kool et al., 2014; Northcott et al., 2017; Pei et al., 2012; Schwalbe et al., 2017), and the PI3K cascade

has been revealed using proteomics (Archer et al., 2018; Forget et al., 2018). Consequently, PI3K pathway inhibitors have been suggested as therapeutic agents in MB (Gröbner et al., 2018), and PI3K inhibitors have been applied in animal models either alone or with other drugs (Metcalfe et al., 2013; Pei et al., 2016; Pei et al., 2012). Furthermore, a phase II clinical trial is currently underway to test the inhibitor LY3023414 on PI3K pathway mutant tumors from pediatric patients, including those with MB (NCT03213678).

All of this begs the question, "does aberrant activation of PI3K upregulate myogenic markers in human MB?" We are currently pursuing this question although we have yet to find a strong correlation between mutations and gene expression. Multiple factors, such as the timing of the mutation and the cell-type where it occurs, could explain the apparent discord between the mouse and human data. The intensity of pathway activation may be a key determinant as the H1047R mutation is strongly activating. Our model is produced by knocking the mutant *Pik3ca* into the *Rosa26* locus of inbred mice (Adams et al., 2011), so the observed transcriptional phenotype may be enhanced both by the constitutive activation of *Pik3ca* and by a reduction in differences caused by inter-patient heterogeneity. The transgene cannot itself explain the discrepancies because the spontaneous $Pik3ca^{H1047R}$ sample also exhibited a myogenic phenotype. Because the number of myogenic cells is low, bulk sequencing of a portion of the tumor may not be sensitive enough to detect their presence; even in the transgenic mice, two of the samples showed weak transcriptional changes, thus contributing to the variability of MyoD target expression observed **in Figure 4-6B**. Nonetheless, I could identify positive cells by immunofluorescence. Hence, it will be worth screening *PIK3CA* mutant tumors with a panel of muscle markers to determine if there are rare myogenic cells in human samples.

4.3.2 ASXL3 and EZH2 in MB and MMB

When case reports ventured into the cytogenetic alterations of MMB, they mostly focused on changes commonly found in MB like i17q and MYC amplifications (Helton et al., 2004; Wright et al., 2012). Missing from the literature is either a search for potential MMB-specific mutations or inquiry into the role of MB drivers in the myogenic phenotype. Owing to the consistent tumor sample nomenclature adopted by St. Jude's researchers, we were able to connect one of the human MMBs with its *ASXL3* mutation (Huether et al., 2014; Robinson et al., 2012). Mutations in *ASXL*s have been uncovered in MB at low frequency (Gröbner et al., 2018; Huether et al., 2014; Northcott et al., 2017; Zhang et al., 2015), but the function of ASXLs in the normal cerebellum or MB tumorigenesis has never been addressed.

ASXL, most commonly *ASXL1*, mutations have been described in multiple cancers (Micol and Abdel-Wahab, 2016), and germline mutations in *ASXL1* are associated with Bohring-Opritz Syndrome, which phenotypically overlaps with BRPS (Bainbridge et al., 2013). Regardless of disease type or ASXL member, these mutations, which exist as either nonsense or frameshift, generate truncated transcripts and occur almost exclusively in exons 11 and 12 (Micol and Abdel-Wahab, 2016). Some studies suggest that these transcripts were either loss-of-function or triggered RNA degradation (Abdel-Wahab et al., 2012; Matheus et al., 2019; Srivastava et al., 2016), yet other groups have suggested that these may lead to gain-of-function (Balasubramani et al., 2015; Yang et al., 2018). Reports have also claimed a link between Asxl1 and PI3K/Akt signaling, but again one proposes a positive relationship where Asxl1 interacts with and is important for the activity of Akt while the other supports an inverse connection via regulation of *Pten* expression, which is reduced when *Asxl1* is deleted (Cao et al., 2020; Youn et al., 2017).

The MMB *ASXL3* mutation is striking because it is predicted to cause a truncation at exon 8, which is located within the conserved ASXH domain (Micol and Abdel-Wahab, 2016). This more strongly indicates loss-of-function as the ASXH domain is necessary for interaction with Brca1-associated protein 1 (BAP1), the mammalian orthologue of Calypso (Scheuermann et al., 2010). In fact, our collaborator has demonstrated that the truncated ASXL3 protein cannot interact with BAP1 and thus impedes BAP1 function (data not shown). Through CRISPR targeted deletion of *Asxl3* and *Ptch1*, one tumor did exhibit muscle marker expression, but more experimental evidence is needed before drawing strong conclusions.

We chose, however, to pursue Ezh2 loss-of-function to modulate H3K27me^3 because this posed a potential link between Asxl3 and PI3K function, because the *in vivo* CRISPR deletion of *Ezh2* appear to induce a more robust myogenic phenotype, and because the tools needed were easily accessed and well-established. The function of Ezh2 in cancer is context dependent as it can act as either an oncogene or a tumor suppressor (Kim and Roberts, 2016), and though current evidence implicates Ezh2 activity in MB, its role is still unclear. For instance, human data indicate that a subset of G3- and G4-MBs contain chromosome 7(q) amplifications correlating with increased *EZH2* expression and H3K27me^3, suggesting that EZH2 is oncogenic (Alimova et al., 2012; Dubuc et al., 2013; Robinson et al., 2012). Supporting this, Ezh2 inhibition reduced cell viability in either D425 cells or in human cerebellar organoids overexpressing Otx2 and Myc (Ballabio et al., 2020; Natsumeda et al., 2019). Also, xenograft transplantation of an immortalized NSC cell line overexpressing Ezh2 and Myc was pro-tumorigenic (Sola, 2019); on the other hand, deleting *Ezh2* in a Myc-p53 G3-MB mouse model also led to more rapid tumor formation, suggestive of a tumor suppressive role (Vo et al., 2017). Although *EZH2* expression itself has not been associated with human SHH-MB, Ezh2 inhibition blocked the growth of

DAOY cells, an SHH-MB line (Alimova et al., 2012). It also reduced proliferation and increased differentiation of *Ptch1*$^{+/-}$ tumor cells *in vitro* and *in vivo* (Cheng et al., 2020). Conditional expression – using the *Nestin*-cre – of H3K27M, a methylation-resistant and dominant mutant, with *p53* deletion strongly favors development of Shh-MBs in mice (Larson et al., 2019; Roussel and Stripay, 2020), yet orthotopic transplantation of H3K27M-transduced *p53*$^{-/-}$ NSCs did not yield tumors (Mohammad et al., 2017).

Along with resolving the impact of Ezh2 activity on MB, future work is needed to assess its influence in human MMB. Based on our work, repressing Ezh2 or reducing H3K27me^3 could contribute to myogenic differentiation within SHH-MBs, such as the two SHH-MB cases reported in the literature (Rao et al., 2020; Wright et al., 2012). It is uncertain whether the same mechanism would apply to other subgroups, which could explain why the *Ezh2* knock-out G3-MB model does not display changes in muscle gene expression compared to control (data not shown) (Vo et al., 2017).

Cumulatively, one notion to draw from the above is the putative significance of Polycomb group proteins in MMB; an idea that could more broadly apply to chromatin regulators and is particularly enticing because muscle-like cells are not the only non-neural lineage observed in rare MB variants. Not only has melanotic differentiation been described in the literature, but there are quite a few examples of MBs that contain both myogenic and melanotic cells hinting at a molecular environment permissive to cell identity alterations (Rajeshwari et al., 2016; Sachdeva et al., 2008; Stefanits et al., 2014). An interesting question to examine in the future is whether modulating PI3K or Ezh2 activity also leads to rare subsets of other cell types.

It is this concept of a permissive chromatin landscape that partly frames our suspicion that altering PI3K or Ezh2 activity stimulates the myogenic conversion of GCPs through an overlapping mechanism by regulating histone post-translational modifications. PI3K could act by obstructing Ezh2 activity through Akt-dependent phosphorylation of serine 21, thereby diminishing H3K27me^3 (Cha et al., 2005). I was not able to detect global changes in H3K27me^3 in *Pik3ca*^{H1047R} GCPs compared to controls (data not shown), yet it is possible that changes are loci-specific rather than global and would require more sensitive methods to find. Also, we cannot exclude the inverse relationship because impeding H3K27me3 via the K27M mutation in NSCs or *Ezh2* deletion in NSC-derived MB tumors elevates *Igf2bp2* (IGF2 binding protein 2), which encodes the RNA-binding protein IMP2 and is known to activate PI3K signaling in other cancer models (Larson et al., 2019; Mu et al., 2015; Vo et al., 2017; Xu et al., 2019).

Even if PI3K and Ezh2 do not act in the same pathway, they could regulate a common target, such as the acetylation of H3K27. The H3K27M substitution blocks the regionally broad spread of H3K27me^3 leading to deviant acetylation (Harutyunyan et al., 2019; Krug et al., 2019), and in neuroblastoma cell lines, PI3K signaling triggered drug resistance by activating super enhancers, as measured by H3K27 acetylation (Iniguez et al., 2018). The histone acetyltransferase p300 is another known Akt target (Huang and Chen, 2005); as a result, impeding PI3K signaling in myoblasts *in vitro* decreases phosphorylation of p300, which leads to reduced H3 acetylation at MyoD transcriptional targets without changing global levels (Serra et al., 2007). Future work aimed at elucidating the specific cascade(s) downstream of PI3K or Ezh2 responsible for muscle gene expression may support or negate these possibilities.

4.3.3 Regulation of MyoD activity

We predict from our working model that PI3K and Ezh2 signaling coalesce at some point to activate MyoD-dependent transcription. MyoD is a member of the basic helix-loop-helix (bHLH) superfamily of transcription factors, like Math1 and NeuroD, and it promotes transcription by binding to the DNA consensus sequence CANNTG, known as E-boxes (Tapscott, 2005). Due to the large number of bHLH factors and the prevalence of E-boxes in the genome, there are many questions surrounding activity regulation within the cell. One determinant of MyoD specificity as an MRF is its preferential binding to particular E-box sequences, of which CAGGTG is primarily associated with myogenic genes (Cao et al., 2010; Fong et al., 2012). In fact, mutating MyoD to change its sequence binding affinity can transform it into a neurogenic factor like NeuroD2 (Fong et al., 2015).

Another straightforward way to limit MyoD activity is through spatially and temporally restricted expression. MyoD, the original reprogramming factor, was first discovered because aberrant expression by chemically induced DNA demethylation or transfection of C3H10 T1/2 fibroblasts triggered myogenesis (Davis et al., 1987; Lassar, 2017; Lassar et al., 1986; Taylor and Jones, 1979). Even postnatal satellite cells repress MyoD expression in the resting state (Lassar, 2017). However, GCPs and MB cells are a glaring exception to this principle as they endogenously express MyoD but not its transcriptional targets *in vivo* (Dey et al., 2013; Ocasio et al., 2019). Viral mediated overexpression of MyoD in DAOY cells but not in UW228 cells, another SHH-MB cell line, has been shown to induce myogenesis (Gerber and Tapscott, 1996), and the effect we observed in primary GCPs was highly variable and therefore not statistically significant. Overall, this suggests that naïve and even some transformed GCPs are resistant to MyoD reprogramming.

Control of DNA binding is also an important step in MyoD transcriptional activation, but it is not necessarily the rate-limiting step. ChIP- and RNA-sequencing data show that many of the genes upregulated in myotubes display increased MyoD-binding during differentiation, yet MyoD binds tens of thousands of loci without changing levels of transcription (Cao et al., 2010). Moreover, interfering with p38 MAPK activity *in vitro* does not alter MyoD binding at either the *Myogenin* promoter or *Ckm* enhancer but does delay and reduce recruitment of the SWI/SNF complex, thereby blocking transcription of targets and myoblast differentiation (Serra et al., 2007). In cell types, such as P19 cells, that are resistant to MyoD reprogramming, DNA accessibility is a major impediment for MyoD binding at its myogenic targets (Fong et al., 2012). Even though the *Pik3ca*^{H1047R} mutation and EPZ6438-treatment are applied broadly to GCPs, only rare cells express muscle-related markers, which suggests that the chromatin of muscle-specific genes is likely in a closed confirmation and that neither condition efficiently triggers remodeling.

Both Ezh2 and PI3K signaling are involved in regulating normal myogenesis, so it is probable that Ezh2 inhibition or *Pik3ca*^{H1047R} affect one or more of these factors to promote muscle-specific gene expression in GCPs. For example, ectopic expression of HLH-1, the MyoD orthologue in *C. Elegans*, induces myogenic conversion in the undifferentiated blastomere, an effect that is limited by subsequent lineage specification (Fukushige and Krause, 2005). Knock-down of PRC2 components including the Ezh2 orthologue, *mes-2*, can overcome these limitations (Patel et al., 2012; Yuzyuk et al., 2009). In C2C12 cells, a discrete set of genes with higher expression in myotubes show a corresponding loss of H3K27me^3, including *Myogenin* and *Acta1* (Asp et al., 2011). Depletion of the PRC2 component *Suz12*, which reduced the levels of H3K27me^3 at these genes in myoblasts, did not trigger differentiation itself but did

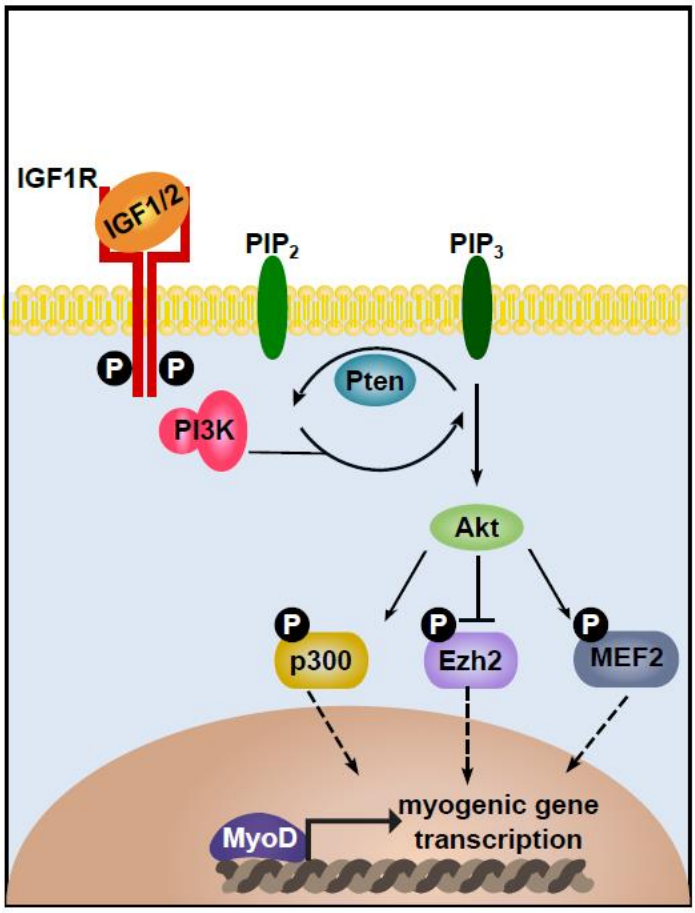

Figure 4-9. PI3K signaling and myogenic gene expression
Model highlighting the potential mediators of PI3K-dependent myogenic conversion. Inhibition of Ezh2, resulting from phosphorylation by Akt, and activation of p300, a known target of Akt, can both enhance transcription of muscle-related genes via the post-translational modification of H3K27. In addition, p300 and MEF2 can function as co-activators of the myogenesis master regulator MyoD. Figure adapted from (Yam and Charron, 2013).

prematurely induce the expression of target genes and increased the speed of differentiation, indicating that other factors contribute to the repression of MyoD transcriptional activity in myoblasts.

PI3K signaling is required for myogenic differentiation *in vitro*, and constitutive activation can strongly enhance myogenin levels upon differentiation (Xu and Wu, 2000). Not only is it possible that PI3K could affect myoblast differentiation through Ezh2 inhibition but, as mentioned earlier, p300 is an Akt target (**Figure 4-9**) (Badeaux and Shi, 2013; Cha et al., 2005; Serra et al., 2007). Inhibition of PI3K or Akt blocks p300 phosphorylation, thus preventing MyoD acetylation and impeding the interaction of MyoD with both p300 and the DNA of its transcriptional targets (Serra et al., 2007). In both myoblasts and granule neurons, where it is involved in cell survival, the PI3K/Akt cascade is important for activity of MEF2 (Myocyte enhancing factor 2), a known MyoD co-activator that can also interact with p300 (**Figure 4-9**) (Sartorelli and Puri, 2018; Tamir and Bengal, 2000; Wiedmann et al., 2005). Modulating MEF2 activity may also play a role in regulating MyoD binding because one intriguing feature of genes where DNA binding of MyoD correlates with transcription is the enrichment of binding motifs for MEF2 (Cao et al., 2010). In summary, the totality of material covered in this section and the one above conveys a plethora of potential avenues for exploring the molecular mechanisms underlying the myogenic fate switch of GCPs.

4.3.4 The multilineage potential of GCPs

The dominant discussion surrounding the study of MMB is the source of the muscle cells within the tumor. Our model affirms earlier theories that the muscular component originates from the same cell as the tumor bulk. Earlier work using FISH has found that both cell

populations contain the same genomic amplifications (Bai et al., 2012; Lindberg et al., 2007). Moreover, our work indicates that myogenic conversion represents a form of reprogramming, an idea that is supported by co-labeling with muscle and neuronal markers both *in vitro* and *in vivo* (Bai et al., 2012; Kido et al., 2009). Because MMB is currently considered a histopathological variant that can occur in multiple subgroups and because these subgroups arise from distinct cell types, it is expected that these other cells can also undergo a myogenic switch.

However, our data contradicts the speculation from some groups that the existence of multilineage differentiation in MBs is evidence that these tumors arise from multipotent progenitors/stem cells (Borcek et al., 2011; Fathaddin et al., 2014). Although GCPs only produce granule neurons during normal development, we show that either *in vitro* or *in vivo* manipulation can convert GCPs to a myogenic fate. Likewise, BMP2 stimulation of GCP cultures triggered progressive expression of astroglial markers in a subpopulation of cells that corresponded with loss of neuronal markers (Okano-Uchida et al., 2004), and tumors from a murine Shh-MB model contain a population of astrocytes generated by trans-differentiation of GCPs (Yao et al., 2020).

Our experiments also favor a trans-differentiation mechanism because of the endogenous expression of MyoD and the relatively rapid cell fate transition *in vitro,* yet this does not exclude the possibility of de-differentiation. Notably, oncogenic transformation of GCPs is not only associated with the persistence of transient progenitor population(s) but also with the expansion of markers, like Olig2 and Nestin, that corresponds with less differentiated states (Li et al., 2016; Selvadurai et al., 2020; Zhang et al., 2019). The possible de-differentiation of GCPs merits future exploration in our two experimental paradigms because PI3K and Ezh2 play pleiotropic roles during normal development that may delineate their impact on tumor formation and myogenic conversion. For instance, aberrant activation of PI3K signaling and deletion of Ezh2 have

opposing effects on the cell cycle entry of muscle-specific stem cells (known as satellite cells) as measured by thymidine analog incorporation (Juan et al., 2011; Wang et al., 2018; Yue et al., 2017). On the other hand, the consequence of both leads to depletion of the stem cell pool with concomitant upregulation of myogenin expression suggesting that resting satellite cells and active satellite cells/myoblasts respond differently to perturbation of PI3K or Ezh2 activity. Understanding the functional consequences of PI3K and Ezh2 on the various cell populations of the granule cell lineage may provide clues about the prognostic implication of myogenic differentiation within Shh-MB.

In conclusion, GCPs possess an underappreciated multilineage potential that can be exploited during tumorigenesis, and in these cells, the activation of PI3K or inhibition of Ezh2 represent a mode of inducing myogenic differentiation, the defining feature of MMB.

Chapter 5

Discussion

5.1 Looking Boc

In 2011, ten years after their original article, Hanahan and Weinberg published an updated list of cancer hallmarks: sustained proliferative signaling, evasion of growth suppressors, resistance to cell death, replicative immortality, angiogenesis, activation of invasion and metastasis, reprogrammed energy metabolism, and evasion of immune destruction. To attain these characteristics, normal cells mostly acquire genetic alterations, and inherent to this process is the breakdown of the mechanisms protecting the integrity of the genome (Hanahan and Weinberg, 2011). In part, this is achieved by the stochastic DNA damage that either transpires or persists during normal cell division, a fact that accounts for the correlation between the lifetime risk of specific cancer types and the overall number of divisions of their respective stem cells (Tomasetti and Vogelstein, 2015). Nevertheless, certain oncogenic drivers can fuel genomic instability by inducing replication stress; for example, Shh causes replication stress in GCPs through which it triggers tumor initiating mutations (Tamayo-Orrego et al., 2020). The resulting DNA lesions lie downstream of the canonical Shh signaling pathway and require the co-receptor Boc (Mille et al., 2014).

Early in my graduate training, I sought to test the hypothesis that Boc enhances tumor formation by actively contributing to DNA damage in GCPs. The key result from the third chapter is that transient overexpression of Boc via electroporation of GCPs – the identity of which was verified by lineage-restricted TdTomato expression – can acutely trigger phosphorylation of H2AX, a proxy of DNA damage. Further work to validate this finding and to test its relevance in MB development will be essential before drawing strong conclusions. Beyond a putative role in DNA damage, clarity in understanding the contribution of Boc to tumorigenesis is still needed.

In *Ptch1*$^{+/-}$ mice, Shh signaling instigates an increase of recombination events resulting in *Ptch1* LOH, which marks the transition to ligand-independent signaling and is coupled with preneoplasia formation, and progression to advanced tumors requires additional alterations of driver genes like *p53* (Tamayo-Orrego et al., 2016a). Thus, our working model places Boc, which acts in conjunction with Ptch1 as a Shh-binding complex, in the early stages of tumorigenesis.

The role of Boc as a Shh co-receptor is a task it shares with Cdo and Gas1 when their expressions overlap. Due to this functional redundancy, Shh signaling phenotypes (or lack thereof) in *Boc*-null mice vary. For instance, loss of *Boc* alone is insufficient to cause holoprosencephaly nor does it disrupt patterning of the neural tube even though ectopic expression of Boc can trigger ventralization of cell fates in a ligand-dependent manner (Allen et al., 2011; Tenzen et al., 2006; Zhang et al., 2011b). On the other hand, *Boc*$^{-/-}$ mice exhibit Shh-related axon guidance defects in both retinal ganglion cells and spinal commissural neurons that phenocopy loss of *Smo*, which acts downstream of ligand-binding (Fabre et al., 2010; Okada et al., 2006; Peng et al., 2018). In cerebellar GCPs, Boc is important though not required for proliferation in response to Shh, due to compensation by Gas1, and this is reflected by the mild phenotype observed in *Boc*-null mice, in which the reduction of the IGL surface area is less than 20% (Izzi et al., 2011). However, Boc is required for Shh-dependent DNA damage, and as such, deletion of *Boc* has a stronger impact on *Ptch1*$^{+/-}$ tumor incidence, which is diminished by more than 60% compared to *Boc* wildtype animals (Mille et al., 2014).

One potential reason Gas1 cannot recoup for loss of Boc during tumor development is that Boc, unlike Gas1, is a Gli transcriptional target (Lee et al., 2010; Liu et al., 2001). Hence, *Ptch1*$^{+/-}$ could drive increased Boc expression that would further potentiate aberrant Shh

signaling, including Shh-dependent DNA damage, to promote *Ptch1* LOH. Another possibility is that oncogenic transformation is more sensitive to modulation of Shh signaling than normal development. For example, low-dose inhibition of Cdc7 (cell division cycle 7), whose activity is critical for origin firing during DNA replication, did not alter proliferation levels in the EGL at P7 but did reduce Shh-dependent genomic instability and preneoplasia incidence (Tamayo-Orrego et al., 2020).

Nonetheless, it is tempting to speculate that other factors may be involved. For example, high Boc expression could prompt it to aggregate with itself or other proteins and activate Shh-independent signaling, potentially through the PI3K/Akt pathway. Recent data generated from our lab shows that IGF1, which is known to activate PI3K/Akt signaling and stimulate GCP proliferation, does not trigger DNA damage (Tamayo-Orrego et al., 2020). Therefore, any link between Boc and PI3K activation would modulate tumor development by other mechanisms and would likely act to drive tumor progression because changing IGF1/2 expression affects tumor but not preneoplasia incidence (Corcoran et al., 2008; Tanori et al., 2010). Alternatively, Boc expression can be detected by single cell RNA sequencing in early cerebellar progenitors and by immunofluorescence in the embryonic ventricular zone of the cerebellum (Carter et al., 2018; Izzi et al., 2011). Shh signaling plays a multifaceted role in the cerebellum (Dahmane and Ruiz-i-Altaba, 1999; Farmer et al., 2016; Huang et al., 2010), so the role of Boc in non-GCPs may augment the development of MB in mice with *Ptch1*$^{+/-}$, which is also germline and which does not lead to tumor formation in all animals.

One way to assess these suppositions would be to engineer a conditional *Boc* allele that can be selectively deleted via Cre-recombinase. If tumor incidence is reduced in *Ptch1*$^{+/-}$*;Math1-cre;Boc*$^{fl/fl}$ mice compared to *Boc* wildtype animals, then it would indicate that loss of Boc

expression in GCPs is sufficient to impede tumorigenesis. Temporal control of *Boc* deletion with a *Math1*-Cre^{ER} line could also specifically test if Boc expression is important for tumor formation after *Ptch1* LOH (Machold and Fishell, 2005). Administration of tamoxifen around P10 would likely ensure recombination and loss of Boc expression by P14, an age corresponding with the preneoplastic stage and characterized by *Ptch1* LOH (Tamayo-Orrego et al., 2016b). Digging a little deeper may uncover hidden secrets behind the impact of Boc in cerebellar development and tumorigenesis.

5.2 Looking forward – Implications of an MMB model

Thanks to a corollary and serendipitous discovery initially uncovered while investigating the role of Boc in MB, I embarked on the scientific journey detailed in Chapter 4 characterizing a mouse model of MMB and exploring the myogenic potential of GCPs. Using transcriptional profiling and immunolabeling, we demonstrated that $Ptch1^{+/-}$;$Pik3ca^{H1047R}$ tumors mirror human MMB. Moreover, conditional expression of the mutant p110α in the *Math1*-lineage is sufficient to produce myogenic cells in the EGL. Like $Pik3ca^{H1047R}$, obstructing Ezh2 function can also trigger muscle marker expression in GCPs and MB cells. This myogenic conversion likely relies on the transcriptional activity of endogenous MyoD and corresponds with loss of Pax6 expression.

Although MMB was removed as a discrete variant in 2016, the 2007 WHO classification of CNS tumors states, “The descriptive term ‘medulloblastoma with myogenic differentiation’ may be used for any variant (desmoplastic/nodular, large cell medulloblastoma, etc.) containing focal rhabdomyoblastic elements with immunoreactivity to desmin, myoglobin, and fast myosin but not smooth muscle α-actin alone (Louis et al., 2007).” This definition does not restrict

categorization based on the number of myoblastic cells or the specific morphology, such as the presence of striations; therefore, our murine tumors can be considered models of medulloblastoma with myogenic differentiation (formerly MMB) based on the myoglobin immunolabeling alone. As such, one consideration stemming from this work is the need to update how myogenic differentiation is detected in human MBs. In many instances, an MMB diagnosis initiates due to unusual histology patterns, such as the presence of strap cells, and is confirmed through immunohistochemistry (Sarkar et al., 2017; Wright et al., 2012). In this way, more subtle phenotypes like those of the *Pik3ca*^{H1047R} murine tumors are prone to be missed. In the literature, there are some examples where the MMB nomenclature was applied as a part of a larger retrospective analysis (Gupta et al., 2018; Sachdeva et al., 2008). Because myogenic differentiation in MB is a rare event, an antibody screen of every MB diagnosis would be inefficient; nonetheless, as we identify MMB-associated mutations, potentially including *PIK3CA* mutations and *EZH2* deletions, then targeted immunohistochemistry of select samples may complement a bioinformatic approach.

Both the PI3K and Ezh2 experimental paradigms display subtle histological phenotypes where the myocytic population is mostly blast-like and makes up a small percentage of the total tumor bulk, and we propose that the human equivalent of these MMBs is currently undiagnosed. On the flip side, these animal models do not recapitulate the full spectrum of myogenic differentiation because we have not detected tumors containing regions with copious numbers of strap cells. In the future, if we can elucidate how *Pik3ca*^{H1047R} and/or Ezh2 inhibition activate a myogenic program in GCPs, then we can leverage that knowledge to develop more efficient models of myogenic conversion. Of particular interest is the role of histone modifiers and chromatin remodelers in this process. Illuminating the molecular mechanisms underlying the

myogenic switch will afford us with a golden opportunity to potentially establish myogenic differentiation as a biomarker for specific therapeutic strategies, such as BET inhibitors.

5.3 Myogenic conversion, triggering an identity crisis in GCPs

Cell fate specification – and by extension cell identity plasticity – is multifactorial. In his now famous "epigenetic landscape," Conrad Waddington attempted to visualize these complex factors with a ball rolling down a sloping hill (**Figure 5-1A**) (1957). As someone who prefers words to pictures, I have provided a simpler model of cell fate specification (**Figure 5-1B**), which admittedly is less elegant by virtue of losing some of the symbolism created by drawing a three-dimensional space. Although pseudotemporal analysis of single cell RNA sequencing has demonstrated that individual cells comprise a continuum of identities, I have chosen to represent cell states as discrete entities that better reflect the lexicon applied *in situ* (Carter et al., 2018; Ocasio et al., 2019; Selvadurai et al., 2020). Nevertheless, I have tried to compensate for this discrepancy by adopting a four-tier hierarchy: multipotent stem cells, bi- or unipotent progenitors, transit amplifying precursors, and terminally differentiated cells. The exact terminology, though not universal, applies to the granule lineage reasonably well as the NSCs of the early cerebellar primordium, which potentially initiate G3-MBs, give rise to both the ventricular zone or rhombic lip progenitors, and this is followed by specification of GCPs (or the other glutamatergic neuronal populations) (Leto et al., 2016). Finally, GCPs exit the cell cycle and differentiate into granule neurons.

Dysregulation of this process is critical not only for tumorigenesis, which I will expand upon later, but also for directed cell reprogramming, which is our aim in developing a more robust MMB model. Critical barriers to reprogramming, whether through de-differentiation to a

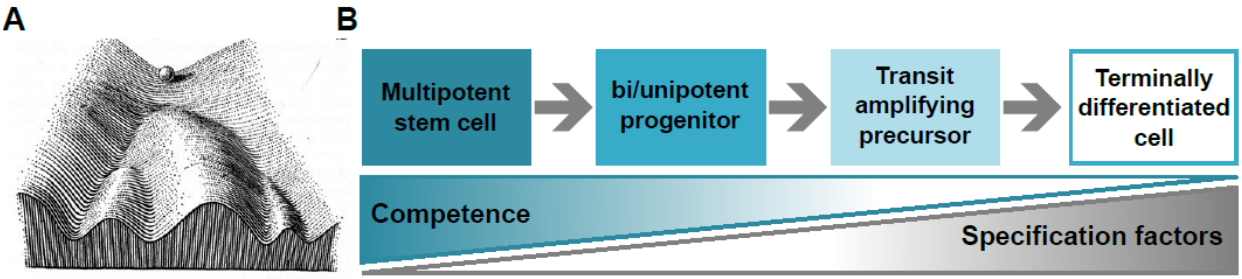

Figure 5-1. Cell fate specification and differentiation

A) Waddington's classic epigenetic landscape visualizes development as a ball rolling along a tilted and "undulating surface" within canals. In this model, change is continuous and gradual, and inducers push the ball at choice points towards one canal, indicative of an individual cell's competence (Gilbert, 1991; Waddington, 1957). Figure from (Waddington, 1957).

B) A simplified two-dimensional representation of the same process broken down into a series of boxes that represent the discrete cell states commonly denoted in developmental cell biology, where the color gradient represents the gradual change in competence, the arrows give directionality, and the fill color of the arrows designates the presence of specification factors that instruct shifts in cell identity.

pluripotent state or trans-differentiation, are (1) the expression of specification factors, specifically transcription factors that regulate gene expression programs, and (2) the intrinsic cell competence restricting lineage plasticity, usually defined by the demarcation of specific epigenetic modifications (**Figure 5-1B**) (Zhou and Melton, 2008).

Here, GCPs present a tantalizing template for myogenesis because a subpopulation endogenously express MyoD, the master regulator of myogenesis, thereby circumventing the need for ectopic expression with strong promoters impervious to normal modulation (**Figure 5-2A** right) (Dey et al., 2013). In addition, many important co-factors are well expressed, such as *Pbx1*, *Meis1*, *Mef2a*, *Mef2c*, and *Mef2d* (**Figure 5-2A** left) (Tapscott, 2005). GCPs even express the switch factor *Trim28* (*Triparte motif-containing protein 28*, aka Kap1) and its regulatory kinase Msk1 (Mitogen- and stress-activated protein kinase 1), which is encoded by *Rps6ka5* (Singh et al., 2015). On the other hand, FPKM of *Six4* is very low and *Six1* is borderline for our threshold of expression (**Figure 5-2A** right) (Tapscott, 2005). Although tissue-specific splice isoforms, known to be involved in myogenesis, are not accounted for in these graphs, it has been previously demonstrated that muscle and brain express the same isoforms of MEF2C (Trapnell et al., 2010; Zhu et al., 2005). MEF2Dα2, the key isoform for late myoblast differentiation, is absent in brain, but its binding profile largely coincides with the ubiquitously expressed MEF2Dα1 (Martin et al., 1994; Sebastian et al., 2013). Moreover, the regulation of these splice variants would not explain the inability of MyoD to drive intermediate differentiation genes like *Myog* and *Ckm* in wildtype GCPs (Sebastian et al., 2013).

I predict that the chromatin landscape restricts the competence of GCPs to undergo myogenic reprogramming. This is a rather obvious prediction because GCPs are derived from the ectoderm while myoblasts are of mesodermal origin meaning that the lineage bifurcation of these

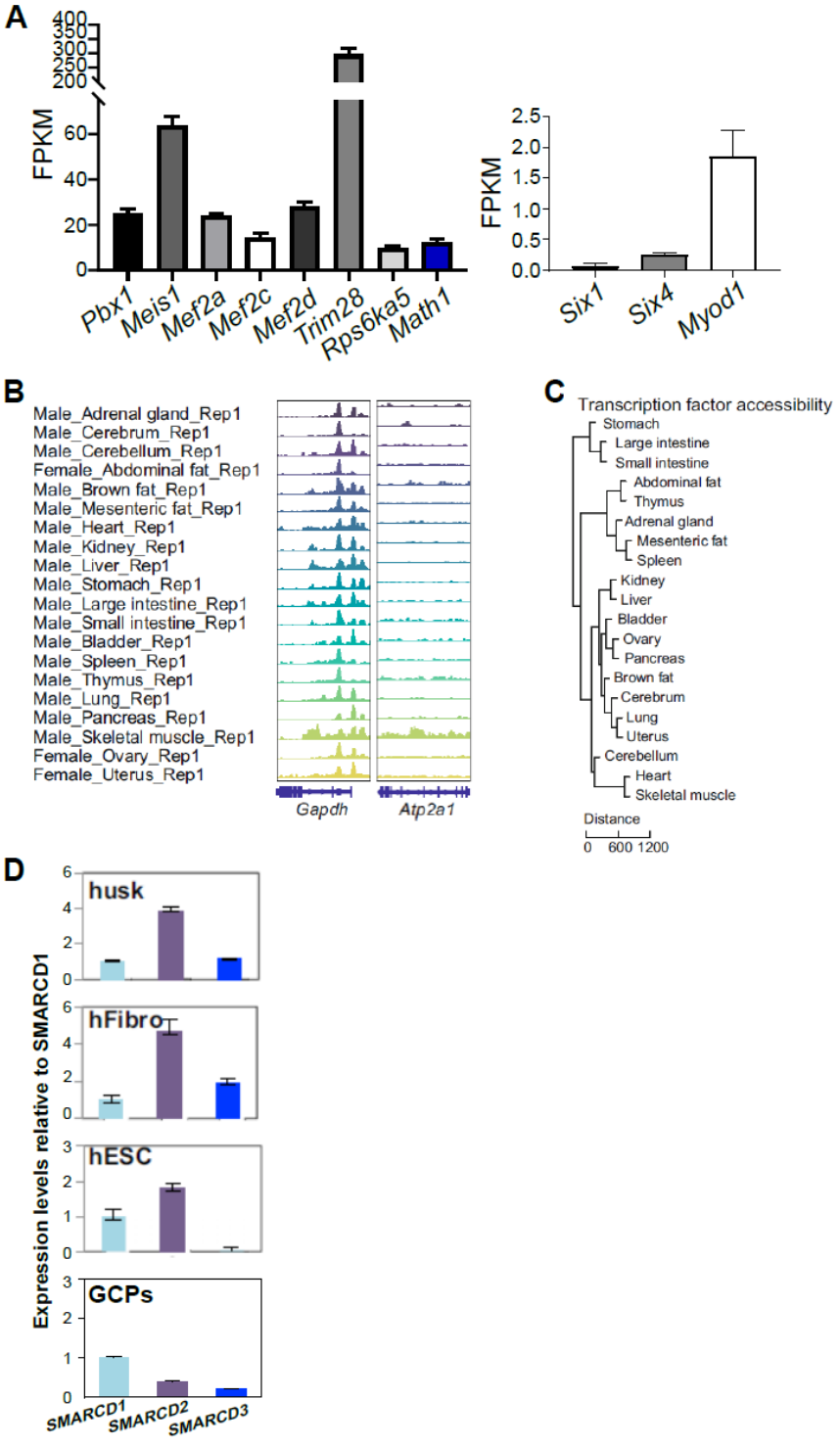

Figure 5-2. GCPs express many MyoD co-factors but lack the competence to undergo myogenic reprogramming

A) GCPs express many but not all MyoD co-activators. FPKMs of RNA sequencing from P7 GCPs show expression of *Pbx1*, *Meis1*, *Mef2a-c*, *Trim28*, and *Rps6ka5* with *Math1* as a reference (left). *Six1*, *Six4*, and *Myod1* are graphed separately due to their low FPKMs (right). Data from 3 animals represented at mean + standard deviation.

B) Muscle-specific *Atp2a1* locus is not accessible in cerebellum, but housekeeping gene *Gapdh* is accessible in all tissues. ATAC-seq of adult murine tissues and graph adapted from (Liu et al., 2019).

C) Hierarchical clustering of transcription factor motifs represented in Euclidean distance. Image from (Liu et al., 2019).

D) Human embryonic stem cells (hESCs) and P7 GCPs show low expression of *SMARCD3* (normalized to *SMARCD1*) compared to human skeletal myoblasts (husk) and myogenic competent fibroblasts (hFibro). GCP data from same RNA sequencing as *A*. Data represented as mean + standard deviation. Graphs adapted from (Albini et al., 2013).

cells occurs during gastrulation. Indeed, Liu *et al.* recently created an atlas of chromatin accessibility in adult mouse tissues using the assay for transposase-accessible chromatin with sequencing (ATAC-seq) where they showed that the cerebellum and skeletal muscle have distinct tissue-specific peaks (2019). For example, *Atp2a1*, whose product SERCA1 is one of the muscle markers utilized in Chapter 4, is accessible in skeletal muscle but not the cerebellum (**Figure 5-2B**). Nonetheless, when they performed hierarchical clustering on transcription factor motifs that they identified within the tissue specific peaks, the cerebellum was closer to the heart and skeletal muscle than it was to the cerebrum reinforcing the theory that these tissues have high overlap of specification factors (**Figure 5-2C**).

One way access to transcriptional targets can be cut off is through the presence of nucleosomes, which are composed of a single histone octamer around which DNA is wrapped. The SWI/SNF complex remodels the chromatin through either nucleosome insertion/exclusion or sliding, thereby changing DNA accessibility, and MyoD can recruit SWI/SNF to its target loci via interaction with the SMARCD3 (aka BAF60c) subunit (Forcales et al., 2012; Wilson and Roberts, 2011). Of the three SMARCD variants, which form mutually exclusive SWI/SNF complexes, SMARCD3 is exclusively required for C2C12 differentiation although SMARCD2 performs an auxiliary role. Furthermore, human embryonic stem cells (hESCs), which are resistant to MyoD-induced myogenesis, express low levels of *SMARCD3* relative to the other variants, whereas *SMARCD3* and *SMARCD1* are present at comparable levels in human skeletal fibroblasts (husk) or human fibroblasts (hFibro) (**Figure 5-2D**) (Albini et al., 2013). Co-expression of MyoD with SMARCD3 can significantly enhance myogenic conversion. As GCPs not only exhibit diminished *SMARCD3* levels but also utilize an alternative promoter to express a novel variant, this poses a potential route for boosting myogenesis (**Figure 5-2D**) (Pal et al.,

2011). Exposing the critical differences in chromatin regulation between GCPs and myoblasts will both assist our understanding and modeling of MMB and may also provide important insights for improving MyoD-triggered reprogramming applications in regenerative therapy.

5.4 Dysregulation of cell fate specification: an emerging cancer hallmark?

Normal developmental hierarchies are unidirectional, which is represented by the incline of Waddington's landscape and by the arrows of the simpler schematic (**Figure 5-1**). Moreover, Waddington opted to place the ball's trajectory within channels to signify that the system can compensate for small disturbances (1957). Yet, the disturbances involved in tumorigenesis are anything but small, and the assignment of cancer hallmarks was designed to recognize unifying precepts of tumor formation with an eye towards therapeutic opportunities (Hanahan and Weinberg, 2011). Now, as we approach 2021, a decade since the last update, it is time to again revisit these hallmarks. In the last version, the authors themselves alluded to cancer stem cells and their potential function in primary tumor development and relapse. Using a few illustrative examples, I hope to substantiate that the alterations in cell identity within tumors encompass more than just cancer stem cells and so should an additional entry to the list of cancer hallmarks.

Cancer stem cells are involved in tumor development and maintenance, where they control the persistence of developmental hierarchies (Azzarelli et al., 2018). For instance, Lgr5-positive stem cells of the normal epithelium can give rise to benign adenomas, a portion of which retain both the gene expression profile and the crypt-villus organoid forming function of normal stem cells (Schepers et al., 2012). These Lgr5-expressing cells, which are only 5-10% of the entire tumor population, maintain growth and generate multilineage progeny in a manner

reminiscent of the normal tissue. Additionally, they can be found in malignant colorectal carcinomas (Beck and Blanpain, 2013).

In the first week of murine postnatal life, the EGL contains a small and transient subset of cells that express neural progenitor markers Nestin, Sox2, and/or even an *hGFAP*-driven dsRed reporter but do not express Prominin1 (aka CD133) or Olig2 (Lee et al., 2005; Li et al., 2013; Selvadurai et al., 2020; Silbereis et al., 2010; Zhang et al., 2019). These cells persist in both preneoplastic lesions and advanced tumors, which also include proliferating GCPs and differentiated granule neurons (Cheng et al., 2020; Vanner et al., 2014). These less differentiated progenitors have heightened tumor propagating properties fueling both relapse and metastasis (Singh et al., 2004; Vanner et al., 2014; Zhang et al., 2019). In this case, it is evident that the normal hierarchy is present yet aberrant because a subpopulation of tumor cells expresses Prominin1 and Olig2 (Ocasio et al., 2019; Singh et al., 2004; Zhang et al., 2019). Deviation from the normal hierarchy occurs early in tumor development because there are Olig2-expressing cells and more Sox2- and Nestin-positve cells in the EGL of P7 *Ptch1* conditional knockout mice compared to wildtype (Li et al., 2016; Selvadurai et al., 2020; Zhang et al., 2019). This could represent a block in GCP specification from rhombic-lip progenitors as Olig2 is expressed there (Schüller et al., 2008), but it could also be the consequence of GCP de-differentiation. Importantly for this latter theory, inducing *Ptch1* deletion in *Math1*-expressing cells at P10 produces tumors while no tumors result when *Ptch1* is deleted in *Sox2*-expressing cells at P7, which suggests that the tumor specific hierarchy can be re-established even after it has been lost during development (Selvadurai et al., 2020; Yang et al., 2008).

This example of how tumorigenesis is marked by the subversion of normal hierarchies is not specific to Shh-MB. In G3-MB, most cells are undifferentiated with stem-like characteristics

with sparse (if any) differentiated cells (Hovestadt et al., 2019b; Vladoiu et al., 2019). Overexpression of Myc, a known reprogramming factor, can trigger tumor formation in NSCs and multiple unipotent progenitor cells including GCPs – demonstrative of an oncogene capable of both blocking and reverting normal differentiation (Kawauchi et al., 2017; Kawauchi et al., 2012; Pei et al., 2012). Similarly, *Pik3ca*^{H1047R}, a recurrent mutation in breast cancer (though less frequent in triple-negative tumors), can instigate an identity switch when expressed in a lineage-restricted manner such that luminal-like cells appear when the mutation is activated in basal cells and vice versa (Koren et al., 2015; Van Keymeulen et al., 2015). These cell types share a common progenitor, and Koren *et al.* showed that mutant basal and luminal cells displayed enhanced mammary repopulating abilities and could produce both lineages, suggesting that it acts via de-differentiation (2015).

De-differentiation is not the only distortion of normal specification relevant to tumorigenesis. During the ageing process, hematopoietic stem cells lose their lymphoid-generating potential leading to myeloid skewing, which is associated with an increase of myeloid malignancies in the elderly (Konieczny and Arranz, 2018). Mutations in *ASXL1* and *EZH2* are associated with myeloid dysplastic diseases and malignancies (Micol and Abdel-Wahab, 2016; Triviai et al., 2019), and deletion of *Asxl1* in bone marrow stromal cells triggered myeloid skewing (Zhang et al., 2018).

Finally, there are instances where oncogenic identity changes are so drastic that they utterly defy the structure of a hierarchy. Rhabdomyosarcoma (RMS) is the most common soft tissue sarcoma in children, and the heterogeneous embryonal RMS (eRMS) subgroup is associated with SHH pathway activating mutations (sporadic and germline), *TP53* mutations (sporadic and germline), and even PI3K activating mutations (Hatley et al., 2012; Kohsaka et al.,

2014). Although eRMS tumors are composed of mainly myoblastic cells, the cell-of-origin is still contested because tumors can arise in regions devoid of skeletal muscle. Driving Shh signaling with the *SmoM2* allele is embryonic lethal in early myoblast cells (*Myf5*-Cre or *Myod1*-Cre) and does not trigger tumor formation in postnatal satellite cells, the adult muscle stem cell (Hatley et al., 2012); however, conditional expression of *SmoM2* in cells expressing *Myogenin*, an early differentiation marker usually restricted to postmitotic myoblasts, produced tongue tumors in 100% of mice, suggesting that early intervention can revert myoblasts back into a proliferative state. Crucially, *SmoM2* can also fuel tumorigenesis in the head and neck, a common tumor site for eRMS, when expressed in endothelial progenitors using an *AP2*-Cre (Drummond et al., 2018; Hatley et al., 2012). Together, these studies show that strong activation of Shh signaling can both impede normal myogenesis and force myoblast-like specification in certain non-muscle lineages. Last, but not least, myogenic differentiation in a subset of MBs is indicative of oncogenic processes that obliterate normal cerebellar lineage management.

Fate plasticity can also play a role in chemotherapy resistance. For example, vismodegib has received FDA approval to treat Basal cell carcinoma, another SHH-driven cancer (Biehs et al., 2018). In a conditional *Ptch1* and *p53* double knockout model, a subset of tumor cells can evade drug-induced apoptosis by altering their identity. These cells are responsible for the residual disease present in vismodegib-treated animals and can then drive tumor relapse upon treatment cessation. Overall, I hope I have sufficiently demonstrated that we cannot assume that fate choice points are unidirectional in cancer; consequently, it would behoove us to cultivate multimodal therapies that target many cell populations in the future to improve initial responses and impede relapse.

5.5 Conclusions

Genomic instability is an accelerant of neoplastic transformation, and in this thesis, I propose for the first time that high levels of the Shh co-receptor Boc can trigger DNA damage in GCPs, a tumor-initiating cell for Shh-MB. I was unable to identify downstream mediators of Boc-induced H2AX phosphorylation, so like the GCPs I have studied for seven years, I too learned that plasticity is a weapon to wield in the world of cancer biology. Using a fluorescence reporter to identify *Math1*-expressing GCPs, I learned that most BocGFP-positive cells were not GCPs, provoking the idea that Boc may trigger DNA damage in other cerebellar cell types. Moving forward, it will be important to substantiate my current findings and to inquire further into the potential of Boc to promote tumorigenesis in GCPs and other cell (and maybe even other cancer) types.

The second part of the thesis covers the characterization of the first transgenic ($Ptch1^{+/-};Pik3ca^{H1047R}$) murine model of MB with myogenic differentiation, also known as medullomyoblastoma. In addition, we show, using two different techniques, that blocking Ezh2 function can induce myogenic marker expression. In summary, our results indicate that the GCPs possess the potential to undergo myogenic conversion, thus contributing one small piece to an ever-growing puzzle that depicts the significance of upsetting developmental cell fate hierarchies in tumor formation. Optimistically looking to the future, I hope that implementing these experimental paradigms in ongoing studies can help fill the void in our understanding of MMB, replacing the current uncertainty for patients and their families with the reassurance of knowledge and potentially uncovering novel therapeutic targets.

Bibliography

Abdel-Wahab, O., Adli, M., LaFave, L.M., Gao, J., Hricik, T., Shih, A.H., Pandey, S., Patel, J.P., Chung, Y.R., Koche, R., *et al.* (2012). ASXL1 mutations promote myeloid transformation through loss of PRC2-mediated gene repression. Cancer Cell *22*, 180-193.

Adams, J.R., Xu, K., Liu, J.C., Agamez, N.M., Loch, A.J., Wong, R.G., Wang, W., Wright, K.L., Lane, T.F., Zacksenhaus, E., *et al.* (2011). Cooperation between Pik3ca and p53 mutations in mouse mammary tumor formation. Cancer research *71*, 2706-2717.

Ahn, J.Y., Schwarz, J.K., Piwnica-Worms, H., and Canman, C.E. (2000). Threonine 68 phosphorylation by ataxia telangiectasia mutated is required for efficient activation of Chk2 in response to ionizing radiation. Cancer research *60*, 5934-5936.

Albini, S., Coutinho, P., Malecova, B., Giordani, L., Savchenko, A., Forcales, S.V., and Puri, P.L. (2013). Epigenetic reprogramming of human embryonic stem cells into skeletal muscle cells and generation of contractile myospheres. Cell reports *3*, 661-670.

Albrecht, S., von Deimling, A., Pietsch, T., Giangaspero, F., Brandner, S., Kleihuest, P., Wiestler, O.J.N., and neurobiology, a. (1994). Microsatellite analysis of loss of heterozygosity on chromosomes 9q, 11 p and 17p in medulloblastomas. *20*, 74-81.

Aldaregia, J., Errarte, P., Olazagoitia-Garmendia, A., Gimeno, M., Uriz, J.J., Gershon, T.R., Garcia, I., and Matheu, A. (2020). Erbb4 Is Required for Cerebellar Developmentand Malignant Phenotype of Medulloblastoma. Cancers *12*.

Aldosari, N., Bigner, S.H., Burger, P.C., Becker, L., Kepner, J.L., Friedman, H.S., McLendon, R.E.J.A.o.p., and medicine, l. (2002). MYCC and MYCN oncogene amplification in medulloblastoma: a fluorescence in situ hybridization study on paraffin sections from the Children's Oncology Group. *126*, 540-544.

Alimova, I., Venkataraman, S., Harris, P., Marquez, V.E., Northcott, P.A., Dubuc, A., Taylor, M.D., Foreman, N.K., and Vibhakar, R. (2012). Targeting the enhancer of zeste homologue 2 in medulloblastoma. International journal of cancer *131*, 1800-1809.

Allen, B.L., Song, J.Y., Izzi, L., Althaus, I.W., Kang, J.S., Charron, F., Krauss, R.S., and McMahon, A.P. (2011). Overlapping roles and collective requirement for the coreceptors GAS1, CDO, and BOC in SHH pathway function. Developmental cell *20*, 775-787.

Alter, B.P., Rosenberg, P.S., and Brody, L.C. (2007). Clinical and molecular features associated with biallelic mutations in FANCD1/BRCA2. Journal of medical genetics *44*, 1-9.

Anders, S., Pyl, P.T., and Huber, W. (2015). HTSeq--a Python framework to work with high-throughput sequencing data. Bioinformatics (Oxford, England) *31*, 166-169.

Andrews, S. (2010). FastQC: a quality control tool for high throughput sequence data (Babraham Bioinformatics, Babraham Institute, Cambridge, United Kingdom).

Archer, T.C., Ehrenberger, T., Mundt, F., Gold, M.P., Krug, K., Mah, C.K., Mahoney, E.L., Daniel, C.J., LeNail, A., Ramamoorthy, D., *et al.* (2018). Proteomics, Post-translational Modifications, and Integrative Analyses Reveal Molecular Heterogeneity within Medulloblastoma Subgroups. Cancer Cell *34*, 396-410.e398.

Armstrong, L. (2013). Epigenetics (Garland science).

Asp, P., Blum, R., Vethantham, V., Parisi, F., Micsinai, M., Cheng, J., Bowman, C., Kluger, Y., and Dynlacht, B.D. (2011). Genome-wide remodeling of the epigenetic landscape during myogenic differentiation. Proceedings of the National Academy of Sciences of the United States of America *108*, E149-158.

Ayrault, O., Zhao, H., Zindy, F., Qu, C., Sherr, C.J., and Roussel, M.F. (2010). Atoh1 inhibits neuronal differentiation and collaborates with Gli1 to generate medulloblastoma-initiating cells. Cancer research *70*, 5618-5627.

Ayrault, O., Zindy, F., Rehg, J., Sherr, C.J., and Roussel, M.F. (2009). Two tumor suppressors, p27Kip1 and patched-1, collaborate to prevent medulloblastoma. Molecular cancer research : MCR *7*, 33-40.

Azzarelli, R., Simons, B.D., and Philpott, A. (2018). The developmental origin of brain tumours: a cellular and molecular framework. Development (Cambridge, England) *145*.

Badeaux, A.I., and Shi, Y. (2013). Emerging roles for chromatin as a signal integration and storage platform. Nature reviews Molecular cell biology *14*, 211-224.

Bae, G.U., Lee, J.R., Kim, B.G., Han, J.W., Leem, Y.E., Lee, H.J., Ho, S.M., Hahn, M.J., and Kang, J.S. (2010). Cdo interacts with APPL1 and activates Akt in myoblast differentiation. Molecular biology of the cell *21*, 2399-2411.

Bai, R.Y., Staedtke, V., Lidov, H.G., Eberhart, C.G., and Riggins, G.J. (2012). OTX2 represses myogenic and neuronal differentiation in medulloblastoma cells. Cancer research *72*, 5988-6001.

Bailey, P., and Cushing, H. (1925). Medulloblastoma cerebelli: a common type of midcerebellar glioma of childhood. *14*, 192-224.

Bainbridge, M.N., Hu, H., Muzny, D.M., Musante, L., Lupski, J.R., Graham, B.H., Chen, W., Gripp, K.W., Jenny, K., Wienker, T.F., *et al.* (2013). De novo truncating mutations in ASXL3 are associated with a novel clinical phenotype with similarities to Bohring-Opitz syndrome. Genome medicine *5*, 11.

Balasubramani, A., Larjo, A., Bassein, J.A., Chang, X., Hastie, R.B., Togher, S.M., Lähdesmäki, H., and Rao, A. (2015). Cancer-associated ASXL1 mutations may act as gain-of-function mutations of the ASXL1-BAP1 complex. Nature communications *6*, 7307.

Ballabio, C., Anderle, M., Gianesello, M., Lago, C., Miele, E., Cardano, M., Aiello, G., Piazza, S., Caron, D., Gianno, F., *et al.* (2020). Modeling medulloblastoma in vivo and with human cerebellar organoids. Nature communications *11*, 583.

Banin, S., Moyal, L., Shieh, S., Taya, Y., Anderson, C.W., Chessa, L., Smorodinsky, N.I., Prives, C., Reiss, Y., Shiloh, Y., *et al.* (1998). Enhanced phosphorylation of p53 by ATM in response to DNA damage. Science (New York, NY) *281*, 1674-1677.

Bartek, J., Jr., Fornara, O., Merchut-Maya, J.M., Maya-Mendoza, A., Rahbar, A., Stragliotto, G., Broholm, H., Svensson, M., Sehested, A., Söderberg Naucler, C., *et al.* (2017). Replication stress, DNA damage signalling, and cytomegalovirus infection in human medulloblastomas. Molecular oncology *11*, 945-964.

Bartek, J., and Lukas, J. (2003). Chk1 and Chk2 kinases in checkpoint control and cancer. Cancer Cell *3*, 421-429.

Bartkova, J., Rezaei, N., Liontos, M., Karakaidos, P., Kletsas, D., Issaeva, N., Vassiliou, L.V., Kolettas, E., Niforou, K., Zoumpourlis, V.C., *et al.* (2006). Oncogene-induced senescence is part of the tumorigenesis barrier imposed by DNA damage checkpoints. Nature *444*, 633-637.

Bautista, F., Fioravantti, V., de Rojas, T., Carceller, F., Madero, L., Lassaletta, A., and Moreno, L.J.C.m. (2017). Medulloblastoma in children and adolescents: a systematic review of contemporary phase I and II clinical trials and biology update. *6*, 2606-2624.

Bayani, J., Zielenska, M., Marrano, P., Ng, Y.K., Taylor, M.D., Jay, V., Rutka, J.T., and Squire, J.A.J.J.o.n. (2000). Molecular cytogenetic analysis of medulloblastomas and supratentorial primitive neuroectodermal tumors by using conventional banding, comparative genomic hybridization, and spectral karyotyping. *93*, 437-448.

Beck, B., and Blanpain, C. (2013). Unravelling cancer stem cell potential. Nature reviews Cancer *13*, 727-738.

Ben-Arie, N., Bellen, H.J., Armstrong, D.L., McCall, A.E., Gordadze, P.R., Guo, Q., Matzuk, M.M., and Zoghbi, H.Y. (1997). Math1 is essential for genesis of cerebellar granule neurons. Nature *390*, 169-172.

Bergstrom, D.A., Penn, B.H., Strand, A., Perry, R.L., Rudnicki, M.A., and Tapscott, S.J. (2002). Promoter-specific regulation of MyoD binding and signal transduction cooperate to pattern gene expression. Molecular cell *9*, 587-600.

Berkes, C.A., and Tapscott, S.J. (2005). MyoD and the transcriptional control of myogenesis. Seminars in cell & developmental biology *16*, 585-595.

Biehs, B., Dijkgraaf, G.J.P., Piskol, R., Alicke, B., Boumahdi, S., Peale, F., Gould, S.E., and de Sauvage, F.J. (2018). A cell identity switch allows residual BCC to survive Hedgehog pathway inhibition. Nature *562*, 429-433.

Bigner, S.H., Mark, J., Friedman, H.S., Biegel, J.A., Bigner, D.D.J.C.g., and cytogenetics (1988). Structural chromosomal abnormalities in human medulloblastoma. *30*, 91-101.

Blais, A., Tsikitis, M., Acosta-Alvear, D., Sharan, R., Kluger, Y., and Dynlacht, B.D. (2005). An initial blueprint for myogenic differentiation. Genes & development *19*, 553-569.

Bloom, H., Wallace, E., and Henk, J.J.A.J.o.R. (1969). The treatment and prognosis of medulloblastoma in children: a study of 82 verified cases. *105*, 43-62.

Borcek, A.O., Durdag, E., Emmez, H., Kurt, G., and Baykaner, M.K. (2011). Myogenic and melanotic differentiated medulloblastoma: case report. Turkish neurosurgery *21*, 438-442.

Bourdeaut, F., Miquel, C., Richer, W., Grill, J., Zerah, M., Grison, C., Pierron, G., Amiel, J., Krucker, C., Radvanyi, F., *et al.* (2014). Rubinstein-Taybi syndrome predisposing to non-WNT, non-SHH, group 3 medulloblastoma. Pediatric blood & cancer *61*, 383-386.

Brand, M., Nakka, K., Zhu, J., and Dilworth, F.J. (2019). Polycomb/Trithorax Antagonism: Cellular Memory in Stem Cell Fate and Function. Cell stem cell *24*, 518-533.

Briscoe, J., and Thérond, P.P.J.N.r.M.c.b. (2013). The mechanisms of Hedgehog signalling and its roles in development and disease. *14*, 416-429.

Brown, A.L., Lee, C.H., Schwarz, J.K., Mitiku, N., Piwnica-Worms, H., and Chung, J.H. (1999). A human Cds1-related kinase that functions downstream of ATM protein in the cellular response to DNA damage. Proceedings of the National Academy of Sciences of the United States of America *96*, 3745-3750.

Brugières, L., Remenieras, A., Pierron, G., Varlet, P., Forget, S., Byrde, V., Bombled, J., Puget, S., Caron, O., and Dufour, C.J.J.C.O. (2012). High frequency of germline SUFU mutations in children with desmoplastic/nodular medulloblastoma younger than 3 years of age. *30*, 2087-2093.

Campagne, O., Davis, A., Maharaj, A.R., Zhong, B., Stripay, J., Farmer, D., Roussel, M.F., and Stewart, C.F. (2020). CNS penetration and pharmacodynamics of the CHK1 inhibitor prexasertib in a mouse Group 3 medulloblastoma model. European journal of pharmaceutical sciences : official journal of the European Federation for Pharmaceutical Sciences *142*, 105106.

Canman, C.E., Lim, D.S., Cimprich, K.A., Taya, Y., Tamai, K., Sakaguchi, K., Appella, E., Kastan, M.B., and Siliciano, J.D. (1998). Activation of the ATM kinase by ionizing radiation and phosphorylation of p53. Science (New York, NY) *281*, 1677-1679.

Cao, L., Xia, X., Kong, Y., Jia, F., Yuan, B., Li, R., Li, Q., Wang, Y., Cui, M., Dai, Z., *et al.* (2020). Deregulation of tumor suppressive ASXL1 - PTEN/AKT axis in myeloid malignancies. Journal of molecular cell biology.

Cao, Y., Yao, Z., Sarkar, D., Lawrence, M., Sanchez, G.J., Parker, M.H., MacQuarrie, K.L., Davison, J., Morgan, M.T., Ruzzo, W.L., *et al.* (2010). Genome-wide MyoD binding in skeletal muscle cells: a potential for broad cellular reprogramming. Developmental cell *18*, 662-674.

Capasso, H., Palermo, C., Wan, S., Rao, H., John, U.P., O'Connell, M.J., and Walworth, N.C. (2002). Phosphorylation activates Chk1 and is required for checkpoint-mediated cell cycle arrest. Journal of cell science *115*, 4555-4564.

Carter, R.A., Bihannic, L., Rosencrance, C., Hadley, J.L., Tong, Y., Phoenix, T.N., Natarajan, S., Easton, J., Northcott, P.A., and Gawad, C. (2018). A Single-Cell Transcriptional Atlas of the Developing Murine Cerebellum. Current biology : CB *28*, 2910-2920.e2912.

Castellino, R.C., Barwick, B.G., Schniederjan, M., Buss, M.C., Becher, O., Hambardzumyan, D., Macdonald, T.J., Brat, D.J., and Durden, D.L. (2010). Heterozygosity for Pten promotes tumorigenesis in a mouse model of medulloblastoma. PloS one *5*, e10849.

Cavalli, F.M.G., Remke, M., Rampasek, L., Peacock, J., Shih, D.J.H., Luu, B., Garzia, L., Torchia, J., Nor, C., Morrissy, A.S., *et al.* (2017). Intertumoral Heterogeneity within Medulloblastoma Subgroups. Cancer Cell *31*, 737-754 e736.

Cha, T.L., Zhou, B.P., Xia, W., Wu, Y., Yang, C.C., Chen, C.T., Ping, B., Otte, A.P., and Hung, M.C. (2005). Akt-mediated phosphorylation of EZH2 suppresses methylation of lysine 27 in histone H3. Science (New York, NY) *310*, 306-310.

Chatty, E.M., and Earle, K.M.J.C. (1971). Medulloblastoma. A report of 201 cases with emphasis on the relationship of histologic variants to survival. *28*, 977-983.

Chaturvedi, P., Eng, W.K., Zhu, Y., Mattern, M.R., Mishra, R., Hurle, M.R., Zhang, X., Annan, R.S., Lu, Q., Faucette, L.F., *et al.* (1999). Mammalian Chk2 is a downstream effector of the ATM-dependent DNA damage checkpoint pathway. Oncogene *18*, 4047-4054.

Chaturvedi, S., Gupta, S., Singhal, S., and Kumari, R. (2008). Medullomyoblastoma with calcification: a case report. Neuropathology : official journal of the Japanese Society of Neuropathology *28*, 93-97.

Chen, J.K., Taipale, J., Young, K.E., Maiti, T., and Beachy, P.A. (2002). Small molecule modulation of Smoothened activity. Proceedings of the National Academy of Sciences of the United States of America *99*, 14071-14076.

Chen, Y., and Struhl, G.J.C. (1996). Dual roles for patched in sequestering and transducing Hedgehog. *87*, 553-563.

Cheng, Y., Liao, S., Xu, G., Hu, J., Guo, D., Du, F., Contreras, A., Cai, K.Q., Peri, S., Wang, Y., *et al.* (2020). NeuroD1 Dictates Tumor Cell Differentiation in Medulloblastoma. Cell reports *31*, 107782.

Cho, Y.J., Tsherniak, A., Tamayo, P., Santagata, S., Ligon, A., Greulich, H., Berhoukim, R., Amani, V., Goumnerova, L., Eberhart, C.G., *et al.* (2011). Integrative genomic analysis of medulloblastoma identifies a molecular subgroup that drives poor clinical outcome. Journal of clinical oncology : official journal of the American Society of Clinical Oncology *29*, 1424-1430.

Chowdhury, C., Roy, S., Mahapatra, A.K., and Bhatia, R. (1985). Medullomyoblastoma. A teratoma. Cancer *55*, 1495-1500.

Cogen, P.H., Daneshvar, L., Metzger, A.K., and Edwards, M.S.J.G. (1990). Deletion mapping of the medulloblastoma locus on chromosome 17p. *8*, 279-285.

Corcoran, R.B., Bachar Raveh, T., Barakat, M.T., Lee, E.Y., and Scott, M.P. (2008). Insulin-like growth factor 2 is required for progression to advanced medulloblastoma in patched1 heterozygous mice. Cancer research *68*, 8788-8795.

Crawford, J.R., and Levy, M.L. (2015). Medulloblastoma with myogenic differentiation: a rare medulloblastoma variant in a young child. BMJ case reports *2015*.

Dahmane, N., and Ruiz-i-Altaba, A.J.D. (1999). Sonic hedgehog regulates the growth and patterning of the cerebellum. *126*, 3089-3100.

Davis, R.L., Weintraub, H., and Lassar, A.B. (1987). Expression of a single transfected cDNA converts fibroblasts to myoblasts. Cell *51*, 987-1000.

de Feraudy, S., Revet, I., Bezrookove, V., Feeney, L., and Cleaver, J.E. (2010). A minority of foci or pan-nuclear apoptotic staining of gammaH2AX in the S phase after UV damage contain DNA double-strand breaks. Proceedings of the National Academy of Sciences of the United States of America *107*, 6870-6875.

Del Valle, L., Enam, S., Lassak, A., Wang, J.Y., Croul, S., Khalili, K., and Reiss, K. (2002). Insulin-like growth factor I receptor activity in human medulloblastomas. Clinical cancer research : an official journal of the American Association for Cancer Research *8*, 1822-1830.

Dey, J., Ditzler, S., Knoblaugh, S.E., Hatton, B.A., Schelter, J.M., Cleary, M.A., Mecham, B., Rorke-Adams, L.B., and Olson, J.M. (2012). A distinct Smoothened mutation causes severe cerebellar developmental defects and medulloblastoma in a novel transgenic mouse model. Molecular and cellular biology *32*, 4104-4115.

Dey, J., Dubuc, A.M., Pedro, K.D., Thirstrup, D., Mecham, B., Northcott, P.A., Wu, X., Shih, D., Tapscott, S.J., LeBlanc, M., *et al.* (2013). MyoD is a tumor suppressor gene in medulloblastoma. Cancer research *73*, 6828-6837.

Dhar, S.S., Zhao, D., Lin, T., Gu, B., Pal, K., Wu, S.J., Alam, H., Lv, J., Yun, K., Gopalakrishnan, V., *et al.* (2018). MLL4 Is Required to Maintain Broad H3K4me3 Peaks and Super-Enhancers at Tumor Suppressor Genes. Molecular cell *70*, 825-841.e826.

Dhar, S.S., Zhao, D., Lin, T., Sillitoe, R.V., Chen, K., and Lee, M.G. (2020). Abstract 1083: Heterozygous knockout of the histone modifier MLL4 promotes Ptch+/−-driven medulloblastoma. Paper presented at: AACR Annual Meeting (Philadelphia, PA: AACR).

Di Croce, L., and Helin, K. (2013). Transcriptional regulation by Polycomb group proteins. Nature structural & molecular biology *20*, 1147-1155.

Diede, S.J., Guenthoer, J., Geng, L.N., Mahoney, S.E., Marotta, M., Olson, J.M., Tanaka, H., and Tapscott, S.J. (2010). DNA methylation of developmental genes in pediatric medulloblastomas identified by denaturation analysis of methylation differences. Proceedings of the National Academy of Sciences of the United States of America *107*, 234-239.

Dreszer, T.R., Karolchik, D., Zweig, A.S., Hinrichs, A.S., Raney, B.J., Kuhn, R.M., Meyer, L.R., Wong, M., Sloan, C.A., Rosenbloom, K.R., *et al.* (2012). The UCSC Genome Browser database: extensions and updates 2011. Nucleic acids research *40*, D918-923.

Drummond, C.J., Hanna, J.A., Garcia, M.R., Devine, D.J., Heyrana, A.J., Finkelstein, D., Rehg, J.E., and Hatley, M.E. (2018). Hedgehog Pathway Drives Fusion-Negative Rhabdomyosarcoma Initiated From Non-myogenic Endothelial Progenitors. Cancer Cell *33*, 108-124.e105.

Dubuc, A.M., Remke, M., Korshunov, A., Northcott, P.A., Zhan, S.H., Mendez-Lago, M., Kool, M., Jones, D.T., Unterberger, A., Morrissy, A.S., *et al.* (2013). Aberrant patterns of H3K4 and H3K27 histone lysine methylation occur across subgroups in medulloblastoma. Acta neuropathologica *125*, 373-384.

Dudek, H., Datta, S.R., Franke, T.F., Birnbaum, M.J., Yao, R., Cooper, G.M., Segal, R.A., Kaplan, D.R., and Greenberg, M.E. (1997). Regulation of neuronal survival by the serine-threonine protein kinase Akt. Science (New York, NY) *275*, 661-665.

Dykhuizen, E.C., Hargreaves, D.C., Miller, E.L., Cui, K., Korshunov, A., Kool, M., Pfister, S., Cho, Y.J., Zhao, K., and Crabtree, G.R. (2013). BAF complexes facilitate decatenation of DNA by topoisomerase IIα. Nature *497*, 624-627.

Easton, R.M., Cho, H., Roovers, K., Shineman, D.W., Mizrahi, M., Forman, M.S., Lee, V.M., Szabolcs, M., de Jong, R., Oltersdorf, T., *et al.* (2005). Role for Akt3/protein kinase Bgamma in attainment of normal brain size. Molecular and cellular biology *25*, 1869-1878.

Eberhart, C.G., Kepner, J.L., Goldthwaite, P.T., Kun, L.E., Duffner, P.K., Friedman, H.S., Strother, D.R., and Burger, P.C.J.C. (2002). Histopathologic grading of medulloblastomas: a Pediatric Oncology Group study. *94*, 552-560.

Echelard, Y., Epstein, D.J., St-Jacques, B., Shen, L., Mohler, J., McMahon, J.A., and McMahon, A.P.J.C. (1993). Sonic hedgehog, a member of a family of putative signaling molecules, is implicated in the regulation of CNS polarity. *75*, 1417-1430.

Ellison, D.W., Onilude, O.E., Lindsey, J.C., Lusher, M.E., Weston, C.L., Taylor, R.E., Pearson, A.D., and Clifford, S.C. (2005). beta-Catenin status predicts a favorable outcome in childhood medulloblastoma: the United Kingdom Children's Cancer Study Group Brain Tumour Committee. Journal of clinical oncology : official journal of the American Society of Clinical Oncology *23*, 7951-7957.

Englund, C., Kowalczyk, T., Daza, R.A., Dagan, A., Lau, C., Rose, M.F., and Hevner, R.F. (2006). Unipolar brush cells of the cerebellum are produced in the rhombic lip and migrate through developing white matter. The Journal of neuroscience : the official journal of the Society for Neuroscience *26*, 9184-9195.

Er, U., Yigitkanli, K., Kazanci, B., Ozturk, E., Sorar, M., and Bavbek, M. (2008). Medullomyoblastoma: teratoid nature of a quite rare neoplasm. Surgical neurology *69*, 403-406.

Fabre, P.J., Shimogori, T., and Charron, F. (2010). Segregation of ipsilateral retinal ganglion cell axons at the optic chiasm requires the Shh receptor Boc. The Journal of neuroscience : the official journal of the Society for Neuroscience *30*, 266-275.

Farmer, W.T., Abrahamsson, T., Chierzi, S., Lui, C., Zaelzer, C., Jones, E.V., Bally, B.P., Chen, G.G., Théroux, J.F., Peng, J., *et al.* (2016). Neurons diversify astrocytes in the adult brain through sonic hedgehog signaling. Science (New York, NY) *351*, 849-854.

Farndon, P.A., Del Mastro, R.G., Kilpatrick, M., and Evans, D.J.T.L. (1992). Location of gene for Gorlin syndrome. *339*, 581-582.

Fathaddin, A.A., Bakhash, E.A., Sabbagh, A.J., and Al-Dandan, S.W. (2014). Large cell/anaplastic medulloblastoma with myogenic, melanotic and neuronal differentiation: a case report of a rare tumor. Indian journal of pathology & microbiology *57*, 294-297.

Fattet, S., Haberler, C., Legoix, P., Varlet, P., Lellouch-Tubiana, A., Lair, S., Manie, E., Raquin, M.A., Bours, D., Carpentier, S., *et al.* (2009). Beta-catenin status in paediatric medulloblastomas: correlation of immunohistochemical expression with mutational status, genetic profiles, and clinical characteristics. The Journal of pathology *218*, 86-94.

Feil, S., Valtcheva, N., and Feil, R. (2009). Inducible cre mice. In Gene knockout protocols (Springer), pp. 343-363.

Feng, X., Juan, A.H., Wang, H.A., Ko, K.D., Zare, H., and Sartorelli, V. (2016). Polycomb Ezh2 controls the fate of GABAergic neurons in the embryonic cerebellum. Development (Cambridge, England) *143*, 1971-1980.

Fernandez-Capetillo, O., Lee, A., Nussenzweig, M., and Nussenzweig, A. (2004). H2AX: the histone guardian of the genome. DNA repair *3*, 959-967.

Fernandez, C., Tatard, V.M., Bertrand, N., and Dahmane, N. (2010). Differential modulation of Sonic-hedgehog-induced cerebellar granule cell precursor proliferation by the IGF signaling network. Developmental neuroscience *32*, 59-70.

Fink, A.J., Englund, C., Daza, R.A., Pham, D., Lau, C., Nivison, M., Kowalczyk, T., and Hevner, R.F. (2006). Development of the deep cerebellar nuclei: transcription factors and cell migration from the rhombic lip. The Journal of neuroscience : the official journal of the Society for Neuroscience *26*, 3066-3076.

Fong, A.P., Yao, Z., Zhong, J.W., Cao, Y., Ruzzo, W.L., Gentleman, R.C., and Tapscott, S.J. (2012). Genetic and epigenetic determinants of neurogenesis and myogenesis. Developmental cell *22*, 721-735.

Fong, A.P., Yao, Z., Zhong, J.W., Johnson, N.M., Farr, G.H., 3rd, Maves, L., and Tapscott, S.J. (2015). Conversion of MyoD to a neurogenic factor: binding site specificity determines lineage. Cell reports *10*, 1937-1946.

Forcales, S.V., Albini, S., Giordani, L., Malecova, B., Cignolo, L., Chernov, A., Coutinho, P., Saccone, V., Consalvi, S., Williams, R., *et al.* (2012). Signal-dependent incorporation of MyoD-BAF60c into Brg1-based SWI/SNF chromatin-remodelling complex. The EMBO journal *31*, 301-316.

Forget, A., Martignetti, L., Puget, S., Calzone, L., Brabetz, S., Picard, D., Montagud, A., Liva, S., Sta, A., Dingli, F., *et al.* (2018). Aberrant ERBB4-SRC Signaling as a Hallmark of Group 4 Medulloblastoma Revealed by Integrative Phosphoproteomic Profiling. Cancer Cell *34*, 379-395.e377.

Fouladi, M., Stewart, C.F., Blaney, S.M., Onar-Thomas, A., Schaiquevich, P., Packer, R.J., Gajjar, A., Kun, L.E., Boyett, J.M., and Gilbertson, R.J.J.J.o.c.o. (2010). Phase I trial of lapatinib in children with refractory CNS malignancies: a Pediatric Brain Tumor Consortium study. *28*, 4221.

Fouladi, M., Stewart, C.F., Blaney, S.M., Onar-Thomas, A., Schaiquevich, P., Packer, R.J., Goldman, S., Geyer, J.R., Gajjar, A., and Kun, L.E.J.J.o.n.-o. (2013). A molecular biology and phase II trial of lapatinib in children with refractory CNS malignancies: a pediatric brain tumor consortium study. *114*, 173-179.

Frank, C.L., Liu, F., Wijayatunge, R., Song, L., Biegler, M.T., Yang, M.G., Vockley, C.M., Safi, A., Gersbach, C.A., Crawford, G.E., *et al.* (2015). Regulation of chromatin accessibility and Zic binding at enhancers in the developing cerebellum. Nature neuroscience *18*, 647-656.

Frappart, P.O., Lee, Y., Lamont, J., and McKinnon, P.J. (2007). BRCA2 is required for neurogenesis and suppression of medulloblastoma. The EMBO journal *26*, 2732-2742.

Frappart, P.O., Lee, Y., Russell, H.R., Chalhoub, N., Wang, Y.D., Orii, K.E., Zhao, J., Kondo, N., Baker, S.J., and McKinnon, P.J. (2009). Recurrent genomic alterations characterize medulloblastoma arising from DNA double-strand break repair deficiency. Proceedings of the National Academy of Sciences of the United States of America *106*, 1880-1885.

Fresno Vara, J.A., Casado, E., de Castro, J., Cejas, P., Belda-Iniesta, C., and González-Barón, M. (2004). PI3K/Akt signalling pathway and cancer. Cancer treatment reviews *30*, 193-204.

Fukushige, T., and Krause, M. (2005). The myogenic potency of HLH-1 reveals wide-spread developmental plasticity in early C. elegans embryos. Development (Cambridge, England) *132*, 1795-1805.

Gai, D., Haan, E., Scholar, M., Nicholl, J., and Yu, S. (2015). Phenotypes of AKT3 deletion: a case report and literature review. American journal of medical genetics Part A *167a*, 174-179.

Gailani, M.R., Bale, S.J., Leffell, D.J., DiGiovanna, J.J., Peck, G.L., Poliak, S., Drum, M.A., Pastakia, B., McBride, O., and Kase, R.J.C. (1992). Developmental defects in Gorlin syndrome related to a putative tumor suppressor gene on chromosome 9. *69*, 111-117.

Galli, R., Borello, U., Gritti, A., Minasi, M.G., Bjornson, C., Coletta, M., Mora, M., De Angelis, M.G., Fiocco, R., Cossu, G., *et al.* (2000). Skeletal myogenic potential of human and mouse neural stem cells. Nature neuroscience *3*, 986-991.

Garrè, M.L., Cama, A., Bagnasco, F., Morana, G., Giangaspero, F., Brisigotti, M., Gambini, C., Forni, M., Rossi, A., and Haupt, R.J.C.C.R. (2009). Medulloblastoma variants: age-dependent occurrence and relation to Gorlin syndrome—a new clinical perspective. *15*, 2463-2471.

Gatei, M., Sloper, K., Sorensen, C., Syljuäsen, R., Falck, J., Hobson, K., Savage, K., Lukas, J., Zhou, B.B., Bartek, J., *et al.* (2003). Ataxia-telangiectasia-mutated (ATM) and NBS1-dependent phosphorylation of Chk1 on Ser-317 in response to ionizing radiation. The Journal of biological chemistry *278*, 14806-14811.

Gautier, L., Cope, L., Bolstad, B.M., and Irizarry, R.A. (2004). affy--analysis of Affymetrix GeneChip data at the probe level. Bioinformatics (Oxford, England) *20*, 307-315.

Gaytán de Ayala Alonso, A., Gutiérrez, L., Fritsch, C., Papp, B., Beuchle, D., and Müller, J. (2007). A genetic screen identifies novel polycomb group genes in Drosophila. Genetics *176*, 2099-2108.

Gerber, A.N., and Tapscott, S.J. (1996). Tumor cell complementation groups based on myogenic potential: evidence for inactivation of loci required for basic helix-loop-helix protein activity. Molecular and cellular biology *16*, 3901-3908.

Giangaspero, F., Perilongo, G., Fondelli, M.P., Brisigotti, M., Carollo, C., Burnelli, R., Burger, P.C., and Garrè, M.L.J.J.o.n. (1999). Medulloblastoma with extensive nodularity: a variant with favorable prognosis. *91*, 971-977.

Giangaspero, F., Rigobello, L., Badiali, M., Loda, M., Andreini, L., Basso, G., Zorzi, F., and Montaldi, A.J.T.A.j.o.s.p. (1992). Large-cell medulloblastomas: a distinct variant with highly aggressive behavior. *16*, 687-693.

Gibson, P., Tong, Y., Robinson, G., Thompson, M.C., Currle, D.S., Eden, C., Kranenburg, T.A., Hogg, T., Poppleton, H., Martin, J., *et al.* (2010). Subtypes of medulloblastoma have distinct developmental origins. Nature *468*, 1095-1099.

Gilbert, S.F. (1991). Epigenetic landscaping: Waddington's use of cell fate bifurcation diagrams. Biology and Philosophy *6*, 135-154.

Gilbertson, R., Jaros, E., Perry, R., and PEARSON, A.J.J.L. (1992). Prognostic factors in medulloblastoma. *340*.

Gilbertson, R.J., and Ellison, D.W. (2008). The origins of medulloblastoma subtypes. Annual review of pathology *3*, 341-365.

Gilbertson, R.J., Perry, R.H., Kelly, P.J., Pearson, A.D., and Lunec, J.J.C.r. (1997). Prognostic significance of HER2 and HER4 coexpression in childhood medulloblastoma. *57*, 3272-3280.

Gilbertson, R.J.J.T.o. (2005). ERBB2 in pediatric cancer: innocent until proven guilty. *10*, 508-517.

Goodrich, L.V., Milenković, L., Higgins, K.M., and Scott, M.P. (1997). Altered neural cell fates and medulloblastoma in mouse patched mutants. Science (New York, NY) *277*, 1109-1113.

Gorlin, R.J. (1987). Nevoid Basal-Cell Carcinoma Syndrome. Medicine *66*.

Grammel, D., Warmuth-Metz, M., von Bueren, A.O., Kool, M., Pietsch, T., Kretzschmar, H.A., Rowitch, D.H., Rutkowski, S., Pfister, S.M., and Schüller, U. (2012). Sonic hedgehog-associated medulloblastoma arising from the cochlear nuclei of the brainstem. Acta neuropathologica *123*, 601-614.

Granese, J., Boué, D.R., Elton, S., and Ellison, D.W. (2008). Idiosyncratic differentiation in medulloblastoma--a report of two exceptional cases. Neuropathology and applied neurobiology *34*, 671-674.

Gröbner, S.N., Worst, B.C., Weischenfeldt, J., Buchhalter, I., Kleinheinz, K., Rudneva, V.A., Johann, P.D., Balasubramanian, G.P., Segura-Wang, M., Brabetz, S., *et al.* (2018). The landscape of genomic alterations across childhood cancers. Nature *555*, 321-327.

Groden, J. (1995). Colon-cancer genes and brain tumors. The New England journal of medicine *332*, 884-885.

Guldal, C.G., Ahmad, A., Korshunov, A., Squatrito, M., Awan, A., Mainwaring, L.A., Bhatia, B., Parathath, S.R., Nahle, Z., Pfister, S., *et al.* (2012). An essential role for p38 MAPK in cerebellar granule neuron precursor proliferation. Acta neuropathologica *123*, 573-586.

Gupta, K., Jogunoori, S., Satapathy, A., Salunke, P., Kumar, N., Radotra, B.D., and Vasishta, R.K. (2018). Medulloblastoma with myogenic and/or melanotic differentiation does not align immunohistochemically with the genetically defined molecular subgroups. Human pathology *75*, 26-33.

Hahn, H., Wicking, C., Zaphiropoulos, P.G., Gailani, M.R., Shanley, S., Chidambaram, A., Vorechovsky, I., Holmberg, E., Unden, A.B., and Gillies, S.J.C. (1996). Mutations of the human homolog of Drosophila patched in the nevoid basal cell carcinoma syndrome. *85*, 841-851.

Hahn, H., Wojnowski, L., Specht, K., Kappler, R., Calzada-Wack, J., Potter, D., Zimmer, A., Müller, U., Samson, E., Quintanilla-Martinez, L., *et al.* (2000). Patched target Igf2 is indispensable for the formation of medulloblastoma and rhabdomyosarcoma. The Journal of biological chemistry *275*, 28341-28344.

Hahn, H., Wojnowski, L., Zimmer, A.M., Hall, J., Miller, G., and Zimmer, A. (1998). Rhabdomyosarcomas and radiation hypersensitivity in a mouse model of Gorlin syndrome. Nature medicine *4*, 619-622.

Halazonetis, T.D., Gorgoulis, V.G., and Bartek, J. (2008). An oncogene-induced DNA damage model for cancer development. Science (New York, NY) *319*, 1352-1355.

Haldipur, P., and Millen, K.J. (2019). What cerebellar malformations tell us about cerebellar development. Neuroscience letters *688*, 14-25.

Hallahan, A.R., Pritchard, J.I., Hansen, S., Benson, M., Stoeck, J., Hatton, B.A., Russell, T.L., Ellenbogen, R.G., Bernstein, I.D., Beachy, P.A., *et al.* (2004). The SmoA1 mouse model reveals that notch signaling is critical for the growth and survival of sonic hedgehog-induced medulloblastomas. Cancer research *64*, 7794-7800.

Hamilton, S.R., Liu, B., Parsons, R.E., Papadopoulos, N., Jen, J., Powell, S.M., Krush, A.J., Berk, T., Cohen, Z., Tetu, B., *et al.* (1995). The molecular basis of Turcot's syndrome. The New England journal of medicine *332*, 839-847.

Hanahan, D., and Weinberg, R.A. (2000). The hallmarks of cancer. Cell *100*, 57-70.

Hanahan, D., and Weinberg, R.A. (2011). Hallmarks of cancer: the next generation. Cell *144*, 646-674.

Hartmann, W., Koch, A., Brune, H., Waha, A., Schüller, U., Dani, I., Denkhaus, D., Langmann, W., Bode, U., Wiestler, O.D., *et al.* (2005). Insulin-like growth factor II is involved in the proliferation control of medulloblastoma and its cerebellar precursor cells. The American journal of pathology *166*, 1153-1162.

Harutyunyan, A.S., Krug, B., Chen, H., Papillon-Cavanagh, S., Zeinieh, M., De Jay, N., Deshmukh, S., Chen, C.C.L., Belle, J., Mikael, L.G., *et al.* (2019). H3K27M induces defective chromatin spread of PRC2-mediated repressive H3K27me2/me3 and is essential for glioma tumorigenesis. Nature communications *10*, 1262.

Hatley, M.E., Tang, W., Garcia, M.R., Finkelstein, D., Millay, D.P., Liu, N., Graff, J., Galindo, R.L., and Olson, E.N. (2012). A mouse model of rhabdomyosarcoma originating from the adipocyte lineage. Cancer Cell *22*, 536-546.

Helton, K.J., Fouladi, M., Boop, F.A., Perry, A., Dalton, J., Kun, L., and Fuller, C. (2004). Medullomyoblastoma: a radiographic and clinicopathologic analysis of six cases and review of the literature. Cancer *101*, 1445-1454.

Herzog, K.H., Chong, M.J., Kapsetaki, M., Morgan, J.I., and McKinnon, P.J. (1998). Requirement for Atm in ionizing radiation-induced cell death in the developing central nervous system. Science (New York, NY) *280*, 1089-1091.

Hirao, A., Cheung, A., Duncan, G., Girard, P.M., Elia, A.J., Wakeham, A., Okada, H., Sarkissian, T., Wong, J.A., Sakai, T., *et al.* (2002). Chk2 is a tumor suppressor that regulates apoptosis in both an ataxia telangiectasia mutated (ATM)-dependent and an ATM-independent manner. Molecular and cellular biology *22*, 6521-6532.

Ho, D.M., Shih, C.C., Liang, M.L., Tsai, C.Y., Hsieh, T.H., Tsai, C.H., Lin, S.C., Chang, T.Y., Chao, M.E., Wang, H.W., *et al.* (2015). Integrated genomics has identified a new AT/RT-like yet INI1-positive brain tumor subtype among primary pediatric embryonal tumors. BMC medical genomics *8*, 32.

Holcomb, V.B., Vogel, H., Marple, T., Kornegay, R.W., and Hasty, P. (2006). Ku80 and p53 suppress medulloblastoma that arise independent of Rag-1-induced DSBs. Oncogene *25*, 7159-7165.

Hoshino, M., Nakamura, S., Mori, K., Kawauchi, T., Terao, M., Nishimura, Y.V., Fukuda, A., Fuse, T., Matsuo, N., Sone, M., *et al.* (2005). Ptf1a, a bHLH transcriptional gene, defines GABAergic neuronal fates in cerebellum. Neuron *47*, 201-213.

Hovestadt, V., Ayrault, O., Swartling, F.J., Robinson, G.W., Pfister, S.M., and Northcott, P.A.J.N.R.C. (2019a). Medulloblastomics revisited: biological and clinical insights from thousands of patients. 1-15.

Hovestadt, V., Smith, K.S., Bihannic, L., Filbin, M.G., Shaw, M.L., Baumgartner, A., DeWitt, J.C., Groves, A., Mayr, L., Weisman, H.R., *et al.* (2019b). Resolving medulloblastoma cellular architecture by single-cell genomics. Nature *572*, 74-79.

Howlader, N., Noone, A.M., Krapcho, M., Miller, D., Brest, A., Yu, M., Ruhl, J., Tatalovich, Z., Mariotto, A., Lewis, D.R., *et al.* (2019). SEER Cancer Statistics Review, 1975-2017, National Cancer Institute. Bethesda, MD, (https://seer.cancer.gov/csr/1975_2017/), pp. based on November 2019 SEER data submission.

Huang, M., Tailor, J., Zhen, Q., Gillmor, A.H., Miller, M.L., Weishaupt, H., Chen, J., Zheng, T., Nash, E.K., McHenry, L.K., *et al.* (2019). Engineering Genetic Predisposition in Human Neuroepithelial Stem Cells Recapitulates Medulloblastoma Tumorigenesis. Cell stem cell *25*, 433-446.e437.

Huang, W.C., and Chen, C.C. (2005). Akt phosphorylation of p300 at Ser-1834 is essential for its histone acetyltransferase and transcriptional activity. Molecular and cellular biology *25*, 6592-6602.

Huang, X., Liu, J., Ketova, T., Fleming, J.T., Grover, V.K., Cooper, M.K., Litingtung, Y., and Chiang, C. (2010). Transventricular delivery of Sonic hedgehog is essential to cerebellar ventricular zone development. Proceedings of the National Academy of Sciences of the United States of America *107*, 8422-8427.

Huether, R., Dong, L., Chen, X., Wu, G., Parker, M., Wei, L., Ma, J., Edmonson, M.N., Hedlund, E.K., Rusch, M.C., *et al.* (2014). The landscape of somatic mutations in epigenetic regulators across 1,000 paediatric cancer genomes. Nature communications *5*, 3630.

Hutson, T.H., Buchser, W.J., Bixby, J.L., Lemmon, V.P., and Moon, L.D. (2011). Optimization of a 96-Well Electroporation Assay for Postnatal Rat CNS Neurons Suitable for Cost-Effective Medium-Throughput Screening of Genes that Promote Neurite Outgrowth. Frontiers in molecular neuroscience *4*, 55.

Iniguez, A.B., Alexe, G., Wang, E.J., Roti, G., Patel, S., Chen, L., Kitara, S., Conway, A., Robichaud, A.L., Stolte, B., *et al.* (2018). Resistance to Epigenetic-Targeted Therapy Engenders Tumor Cell Vulnerabilities Associated with Enhancer Remodeling. Cancer Cell *34*, 922-938.e927.

Ismail, A., Lamont, J.M., Tweddle, D.A., Pearson, A.D., Clifford, S.C., and Ellison, D.W.J.B.P. (2005). A 7-year-old boy with midline cerebellar mass. *15*, 261-261.

Izzi, L., Lévesque, M., Morin, S., Laniel, D., Wilkes, B.C., Mille, F., Krauss, R.S., McMahon, A.P., Allen, B.L., and Charron, F. (2011). Boc and Gas1 each form distinct Shh receptor complexes with Ptch1 and are required for Shh-mediated cell proliferation. Developmental cell *20*, 788-801.

Jaiswal, A.K., Jaiswal, S., Mahapatra, A.K., and Sharma, M.C.J.J.o.c.n. (2005). Unusually long survival in a case of medullomyoblastoma. *12*, 961-963.

Jenkins, N.C., Rao, G., Eberhart, C.G., Pedone, C.A., Dubuc, A.M., and Fults, D.W. (2016). Somatic cell transfer of c-Myc and Bcl-2 induces large-cell anaplastic medulloblastomas in mice. Journal of neuro-oncology *126*, 415-424.

Johnson, R.L., Rothman, A.L., Xie, J., Goodrich, L.V., Bare, J.W., Bonifas, J.M., Quinn, A.G., Myers, R.M., Cox, D.R., and Epstein, E.H.J.S. (1996). Human homolog of patched, a candidate gene for the basal cell nevus syndrome. *272*, 1668-1671.

Jones, D.T., Jäger, N., Kool, M., Zichner, T., Hutter, B., Sultan, M., Cho, Y.J., Pugh, T.J., Hovestadt, V., Stütz, A.M., *et al.* (2012). Dissecting the genomic complexity underlying medulloblastoma. Nature *488*, 100-105.

Juan, A.H., Derfoul, A., Feng, X., Ryall, J.G., Dell'Orso, S., Pasut, A., Zare, H., Simone, J.M., Rudnicki, M.A., Sartorelli, V.J.G., *et al.* (2011). Polycomb EZH2 controls self-renewal and safeguards the transcriptional identity of skeletal muscle stem cells. *25*, 789-794.

Kabadi, A.M., Ousterout, D.G., Hilton, I.B., and Gersbach, C.A. (2014). Multiplex CRISPR/Cas9-based genome engineering from a single lentiviral vector. Nucleic acids research *42*, e147.

Kang, J.S., Mulieri, P.J., Hu, Y., Taliana, L., and Krauss, R.S. (2002). BOC, an Ig superfamily member, associates with CDO to positively regulate myogenic differentiation. The EMBO journal *21*, 114-124.

Kawauchi, D., Ogg, R.J., Liu, L., Shih, D.J.H., Finkelstein, D., Murphy, B.L., Rehg, J.E., Korshunov, A., Calabrese, C., Zindy, F., *et al.* (2017). Novel MYC-driven medulloblastoma models from multiple embryonic cerebellar cells. Oncogene *36*, 5231-5242.

Kawauchi, D., Robinson, G., Uziel, T., Gibson, P., Rehg, J., Gao, C., Finkelstein, D., Qu, C., Pounds, S., Ellison, D.W., *et al.* (2012). A mouse model of the most aggressive subgroup of human medulloblastoma. Cancer Cell *21*, 168-180.

Ke, C.-s., Deng, Z.-d., Lei, T., Zeng, L.-c., Wu, S.-m., and Wan, J. (2008). Medullomyoblastoma: report of an adult case and review of literatures. Chinese Journal of contemporary Neurology and Neurosurgery *8*, 567-571.

Kenney, A.M., Cole, M.D., and Rowitch, D.H. (2003). Nmyc upregulation by sonic hedgehog signaling promotes proliferation in developing cerebellar granule neuron precursors. Development (Cambridge, England) *130*, 15-28.

Kenney, A.M., Widlund, H.R., and Rowitch, D.H. (2004). Hedgehog and PI-3 kinase signaling converge on Nmyc1 to promote cell cycle progression in cerebellar neuronal precursors. Development (Cambridge, England) *131*, 217-228.

Khanna, K.K., Keating, K.E., Kozlov, S., Scott, S., Gatei, M., Hobson, K., Taya, Y., Gabrielli, B., Chan, D., Lees-Miller, S.P., *et al.* (1998). ATM associates with and phosphorylates p53: mapping the region of interaction. Nature genetics *20*, 398-400.

Kido, M., Ueno, M., Onodera, M., Matsumoto, K., Imai, T., Haba, R., Tamiya, T., Huang, C.L., and Sakamoto, H. (2009). Medulloblastoma with myogenic differentiation showing double immunopositivity for synaptophysin and myoglobin. Pathology international *59*, 255-260.

Kim, K.H., and Roberts, C.W. (2016). Targeting EZH2 in cancer. Nature medicine *22*, 128-134.

Kim, Y.C., Shim, J.W., Oh, Y.J., Son, H., Lee, Y.S., and Lee, S.H. (2002). Co-transfection with cDNA encoding the Bcl family of anti-apoptotic proteins improves the efficiency of transfection in primary fetal neural stem cells. Journal of neuroscience methods *117*, 153-158.

Kimura, E., Han, J.J., Li, S., Fall, B., Ra, J., Haraguchi, M., Tapscott, S.J., and Chamberlain, J.S. (2008a). Cell-lineage regulated myogenesis for dystrophin replacement: a novel therapeutic approach for treatment of muscular dystrophy. Human molecular genetics *17*, 2507-2517.

Kimura, H., Ng, J.M., and Curran, T. (2008b). Transient inhibition of the Hedgehog pathway in young mice causes permanent defects in bone structure. Cancer Cell *13*, 249-260.

Knoepfler, P.S., Cheng, P.F., and Eisenman, R.N. (2002). N-myc is essential during neurogenesis for the rapid expansion of progenitor cell populations and the inhibition of neuronal differentiation. Genes & development *16*, 2699-2712.

Knutson, S.K., Warholic, N.M., Wigle, T.J., Klaus, C.R., Allain, C.J., Raimondi, A., Porter Scott, M., Chesworth, R., Moyer, M.P., Copeland, R.A., *et al.* (2013). Durable tumor regression in genetically altered malignant rhabdoid tumors by inhibition of methyltransferase EZH2. Proceedings of the National Academy of Sciences of the United States of America *110*, 7922-7927.

Kohsaka, S., Shukla, N., Ameur, N., Ito, T., Ng, C.K., Wang, L., Lim, D., Marchetti, A., Viale, A., Pirun, M., *et al.* (2014). A recurrent neomorphic mutation in MYOD1 defines a clinically aggressive subset of embryonal rhabdomyosarcoma associated with PI3K-AKT pathway mutations. Nature genetics *46*, 595-600.

Konieczny, J., and Arranz, L. (2018). Updates on Old and Weary Haematopoiesis. International journal of molecular sciences *19*.

Kool, M., Jones, D.T., Jäger, N., Northcott, P.A., Pugh, T.J., Hovestadt, V., Piro, R.M., Esparza, L.A., Markant, S.L., Remke, M., *et al.* (2014). Genome sequencing of SHH medulloblastoma predicts genotype-related response to smoothened inhibition. Cancer Cell *25*, 393-405.

Koren, S., Reavie, L., Couto, J.P., De Silva, D., Stadler, M.B., Roloff, T., Britschgi, A., Eichlisberger, T., Kohler, H., Aina, O., *et al.* (2015). PIK3CA(H1047R) induces multipotency and multi-lineage mammary tumours. Nature *525*, 114-118.

Korshunov, A., Sahm, F., Stichel, D., Schrimpf, D., Ryzhova, M., Zheludkova, O., Golanov, A., Lichter, P., Jones, D.T., and von Deimling, A.J.A.n. (2018). Molecular characterization of medulloblastomas with extensive nodularity (MBEN). *136*, 303-313.

Krug, B., De Jay, N., Harutyunyan, A.S., Deshmukh, S., Marchione, D.M., Guilhamon, P., Bertrand, K.C., Mikael, L.G., McConechy, M.K., Chen, C.C.L., *et al.* (2019). Pervasive H3K27 Acetylation Leads to ERV Expression and a Therapeutic Vulnerability in H3K27M Gliomas. Cancer Cell *35*, 782-797.e788.

Krüger, K., Geist, K., Stuhldreier, F., Schumacher, L., Blümel, L., Remke, M., Wesselborg, S., Stork, B., Klöcker, N., Bormann, S., *et al.* (2018). Multiple DNA damage-dependent and DNA damage-independent stress responses define the outcome of ATR/Chk1 targeting in medulloblastoma cells. Cancer letters *430*, 34-46.

Kuramoto, T., Kuwamura, M., and Serikawa, T. (2004). Rat neurological mutations cerebellar vermis defect and hobble are caused by mutations in the netrin-1 receptor gene Unc5h3. Brain research Molecular brain research *122*, 103-108.

Kuwamura, M., Shirota, A., Takada, A., Yamate, J., Kotani, T., and Sakuma, S. (2000). Spontaneous and ethyl-nitrosourea-induced medullomyoblastomas in cerebellar vermis defect (CVD) mutant rats. Acta neuropathologica *99*, 285-288.

Lakin, N.D., Hann, B.C., and Jackson, S.P. (1999). The ataxia-telangiectasia related protein ATR mediates DNA-dependent phosphorylation of p53. Oncogene *18*, 3989-3995.

Lang, P.Y., Nanjangud, G.J., Sokolsky-Papkov, M., Shaw, C., Hwang, D., Parker, J.S., Kabanov, A.V., and Gershon, T.R. (2016). ATR maintains chromosomal integrity during postnatal cerebellar neurogenesis and is required for medulloblastoma formation. Development (Cambridge, England) *143*, 4038-4052.

Larson, J.D., Kasper, L.H., Paugh, B.S., Jin, H., Wu, G., Kwon, C.H., Fan, Y., Shaw, T.I., Silveira, A.B., Qu, C., *et al.* (2019). Histone H3.3 K27M Accelerates Spontaneous Brainstem Glioma and Drives Restricted Changes in Bivalent Gene Expression. Cancer Cell *35*, 140-155.e147.

Lassar, A.B. (2017). Finding MyoD and lessons learned along the way. Seminars in cell & developmental biology *72*, 3-9.

Lassar, A.B., Paterson, B.M., and Weintraub, H. (1986). Transfection of a DNA locus that mediates the conversion of 10T1/2 fibroblasts to myoblasts. Cell *47*, 649-656.

Lauth, M., Bergström, A., Shimokawa, T., and Toftgård, R. (2007). Inhibition of GLI-mediated transcription and tumor cell growth by small-molecule antagonists. Proceedings of the National Academy of Sciences of the United States of America *104*, 8455-8460.

Lee, A., Kessler, J.D., Read, T.A., Kaiser, C., Corbeil, D., Huttner, W.B., Johnson, J.E., and Wechsler-Reya, R.J. (2005). Isolation of neural stem cells from the postnatal cerebellum. Nature neuroscience *8*, 723-729.

Lee, E.Y., Ji, H., Ouyang, Z., Zhou, B., Ma, W., Vokes, S.A., McMahon, A.P., Wong, W.H., and Scott, M.P. (2010). Hedgehog pathway-regulated gene networks in cerebellum development and tumorigenesis. Proceedings of the National Academy of Sciences of the United States of America *107*, 9736-9741.

Lee, Y., Chong, M.J., and McKinnon, P.J. (2001). Ataxia telangiectasia mutated-dependent apoptosis after genotoxic stress in the developing nervous system is determined by cellular

differentiation status. The Journal of neuroscience : the official journal of the Society for Neuroscience *21*, 6687-6693.

Lee, Y., Kawagoe, R., Sasai, K., Li, Y., Russell, H.R., Curran, T., and McKinnon, P.J. (2007). Loss of suppressor-of-fused function promotes tumorigenesis. Oncogene *26*, 6442-6447.

Lee, Y., and McKinnon, P.J. (2002). DNA ligase IV suppresses medulloblastoma formation. Cancer research *62*, 6395-6399.

Lee, Y., Miller, H.L., Jensen, P., Hernan, R., Connelly, M., Wetmore, C., Zindy, F., Roussel, M.F., Curran, T., Gilbertson, R.J., *et al.* (2003). A molecular fingerprint for medulloblastoma. Cancer research *63*, 5428-5437.

Lee, Y., Miller, H.L., Russell, H.R., Boyd, K., Curran, T., and McKinnon, P.J. (2006). Patched2 modulates tumorigenesis in patched1 heterozygous mice. Cancer research *66*, 6964-6971.

Leek, J.T., Johnson, W.E., Parker, H.S., Fertig, E.J., Jaffe, A.E., Storey, J.D., Zhang, Y., and Torres, L.C.J.R.p.v. (2017). sva: Surrogate variable analysis. *3*, 882-883.

Leto, K., Arancillo, M., Becker, E.B., Buffo, A., Chiang, C., Ding, B., Dobyns, W.B., Dusart, I., Haldipur, P., Hatten, M.E., *et al.* (2016). Consensus Paper: Cerebellar Development. Cerebellum (London, England) *15*, 789-828.

Leto, K., Carletti, B., Williams, I.M., Magrassi, L., and Rossi, F. (2006). Different types of cerebellar GABAergic interneurons originate from a common pool of multipotent progenitor cells. The Journal of neuroscience : the official journal of the Society for Neuroscience *26*, 11682-11694.

Lewis, A.J. (1973). Medulloblastoma with striated muscle fibers. Case report. Journal of neurosurgery *38*, 642-646.

Li, H., Choi, Y.J., Hanes, M.A., Marple, T., Vogel, H., and Hasty, P. (2009). Deleting Ku70 is milder than deleting Ku80 in p53-mutant mice and cells. Oncogene *28*, 1875-1878.

Li, P., Du, F., Yuelling, L.W., Lin, T., Muradimova, R.E., Tricarico, R., Wang, J., Enikolopov, G., Bellacosa, A., Wechsler-Reya, R.J., *et al.* (2013). A population of Nestin-expressing progenitors in the cerebellum exhibits increased tumorigenicity. Nature neuroscience *16*, 1737-1744.

Li, P., Lee, E.H., Du, F., Gordon, R.E., Yuelling, L.W., Liu, Y., Ng, J.M., Zhang, H., Wu, J., Korshunov, A., *et al.* (2016). Nestin Mediates Hedgehog Pathway Tumorigenesis. Cancer research *76*, 5573-5583.

Lichtig, H., Artamonov, A., Polevoy, H., Reid, C.D., Bielas, S.L., and Frank, D. (2020). Modeling Bainbridge-Ropers Syndrome in Xenopus laevis Embryos. Frontiers in physiology *11*, 75.

Lindberg, E., Persson, A., Øra, I., Mertens, F., Englund, E., and Gisselsson, D. (2007). Concurrent gain of 17q and the MYC oncogene in a medullomyoblastoma. Neuropathology : official journal of the Japanese Society of Neuropathology *27*, 556-560.

Liu, C., Wang, M., Wei, X., Wu, L., Xu, J., Dai, X., Xia, J., Cheng, M., Yuan, Y., Zhang, P., *et al.* (2019). An ATAC-seq atlas of chromatin accessibility in mouse tissues. Scientific data *6*, 65.

Liu, Q., Guntuku, S., Cui, X.S., Matsuoka, S., Cortez, D., Tamai, K., Luo, G., Carattini-Rivera, S., DeMayo, F., Bradley, A., *et al.* (2000). Chk1 is an essential kinase that is regulated by Atr and required for the G(2)/M DNA damage checkpoint. Genes & development *14*, 1448-1459.

Liu, Y., May, N.R., and Fan, C.M. (2001). Growth arrest specific gene 1 is a positive growth regulator for the cerebellum. Developmental biology *236*, 30-45.

Lohse, M., Bolger, A.M., Nagel, A., Fernie, A.R., Lunn, J.E., Stitt, M., and Usadel, B.J.N.a.r. (2012). R obi NA: A user-friendly, integrated software solution for RNA-Seq-based transcriptomics. *40*, W622-W627.

Louis, D.N., Ohgaki, H., Wiestler, O.D., Cavenee, W.K., Burger, P.C., Jouvet, A., Scheithauer, B.W., and Kleihues, P.J.A.n. (2007). The 2007 WHO classification of tumours of the central nervous system. *114*, 97-109.

Louis, D.N., Perry, A., Reifenberger, G., von Deimling, A., Figarella-Branger, D., Cavenee, W.K., Ohgaki, H., Wiestler, O.D., Kleihues, P., and Ellison, D.W. (2016). The 2016 World Health Organization Classification of Tumors of the Central Nervous System: a summary. Acta neuropathologica *131*, 803-820.

Love, M.I., Huber, W., and Anders, S. (2014). Moderated estimation of fold change and dispersion for RNA-seq data with DESeq2. Genome biology *15*, 550.

Machold, R., and Fishell, G. (2005). Math1 is expressed in temporally discrete pools of cerebellar rhombic-lip neural progenitors. Neuron *48*, 17-24.

Madisen, L., Zwingman, T.A., Sunkin, S.M., Oh, S.W., Zariwala, H.A., Gu, H., Ng, L.L., Palmiter, R.D., Hawrylycz, M.J., Jones, A.R., *et al.* (2010). A robust and high-throughput Cre reporting and characterization system for the whole mouse brain. Nature neuroscience *13*, 133-140.

Mahapatra, A.K., Sinha, A.K., and Sharma, M.C. (1998). Medullomyoblastoma. A rare cerebellar tumour in children. Child's nervous system : ChNS : official journal of the International Society for Pediatric Neurosurgery *14*, 312-316.

Majumdar, K., Tyagi, I., Saran, R.K., Sakhuja, P., and Sharma, A. (2013). Medulloblastoma with focal divergent/teratoid differentiation. Brain tumor pathology *30*, 50-56.

Makihara, S., Morin, S., Ferent, J., Côté, J.F., Yam, P.T., and Charron, F. (2018). Polarized Dock Activity Drives Shh-Mediated Axon Guidance. Developmental cell *46*, 410-425.e417.

Marino, S., Vooijs, M., van Der Gulden, H., Jonkers, J., and Berns, A. (2000). Induction of medulloblastomas in p53-null mutant mice by somatic inactivation of Rb in the external granular layer cells of the cerebellum. Genes & development *14*, 994-1004.

Marti, T.M., Hefner, E., Feeney, L., Natale, V., and Cleaver, J.E. (2006). H2AX phosphorylation within the G1 phase after UV irradiation depends on nucleotide excision repair and not DNA double-strand breaks. Proceedings of the National Academy of Sciences of the United States of America *103*, 9891-9896.

Martin, J.F., Miano, J.M., Hustad, C.M., Copeland, N.G., Jenkins, N.A., and Olson, E.N. (1994). A Mef2 gene that generates a muscle-specific isoform via alternative mRNA splicing. Molecular and cellular biology *14*, 1647-1656.

Matei, V., Pauley, S., Kaing, S., Rowitch, D., Beisel, K.W., Morris, K., Feng, F., Jones, K., Lee, J., and Fritzsch, B. (2005). Smaller inner ear sensory epithelia in Neurog 1 null mice are related to earlier hair cell cycle exit. Developmental dynamics : an official publication of the American Association of Anatomists *234*, 633-650.

Matheus, F., Rusha, E., Rehimi, R., Molitor, L., Pertek, A., Modic, M., Feederle, R., Flatley, A., Kremmer, E., Geerlof, A., *et al.* (2019). Pathological ASXL1 Mutations and Protein Variants Impair Neural Crest Development. Stem cell reports *12*, 861-868.

Matsuoka, S., Huang, M., and Elledge, S.J. (1998). Linkage of ATM to cell cycle regulation by the Chk2 protein kinase. Science (New York, NY) *282*, 1893-1897.

Matsuoka, S., Rotman, G., Ogawa, A., Shiloh, Y., Tamai, K., and Elledge, S.J. (2000). Ataxia telangiectasia-mutated phosphorylates Chk2 in vivo and in vitro. Proceedings of the National Academy of Sciences of the United States of America *97*, 10389-10394.

McCarthy, K.D., and de Vellis, J. (1980). Preparation of separate astroglial and oligodendroglial cell cultures from rat cerebral tissue. The Journal of cell biology *85*, 890-902.

Mehta, A., Patkar, N., Nakra, R., and Nema, S. (2006). A 3 1/2-Year-Old Child With a Posterior Fossa Mass. Archives of pathology $ laboratory medicine *130*.

Merk, D.J., Ohli, J., Merk, N.D., Thatikonda, V., Morrissy, S., Schoof, M., Schmid, S.N., Harrison, L., Filser, S., Ahlfeld, J., *et al.* (2018). Opposing Effects of CREBBP Mutations Govern the Phenotype of Rubinstein-Taybi Syndrome and Adult SHH Medulloblastoma. Developmental cell *44*, 709-724.e706.

Metcalfe, C., Alicke, B., Crow, A., Lamoureux, M., Dijkgraaf, G.J., Peale, F., Gould, S.E., and de Sauvage, F.J. (2013). PTEN loss mitigates the response of medulloblastoma to Hedgehog pathway inhibition. Cancer research *73*, 7034-7042.

Micol, J.B., and Abdel-Wahab, O. (2016). The Role of Additional Sex Combs-Like Proteins in Cancer. Cold Spring Harbor perspectives in medicine *6*.

Miles, J., Bhandari, Y.J.J.o.n., neurosurgery,, and psychiatry (1970). Cerebellar medulloblastomata in adults: review of 18 cases. *33*, 208.

Mille, F., Tamayo-Orrego, L., Lévesque, M., Remke, M., Korshunov, A., Cardin, J., Bouchard, N., Izzi, L., Kool, M., Northcott, P.A., *et al.* (2014). The Shh receptor Boc promotes progression of early medulloblastoma to advanced tumors. Developmental cell *31*, 34-47.

Millen, K.J., Steshina, E.Y., Iskusnykh, I.Y., and Chizhikov, V.V. (2014). Transformation of the cerebellum into more ventral brainstem fates causes cerebellar agenesis in the absence of Ptf1a function. Proceedings of the National Academy of Sciences of the United States of America *111*, E1777-1786.

Miyata, T., Maeda, T., and Lee, J.E. (1999). NeuroD is required for differentiation of the granule cells in the cerebellum and hippocampus. Genes & development *13*, 1647-1652.

Miyazawa, K., Himi, T., Garcia, V., Yamagishi, H., Sato, S., and Ishizaki, Y. (2000). A role for p27/Kip1 in the control of cerebellar granule cell precursor proliferation. The Journal of neuroscience : the official journal of the Society for Neuroscience *20*, 5756-5763.

Mohammad, F., Weissmann, S., Leblanc, B., Pandey, D.P., Højfeldt, J.W., Comet, I., Zheng, C., Johansen, J.V., Rapin, N., Porse, B.T., *et al.* (2017). EZH2 is a potential therapeutic target for H3K27M-mutant pediatric gliomas. Nature medicine *23*, 483-492.

Mu, Q., Wang, L., Yu, F., Gao, H., Lei, T., Li, P., Liu, P., Zheng, X., Hu, X., Chen, Y., *et al.* (2015). Imp2 regulates GBM progression by activating IGF2/PI3K/Akt pathway. Cancer biology & therapy *16*, 623-633.

Natsumeda, M., Liu, Y., Nakata, S., Miyahara, H., Hanaford, A., Ahsan, S., Stearns, D., Skuli, N., Kahlert, U.D., Raabe, E.H., *et al.* (2019). Inhibition of enhancer of zest homologue 2 is a potential therapeutic target for high-MYC medulloblastoma. Neuropathology : official journal of the Japanese Society of Neuropathology *39*, 71-77.

NCT01878617 (2013). US National Library of Medicine. *ClinicalTrials.gov*

NCT02724579 (2016). US National Library of Medicine. *ClinicalTrials.gov*.

NCT03213678 (2017). US National Library of Medicine. *ClinicalTrials.gov*.

NCT04023669 (2019). US National Library of Medicine. *ClinicalTrials.gov*.

Neumann, J.E., Swartling, F.J., and Schüller, U. (2017). Medulloblastoma: experimental models and reality. Acta neuropathologica *134*, 679-689.

Niesen, J., Ohli, J., Sedlacik, J., Dührsen, L., Hellwig, M., Spohn, M., Holsten, T., and Schüller, U. (2020). Pik3ca mutations significantly enhance the growth of SHH medulloblastoma and lead to metastatic tumour growth in a novel mouse model. Cancer letters *477*, 10-18.

Niida, H., Katsuno, Y., Banerjee, B., Hande, M.P., and Nakanishi, M. (2007). Specific role of Chk1 phosphorylations in cell survival and checkpoint activation. Molecular and cellular biology *27*, 2572-2581.

Nishizaki, T., Harada, K., Kubota, H., Harada, K., Ozaki, S., Ito, H., and Sasaki, K.J.P.n. (1999). Genetic alterations in pediatric medulloblastomas detected by comparative genomic hybridization. *31*, 27-32.

Northcott, P.A., Buchhalter, I., Morrissy, A.S., Hovestadt, V., Weischenfeldt, J., Ehrenberger, T., Gröbner, S., Segura-Wang, M., Zichner, T., and Rudneva, V.A.J.N. (2017). The whole-genome landscape of medulloblastoma subtypes. *547*, 311-317.

Northcott, P.A., Lee, C., Zichner, T., Stütz, A.M., Erkek, S., Kawauchi, D., Shih, D.J., Hovestadt, V., Zapatka, M., Sturm, D., *et al.* (2014). Enhancer hijacking activates GFI1 family oncogenes in medulloblastoma. Nature *511*, 428-434.

Northcott, P.A., Shih, D.J., Peacock, J., Garzia, L., Morrissy, A.S., Zichner, T., Stütz, A.M., Korshunov, A., Reimand, J., Schumacher, S.E., *et al.* (2012). Subgroup-specific structural variation across 1,000 medulloblastoma genomes. Nature *488*, 49-56.

Nozza, P., Milanaccio, C., Piatelli, G., Rossi, A., Raso, A., Cama, A., Garré, M.L., Pietsch, T.J.P.b., and cancer (2008). Cerebellar medullomyoblastoma with melanotic tubular structures. *50*, 183-185.

Nüsslein-Volhard, C., and Wieschaus, E.J.N. (1980). Mutations affecting segment number and polarity in Drosophila. *287*, 795-801.

Ocasio, J., Babcock, B., Malawsky, D., Weir, S.J., Loo, L., Simon, J.M., Zylka, M.J., Hwang, D., Dismuke, T., Sokolsky, M., *et al.* (2019). scRNA-seq in medulloblastoma shows cellular heterogeneity and lineage expansion support resistance to SHH inhibitor therapy. Nature communications *10*, 5829.

Okada, A., Charron, F., Morin, S., Shin, D.S., Wong, K., Fabre, P.J., Tessier-Lavigne, M., and McConnell, S.K. (2006). Boc is a receptor for sonic hedgehog in the guidance of commissural axons. Nature *444*, 369-373.

Okano-Uchida, T., Himi, T., Komiya, Y., and Ishizaki, Y. (2004). Cerebellar granule cell precursors can differentiate into astroglial cells. Proceedings of the National Academy of Sciences of the United States of America *101*, 1211-1216.

Oliver, T.G., Grasfeder, L.L., Carroll, A.L., Kaiser, C., Gillingham, C.L., Lin, S.M., Wickramasinghe, R., Scott, M.P., and Wechsler-Reya, R.J. (2003). Transcriptional profiling of the Sonic hedgehog response: a critical role for N-myc in proliferation of neuronal precursors. Proceedings of the National Academy of Sciences of the United States of America *100*, 7331-7336.

Oliver, T.G., Read, T.A., Kessler, J.D., Mehmeti, A., Wells, J.F., Huynh, T.T., Lin, S.M., and Wechsler-Reya, R.J. (2005). Loss of patched and disruption of granule cell development in a pre-neoplastic stage of medulloblastoma. Development (Cambridge, England) *132*, 2425-2439.

Pal, S., Gupta, R., Kim, H., Wickramasinghe, P., Baubet, V., Showe, L.C., Dahmane, N., and Davuluri, R.V. (2011). Alternative transcription exceeds alternative splicing in generating the transcriptome diversity of cerebellar development. Genome research *21*, 1260-1272.

Pan, N., Jahan, I., Lee, J.E., and Fritzsch, B. (2009). Defects in the cerebella of conditional Neurod1 null mice correlate with effective Tg(Atoh1-cre) recombination and granule cell requirements for Neurod1 for differentiation. Cell and tissue research *337*, 407-428.

Park, S.Y., Kim, J.H., Kim, K.T., Kim, Y.J., Kim, T.H., Hwang, K., Sung, K.J., and Park, K.H.J.Y.m.j. (2004). A case of medullomyoblastoma of cerebellopontine angle mimicking acoustic neuroma. *45*, 719-722.

Parsons, D.W., Li, M., Zhang, X., Jones, S., Leary, R.J., Lin, J.C., Boca, S.M., Carter, H., Samayoa, J., Bettegowda, C., *et al.* (2011). The genetic landscape of the childhood cancer medulloblastoma. Science (New York, NY) *331*, 435-439.

Patel, K.J. (2007). Fanconi anemia and breast cancer susceptibility. Nature genetics *39*, 142-143.

Patel, P., Annapurneswari, S., and Ghosh, S. (2007). Fourth ventricular medullomyoblastoma A case report with review of literature. Journal of Pediatric Neurosciences *2*, 82.

Patel, T., Tursun, B., Rahe, D.P., and Hobert, O. (2012). Removal of Polycomb repressive complex 2 makes C. elegans germ cells susceptible to direct conversion into specific somatic cell types. Cell reports *2*, 1178-1186.

Patmore, D.M., Jassim, A., Nathan, E., Gilbertson, R.J., Tahan, D., Hoffmann, N., Tong, Y., Smith, K.S., Kanneganti, T.D., Suzuki, H., *et al.* (2020). DDX3X Suppresses the Susceptibility of Hindbrain Lineages to Medulloblastoma. Developmental cell *54*, 455-470.e455.

Pei, Y., Liu, K.W., Wang, J., Garancher, A., Tao, R., Esparza, L.A., Maier, D.L., Udaka, Y.T., Murad, N., Morrissy, S., *et al.* (2016). HDAC and PI3K Antagonists Cooperate to Inhibit Growth of MYC-Driven Medulloblastoma. Cancer Cell *29*, 311-323.

Pei, Y., Moore, C.E., Wang, J., Tewari, A.K., Eroshkin, A., Cho, Y.J., Witt, H., Korshunov, A., Read, T.A., Sun, J.L., *et al.* (2012). An animal model of MYC-driven medulloblastoma. Cancer Cell *21*, 155-167.

Peng, J., Fabre, P.J., Dolique, T., Swikert, S.M., Kermasson, L., Shimogori, T., and Charron, F. (2018). Sonic Hedgehog Is a Remotely Produced Cue that Controls Axon Guidance Trans-axonally at a Midline Choice Point. Neuron *97*, 326-340.e324.

Pietsch, T., Waha, A., Koch, A., Kraus, J., Albrecht, S., Tonn, J., Sörensen, N., Berthold, F., Henk, B., and Schmandt, N.J.C.r. (1997). Medulloblastomas of the desmoplastic variant carry mutations of the human homologue of Drosophila patched. *57*, 2085-2088.

Polakis, P. (2000). Wnt signaling and cancer. Genes & development *14*, 1837-1851.

Polydorides, A.D., Perry, A., and Edgar, M.A. (2008). Large cell medulloblastoma with myogenic and melanotic differentiation: a case report with molecular analysis. Journal of neuro-oncology *88*, 193-197.

Pomeroy, S.L., Tamayo, P., Gaasenbeek, M., Sturla, L.M., Angelo, M., McLaughlin, M.E., Kim, J.Y., Goumnerova, L.C., Black, P.M., and Lau, C.J.N. (2002). Prediction of central nervous system embryonal tumour outcome based on gene expression. *415*, 436-442.

Pöschl, J., Stark, S., Neumann, P., Gröbner, S., Kawauchi, D., Jones, D.T., Northcott, P.A., Lichter, P., Pfister, S.M., Kool, M., *et al.* (2014). Genomic and transcriptomic analyses match medulloblastoma mouse models to their human counterparts. Acta neuropathologica *128*, 123-136.

Prince, E.W., Balakrishnan, I., Shah, M., Mulcahy Levy, J.M., Griesinger, A.M., Alimova, I., Harris, P.S., Birks, D.K., Donson, A.M., Davidson, N., *et al.* (2016). Checkpoint kinase 1 expression is an adverse prognostic marker and therapeutic target in MYC-driven medulloblastoma. Oncotarget *7*, 53881-53894.

Pugh, T.J., Weeraratne, S.D., Archer, T.C., Pomeranz Krummel, D.A., Auclair, D., Bochicchio, J., Carneiro, M.O., Carter, S.L., Cibulskis, K., Erlich, R.L., *et al.* (2012). Medulloblastoma exome sequencing uncovers subtype-specific somatic mutations. Nature *488*, 106-110.

Rajeshwari, M., Kakkar, A., Nalwa, A., Suri, V., Sarkar, C., Satyarthee, G.D., Garg, A., and Sharma, M.C. (2016). WNT-activated medulloblastoma with melanotic and myogenic differentiation: Report of a rare case. Neuropathology : official journal of the Japanese Society of Neuropathology *36*, 372-375.

Raleigh, D.R., Choksi, P.K., Krup, A.L., Mayer, W., Santos, N., and Reiter, J.F. (2018). Hedgehog signaling drives medulloblastoma growth via CDK6. The Journal of clinical investigation *128*, 120-124.

Rao, G., Pedone, C.A., Del Valle, L., Reiss, K., Holland, E.C., and Fults, D.W. (2004). Sonic hedgehog and insulin-like growth factor signaling synergize to induce medulloblastoma formation from nestin-expressing neural progenitors in mice. Oncogene *23*, 6156-6162.

Rao, R.C., and Dou, Y. (2015). Hijacked in cancer: the KMT2 (MLL) family of methyltransferases. Nature reviews Cancer *15*, 334-346.

Rao, S., Uppar, A.M., and Santosh, V. (2020). Sonic Hedgehog-Activated Large Cell/Anaplastic Medulloblastoma with Myogenic Differentiation. World neurosurgery *135*, 16-18.

Rattenberry, W., McDonough, C.H., Burger, P.C., and Cohen, K.J. (2011). Medulloblastoma with myogenic differentiation: long-term survival in a patient treated with aggressive combination therapy and autologous stem cell transplantation. Journal of neuro-oncology *105*, 659-662.

Rausch, T., Jones, D.T., Zapatka, M., Stütz, A.M., Zichner, T., Weischenfeldt, J., Jäger, N., Remke, M., Shih, D., Northcott, P.A., *et al.* (2012). Genome sequencing of pediatric medulloblastoma links catastrophic DNA rearrangements with TP53 mutations. Cell *148*, 59-71.

Reardon, D.A., Michalkiewicz, E., Boyett, J.M., Sublett, J.E., Entrekin, R.E., Ragsdale, S.T., Valentine, M.B., Behm, F.G., Li, H., and Heideman, R.L.J.C.r. (1997). Extensive genomic abnormalities in childhood medulloblastoma by comparative genomic hybridization. *57*, 4042-4047.

Ritchie, M.E., Phipson, B., Wu, D., Hu, Y., Law, C.W., Shi, W., and Smyth, G.K. (2015). limma powers differential expression analyses for RNA-sequencing and microarray studies. Nucleic acids research *43*, e47.

Robinson, G., Parker, M., Kranenburg, T.A., Lu, C., Chen, X., Ding, L., Phoenix, T.N., Hedlund, E., Wei, L., Zhu, X., *et al.* (2012). Novel mutations target distinct subgroups of medulloblastoma. Nature *488*, 43-48.

Robinson, G.W., Kaste, S.C., Chemaitilly, W., Bowers, D.C., Laughton, S., Smith, A., Gottardo, N.G., Partap, S., Bendel, A., Wright, K.D., *et al.* (2017). Irreversible growth plate fusions in children with medulloblastoma treated with a targeted hedgehog pathway inhibitor. Oncotarget *8*, 69295-69302.

Robinson, G.W., Orr, B.A., Wu, G., Gururangan, S., Lin, T., Qaddoumi, I., Packer, R.J., Goldman, S., Prados, M.D., Desjardins, A., *et al.* (2015). Vismodegib Exerts Targeted Efficacy Against Recurrent Sonic Hedgehog-Subgroup Medulloblastoma: Results From Phase II Pediatric Brain Tumor Consortium Studies PBTC-025B and PBTC-032. Journal of clinical oncology : official journal of the American Society of Clinical Oncology *33*, 2646-2654.

Rodriguez, A., and Flemington, E.K. (1999). Transfection-mediated cell-cycle signaling: considerations for transient transfection-based cell-cycle studies. Analytical biochemistry *272*, 171-181.

Rogakou, E.P., Boon, C., Redon, C., and Bonner, W.M. (1999). Megabase chromatin domains involved in DNA double-strand breaks in vivo. The Journal of cell biology *146*, 905-916.

Rogakou, E.P., Pilch, D.R., Orr, A.H., Ivanova, V.S., and Bonner, W.M. (1998). DNA double-stranded breaks induce histone H2AX phosphorylation on serine 139. The Journal of biological chemistry *273*, 5858-5868.

Romer, J.T., Kimura, H., Magdaleno, S., Sasai, K., Fuller, C., Baines, H., Connelly, M., Stewart, C.F., Gould, S., Rubin, L.L., *et al.* (2004). Suppression of the Shh pathway using a small molecule inhibitor eliminates medulloblastoma in Ptc1(+/-)p53(-/-) mice. Cancer Cell *6*, 229-240.

Roussel, M.F., and Stripay, J.L. (2020). Modeling pediatric medulloblastoma. Brain pathology (Zurich, Switzerland) *30*, 703-712.

Rudin, C.M., Hann, C.L., Laterra, J., Yauch, R.L., Callahan, C.A., Fu, L., Holcomb, T., Stinson, J., Gould, S.E., Coleman, B., *et al.* (2009). Treatment of medulloblastoma with hedgehog pathway inhibitor GDC-0449. The New England journal of medicine *361*, 1173-1178.

Rutkowski, S., Von Hoff, K., Emser, A., Zwiener, I., Pietsch, T., Figarella-Branger, D., Giangaspero, F., Ellison, D.W., Garre, M.-L., and Biassoni, V.J.J.o.c.o. (2010). Survival and prognostic factors of early childhood medulloblastoma: an international meta-analysis. *28*, 4961-4968.

Sachdeva, M.U., Vankalakunti, M., Rangan, A., Radotra, B.D., Chhabra, R., and Vasishta, R.K. (2008). The role of immunohistochemistry in medullomyoblastoma--a case series highlighting divergent differentiation. Diagnostic pathology *3*, 18.

Sakata, H., Kanamori, M., Watanabe, M., Kumabe, T., and Tominaga, T. (2008). Medulloblastoma demonstrating multipotent differentiation: case report. Brain tumor pathology *25*, 39-43.

Sarkar, P., Halder, A., Arun, I., Chatterjee, U., and Chatterjee, S. (2017). Medullomyoblastoma: A report of two cases. Neurology India *65*, 647-650.

Sartorelli, V., and Puri, P.L. (2018). Shaping Gene Expression by Landscaping Chromatin Architecture: Lessons from a Master. Molecular cell *71*, 375-388.

Schepers, A.G., Snippert, H.J., Stange, D.E., van den Born, M., van Es, J.H., van de Wetering, M., and Clevers, H. (2012). Lineage tracing reveals Lgr5+ stem cell activity in mouse intestinal adenomas. Science (New York, NY) *337*, 730-735.

Scheuermann, J.C., de Ayala Alonso, A.G., Oktaba, K., Ly-Hartig, N., McGinty, R.K., Fraterman, S., Wilm, M., Muir, T.W., and Müller, J. (2010). Histone H2A deubiquitinase activity of the Polycomb repressive complex PR-DUB. Nature *465*, 243-247.

Schofield, D., West, D.C., Anthony, D.C., Marshal, R., and Sklar, J.J.T.A.j.o.p. (1995). Correlation of loss of heterozygosity at chromosome 9q with histological subtype in medulloblastomas. *146*, 472.

Schüller, U., Heine, V.M., Mao, J., Kho, A.T., Dillon, A.K., Han, Y.-G., Huillard, E., Sun, T., Ligon, A.H., and Qian, Y.J.C.c. (2008). Acquisition of granule neuron precursor identity is a

critical determinant of progenitor cell competence to form Shh-induced medulloblastoma. *14*, 123-134.

Schwalbe, E.C., Lindsey, J.C., Nakjang, S., Crosier, S., Smith, A.J., Hicks, D., Rafiee, G., Hill, R.M., Iliasova, A., and Stone, T.J.T.L.O. (2017). Novel molecular subgroups for clinical classification and outcome prediction in childhood medulloblastoma: a cohort study. *18*, 958-971.

Sebastian, S., Faralli, H., Yao, Z., Rakopoulos, P., Palii, C., Cao, Y., Singh, K., Liu, Q.C., Chu, A., Aziz, A., *et al.* (2013). Tissue-specific splicing of a ubiquitously expressed transcription factor is essential for muscle differentiation. Genes & development *27*, 1247-1259.

Selvadurai, H.J., Luis, E., Desai, K., Lan, X., Vladoiu, M.C., Whitley, O., Galvin, C., Vanner, R.J., Lee, L., Whetstone, H., *et al.* (2020). Medulloblastoma Arises from the Persistence of a Rare and Transient Sox2(+) Granule Neuron Precursor. Cell reports *31*, 107511.

Serra, C., Palacios, D., Mozzetta, C., Forcales, S.V., Morantte, I., Ripani, M., Jones, D.R., Du, K., Jhala, U.S., Simone, C., *et al.* (2007). Functional interdependence at the chromatin level between the MKK6/p38 and IGF1/PI3K/AKT pathways during muscle differentiation. Molecular cell *28*, 200-213.

Sharma, T., Schwalbe, E.C., Williamson, D., Sill, M., Hovestadt, V., Mynarek, M., Rutkowski, S., Robinson, G.W., Gajjar, A., and Cavalli, F.J.A.n. (2019). Second-generation molecular subgrouping of medulloblastoma: an international meta-analysis of Group 3 and Group 4 subtypes. *138*, 309-326.

Shi, X., Wang, Q., Gu, J., Xuan, Z., and Wu, J.I. (2016). SMARCA4/Brg1 coordinates genetic and epigenetic networks underlying Shh-type medulloblastoma development. Oncogene *35*, 5746-5758.

Silbereis, J., Heintz, T., Taylor, M.M., Ganat, Y., Ment, L.R., Bordey, A., and Vaccarino, F. (2010). Astroglial cells in the external granular layer are precursors of cerebellar granule neurons in neonates. Molecular and cellular neurosciences *44*, 362-373.

Singh, K., Cassano, M., Planet, E., Sebastian, S., Jang, S.M., Sohi, G., Faralli, H., Choi, J., Youn, H.D., Dilworth, F.J., *et al.* (2015). A KAP1 phosphorylation switch controls MyoD function during skeletal muscle differentiation. Genes & development *29*, 513-525.

Singh, S.K., Hawkins, C., Clarke, I.D., Squire, J.A., Bayani, J., Hide, T., Henkelman, R.M., Cusimano, M.D., and Dirks, P.B. (2004). Identification of human brain tumour initiating cells. Nature *432*, 396-401.

Smith, J., Tho, L.M., Xu, N., and Gillespie, D.A. (2010). The ATM-Chk2 and ATR-Chk1 pathways in DNA damage signaling and cancer. Advances in cancer research *108*, 73-112.

Smolle, E., Al-Qubati, S., Stefanits, H., Haberler, C., Kleinert, R., and Haybaeck, J. (2012). Medullomyoblastoma: a case report and literature review of a rare tumor entity. Anticancer research *32*, 4939-4944.

Sola, I. (2019). The role of Ezh2 in Group 3 medulloblastoma. In Cell Biology, Stem Cells, and Developmental Biology Program (University of Colorado).

Song, J.Y., Holtz, A.M., Pinskey, J.M., and Allen, B.L. (2015). Distinct structural requirements for CDON and BOC in the promotion of Hedgehog signaling. Developmental biology *402*, 239-252.

Srivastava, A., Ritesh, K.C., Tsan, Y.C., Liao, R., Su, F., Cao, X., Hannibal, M.C., Keegan, C.E., Chinnaiyan, A.M., Martin, D.M., *et al.* (2016). De novo dominant ASXL3 mutations alter H2A deubiquitination and transcription in Bainbridge-Ropers syndrome. Human molecular genetics *25*, 597-608.

Stefanits, H., Ebetsberger-Dachs, G., Weis, S., and Haberler, C. (2014). Medulloblastoma with multi-lineage differentiation including myogenic and melanotic elements: a case report with molecular data. Clinical neuropathology *33*, 122-127.

Sulli, G., Di Micco, R., and d'Adda di Fagagna, F. (2012). Crosstalk between chromatin state and DNA damage response in cellular senescence and cancer. Nature reviews Cancer *12*, 709-720.

Swartling, F.J., Savov, V., Persson, A.I., Chen, J., Hackett, C.S., Northcott, P.A., Grimmer, M.R., Lau, J., Chesler, L., Perry, A., *et al.* (2012). Distinct neural stem cell populations give rise to disparate brain tumors in response to N-MYC. Cancer Cell *21*, 601-613.

Tamayo-Orrego, L., Gallo, D., Racicot, F., Bemmo, A., Mohan, S., Ho, B., Salameh, S., Hoang, T., Jackson, A.P., Brown, G.W., *et al.* (2020). Sonic hedgehog accelerates DNA replication to cause replication stress promoting cancer initiation in medulloblastoma. Nature Cancer, 1-15.

Tamayo-Orrego, L., Swikert, S.M., and Charron, F. (2016a). Evasion of cell senescence in SHH medulloblastoma. Cell cycle (Georgetown, Tex) *15*, 2102-2107.

Tamayo-Orrego, L., Wu, C.L., Bouchard, N., Khedher, A., Swikert, S.M., Remke, M., Skowron, P., Taylor, M.D., and Charron, F. (2016b). Evasion of Cell Senescence Leads to Medulloblastoma Progression. Cell reports *14*, 2925-2937.

Tamir, Y., and Bengal, E. (2000). Phosphoinositide 3-kinase induces the transcriptional activity of MEF2 proteins during muscle differentiation. The Journal of biological chemistry *275*, 34424-34432.

Tanori, M., Mancuso, M., Pasquali, E., Leonardi, S., Rebessi, S., Di Majo, V., Guilly, M.N., Giangaspero, F., Covelli, V., Pazzaglia, S., *et al.* (2008). PARP-1 cooperates with Ptc1 to suppress medulloblastoma and basal cell carcinoma. Carcinogenesis *29*, 1911-1919.

Tanori, M., Santone, M., Mancuso, M., Pasquali, E., Leonardi, S., Di Majo, V., Rebessi, S., Saran, A., and Pazzaglia, S. (2010). Developmental and oncogenic effects of insulin-like growth factor-I in Ptc1+/- mouse cerebellum. Molecular cancer *9*, 53.

Tao, R., Murad, N., Xu, Z., Zhang, P., Okonechnikov, K., Kool, M., Rivero-Hinojosa, S., Lazarski, C., Zheng, P., Liu, Y., *et al.* (2019). MYC Drives Group 3 Medulloblastoma through Transformation of Sox2(+) Astrocyte Progenitor Cells. Cancer research *79*, 1967-1980.

Tapscott, S.J. (2005). The circuitry of a master switch: Myod and the regulation of skeletal muscle gene transcription. Development (Cambridge, England) *132*, 2685-2695.

Taylor, M.D., Liu, L., Raffel, C., Hui, C.C., Mainprize, T.G., Zhang, X., Agatep, R., Chiappa, S., Gao, L., Lowrance, A., *et al.* (2002). Mutations in SUFU predispose to medulloblastoma. Nature genetics *31*, 306-310.

Taylor, M.D., Mainprize, T.G., and Rutka, J.T. (2000). Molecular insight into medulloblastoma and central nervous system primitive neuroectodermal tumor biology from hereditary syndromes: a review. Neurosurgery *47*, 888-901.

Taylor, M.D., Mainprize, T.G., Rutka, J.T., Becker, L., Bayani, J., and Drake, J.M. (2001). Medulloblastoma in a child with Rubenstein-Taybi Syndrome: case report and review of the literature. Pediatric neurosurgery *35*, 235-238.

Taylor, S.M., and Jones, P.A. (1979). Multiple new phenotypes induced in 10T1/2 and 3T3 cells treated with 5-azacytidine. Cell *17*, 771-779.

Tenzen, T., Allen, B.L., Cole, F., Kang, J.S., Krauss, R.S., and McMahon, A.P. (2006). The cell surface membrane proteins Cdo and Boc are components and targets of the Hedgehog signaling pathway and feedback network in mice. Developmental cell *10*, 647-656.

Tibbetts, R.S., Brumbaugh, K.M., Williams, J.M., Sarkaria, J.N., Cliby, W.A., Shieh, S.Y., Taya, Y., Prives, C., and Abraham, R.T. (1999). A role for ATR in the DNA damage-induced phosphorylation of p53. Genes & development *13*, 152-157.

Tiberi, L., Bonnefont, J., van den Ameele, J., Le Bon, S.D., Herpoel, A., Bilheu, A., Baron, B.W., and Vanderhaeghen, P. (2014). A BCL6/BCOR/SIRT1 complex triggers neurogenesis and suppresses medulloblastoma by repressing Sonic Hedgehog signaling. Cancer Cell *26*, 797-812.

Tomasetti, C., and Vogelstein, B. (2015). Cancer etiology. Variation in cancer risk among tissues can be explained by the number of stem cell divisions. Science (New York, NY) *347*, 78-81.

Tominaga, K., Morisaki, H., Kaneko, Y., Fujimoto, A., Tanaka, T., Ohtsubo, M., Hirai, M., Okayama, H., Ikeda, K., and Nakanishi, M. (1999). Role of human Cds1 (Chk2) kinase in DNA damage checkpoint and its regulation by p53. The Journal of biological chemistry *274*, 31463-31467.

Tong, W.M., Ohgaki, H., Huang, H., Granier, C., Kleihues, P., and Wang, Z.Q. (2003). Null mutation of DNA strand break-binding molecule poly(ADP-ribose) polymerase causes medulloblastomas in p53(-/-) mice. The American journal of pathology *162*, 343-352.

Trapnell, C., Williams, B.A., Pertea, G., Mortazavi, A., Kwan, G., van Baren, M.J., Salzberg, S.L., Wold, B.J., and Pachter, L. (2010). Transcript assembly and quantification by RNA-Seq reveals unannotated transcripts and isoform switching during cell differentiation. Nature biotechnology *28*, 511-515.

Triviai, I., Zeschke, S., Rentel, J., Spanakis, M., Scherer, T., Gabdoulline, R., Panagiota, V., Thol, F., Heuser, M., Stocking, C., *et al.* (2019). ASXL1/EZH2 mutations promote clonal expansion of neoplastic HSC and impair erythropoiesis in PMF. Leukemia *33*, 99-109.

Tschopp, O., Yang, Z.Z., Brodbeck, D., Dummler, B.A., Hemmings-Mieszczak, M., Watanabe, T., Michaelis, T., Frahm, J., and Hemmings, B.A. (2005). Essential role of protein kinase B gamma (PKB gamma/Akt3) in postnatal brain development but not in glucose homeostasis. Development (Cambridge, England) *132*, 2943-2954.

Turcot, J., Despres, J.P., and St Pierre, F. (1959). Malignant tumors of the central nervous system associated with familial polyposis of the colon: report of two cases. Diseases of the colon and rectum *2*, 465-468.

Uziel, T., Zindy, F., Xie, S., Lee, Y., Forget, A., Magdaleno, S., Rehg, J.E., Calabrese, C., Solecki, D., Eberhart, C.G., *et al.* (2005). The tumor suppressors Ink4c and p53 collaborate independently with Patched to suppress medulloblastoma formation. Genes & development *19*, 2656-2667.

Valtz, N.L., Hayes, T.E., Norregaard, T., Liu, S.M., and McKay, R.D. (1991). An embryonic origin for medulloblastoma. The New biologist *3*, 364-371.

Van Keymeulen, A., Lee, M.Y., Ousset, M., Brohée, S., Rorive, S., Giraddi, R.R., Wuidart, A., Bouvencourt, G., Dubois, C., Salmon, I., *et al.* (2015). Reactivation of multipotency by oncogenic PIK3CA induces breast tumour heterogeneity. Nature *525*, 119-123.

Van Meir, E.G. (1998). "Turcot's syndrome": phenotype of brain tumors, survival and mode of inheritance. International journal of cancer *75*, 162-164.

Vanner, R.J., Remke, M., Gallo, M., Selvadurai, H.J., Coutinho, F., Lee, L., Kushida, M., Head, R., Morrissy, S., Zhu, X., *et al.* (2014). Quiescent sox2(+) cells drive hierarchical growth and relapse in sonic hedgehog subgroup medulloblastoma. Cancer Cell *26*, 33-47.

Vladoiu, M.C., El-Hamamy, I., Donovan, L.K., Farooq, H., Holgado, B.L., Sundaravadanam, Y., Ramaswamy, V., Hendrikse, L.D., Kumar, S., Mack, S.C., *et al.* (2019). Childhood cerebellar tumours mirror conserved fetal transcriptional programs. Nature *572*, 67-73.

Vo, B.T., Kwon, J.A., Li, C., Finkelstein, D., Xu, B., Orr, B.A., Sherr, C.J., and Roussel, M.F. (2018). Mouse medulloblastoma driven by CRISPR activation of cellular Myc. Scientific reports *8*, 8733.

Vo, B.T., Li, C., Morgan, M.A., Theurillat, I., Finkelstein, D., Wright, S., Hyle, J., Smith, S.M.C., Fan, Y., Wang, Y.D., *et al.* (2017). Inactivation of Ezh2 Upregulates Gfi1 and Drives Aggressive Myc-Driven Group 3 Medulloblastoma. Cell reports *18*, 2907-2917.

Voronova, A., Coyne, E., Al Madhoun, A., Fair, J.V., Bosiljcic, N., St-Louis, C., Li, G., Thurig, S., Wallace, V.A., Wiper-Bergeron, N., *et al.* (2013). Hedgehog signaling regulates MyoD expression and activity. The Journal of biological chemistry *288*, 4389-4404.

Waddington, C. (1957). The Cybernetics of Development. In The Strategy of Genes (Bristol: George Allen & Unwin).

Wallace, V.A.J.C.B. (1999). Purkinje-cell-derived Sonic hedgehog regulates granule neuron precursor cell proliferation in the developing mouse cerebellum. *9*, 445-448.

Walter, G.F., and Brucher, J.M. (1979). Ultrastructural study of medullomyoblastoma. Acta neuropathologica *48*, 211-214.

Wang, G., Zhu, H., Situ, C., Han, L., Yu, Y., Cheung, T.H., Liu, K., and Wu, Z.J.T.E.j. (2018). p110α of PI3K is necessary and sufficient for quiescence exit in adult muscle satellite cells. *37*, e98239.

Wang, V.Y., Rose, M.F., and Zoghbi, H.Y. (2005). Math1 expression redefines the rhombic lip derivatives and reveals novel lineages within the brainstem and cerebellum. Neuron *48*, 31-43.

Ward, I.M., and Chen, J. (2001). Histone H2AX is phosphorylated in an ATR-dependent manner in response to replicational stress. The Journal of biological chemistry *276*, 47759-47762.

Waszak, S.M., Northcott, P.A., Buchhalter, I., Robinson, G.W., Sutter, C., Groebner, S., Grund, K.B., Brugières, L., Jones, D.T., and Pajtler, K.W.J.T.L.O. (2018). Spectrum and prevalence of genetic predisposition in medulloblastoma: a retrospective genetic study and prospective validation in a clinical trial cohort. *19*, 785-798.

Wechsler-Reya, R.J., and Scott, M.P.J.N. (1999). Control of neuronal precursor proliferation in the cerebellum by Sonic Hedgehog. *22*, 103-114.

Weinberg, R. (2007). The Biology of Cancer (New York: Garland Science).

Weishaupt, H., Johansson, P., Sundström, A., Lubovac-Pilav, Z., Olsson, B., Nelander, S., and Swartling, F.J. (2019). Batch-normalization of cerebellar and medulloblastoma gene expression datasets utilizing empirically defined negative control genes. Bioinformatics (Oxford, England) *35*, 3357-3364.

Wetmore, C., Eberhart, D.E., and Curran, T. (2001). Loss of p53 but not ARF accelerates medulloblastoma in mice heterozygous for patched. Cancer research *61*, 513-516.

Wiedmann, M., Wang, X., Tang, X., Han, M., Li, M., and Mao, Z. (2005). PI3K/Akt-dependent regulation of the transcription factor myocyte enhancer factor-2 in insulin-like growth factor-1- and membrane depolarization-mediated survival of cerebellar granule neurons. Journal of neuroscience research *81*, 226-234.

Wilsker, D., Petermann, E., Helleday, T., and Bunz, F. (2008). Essential function of Chk1 can be uncoupled from DNA damage checkpoint and replication control. Proceedings of the National Academy of Sciences of the United States of America *105*, 20752-20757.

Wilson, B.G., and Roberts, C.W.J.N.R.C. (2011). SWI/SNF nucleosome remodellers and cancer. *11*, 481-492.

Wilson, B.G., Wang, X., Shen, X., McKenna, E.S., Lemieux, M.E., Cho, Y.J., Koellhoffer, E.C., Pomeroy, S.L., Orkin, S.H., and Roberts, C.W. (2010). Epigenetic antagonism between polycomb and SWI/SNF complexes during oncogenic transformation. Cancer Cell *18*, 316-328.

Wojcinski, A., Lawton, A.K., Bayin, N.S., Lao, Z., Stephen, D.N., and Joyner, A.L. (2017). Cerebellar granule cell replenishment postinjury by adaptive reprogramming of Nestin(+) progenitors. Nature neuroscience *20*, 1361-1370.

Wright, K.D., von der Embse, K., Coleman, J., Patay, Z., Ellison, D.W., and Gajjar, A. (2012). Isochromosome 17q, MYC amplification and large cell/anaplastic phenotype in a case of medullomyoblastoma with extracranial metastases. Pediatric blood & cancer *59*, 561-564.

Xu, Q., and Wu, Z. (2000). The insulin-like growth factor-phosphatidylinositol 3-kinase-Akt signaling pathway regulates myogenin expression in normal myogenic cells but not in rhabdomyosarcoma-derived RD cells. The Journal of biological chemistry *275*, 36750-36757.

Xu, X., Yu, Y., Zong, K., Lv, P., and Gu, Y. (2019). Up-regulation of IGF2BP2 by multiple mechanisms in pancreatic cancer promotes cancer proliferation by activating the PI3K/Akt signaling pathway. Journal of experimental & clinical cancer research : CR *38*, 497.

Yam, P.T., and Charron, F. (2013). Signaling mechanisms of non-conventional axon guidance cues: the Shh, BMP and Wnt morphogens. Current opinion in neurobiology *23*, 965-973.

Yam, P.T., Langlois, S.D., Morin, S., and Charron, F. (2009). Sonic hedgehog guides axons through a noncanonical, Src-family-kinase-dependent signaling pathway. Neuron *62*, 349-362.

Yamada, M., Seto, Y., Taya, S., Owa, T., Inoue, Y.U., Inoue, T., Kawaguchi, Y., Nabeshima, Y., and Hoshino, M. (2014). Specification of spatial identities of cerebellar neuron progenitors by ptf1a and atoh1 for proper production of GABAergic and glutamatergic neurons. The Journal of neuroscience : the official journal of the Society for Neuroscience *34*, 4786-4800.

Yamasaki, T., Kawaji, K., Ono, K., Bito, H., Hirano, T., Osumi, N., and Kengaku, M. (2001). Pax6 regulates granule cell polarization during parallel fiber formation in the developing cerebellum. Development (Cambridge, England) *128*, 3133-3144.

Yan, C.T., Kaushal, D., Murphy, M., Zhang, Y., Datta, A., Chen, C., Monroe, B., Mostoslavsky, G., Coakley, K., Gao, Y., *et al.* (2006). XRCC4 suppresses medulloblastomas with recurrent translocations in p53-deficient mice. Proceedings of the National Academy of Sciences of the United States of America *103*, 7378-7383.

Yang, H., Kurtenbach, S., Guo, Y., Lohse, I., Durante, M.A., Li, J., Li, Z., Al-Ali, H., Li, L., Chen, Z., *et al.* (2018). Gain of function of ASXL1 truncating protein in the pathogenesis of myeloid malignancies. Blood *131*, 328-341.

Yang, Z.-J., Ellis, T., Markant, S.L., Read, T.-A., Kessler, J.D., Bourboulas, M., Schüller, U., Machold, R., Fishell, G., and Rowitch, D.H.J.C.c. (2008). Medulloblastoma can be initiated by deletion of Patched in lineage-restricted progenitors or stem cells. *14*, 135-145.

Yao, M., Ventura, P.B., Jiang, Y., Rodriguez, F.J., Wang, L., Perry, J.S.A., Yang, Y., Wahl, K., Crittenden, R.B., Bennett, M.L., *et al.* (2020). Astrocytic trans-Differentiation Completes a Multicellular Paracrine Feedback Loop Required for Medulloblastoma Tumor Growth. Cell *180*, 502-520.e519.

Yauch, R.L., Dijkgraaf, G.J., Alicke, B., Januario, T., Ahn, C.P., Holcomb, T., Pujara, K., Stinson, J., Callahan, C.A., Tang, T., *et al.* (2009). Smoothened mutation confers resistance to a Hedgehog pathway inhibitor in medulloblastoma. Science (New York, NY) *326*, 572-574.

Yin, W.C., Satkunendran, T., Mo, R., Morrissy, S., Zhang, X., Huang, E.S., Uusküla-Reimand, L., Hou, H., Son, J.E., Liu, W., *et al.* (2019). Dual Regulatory Functions of SUFU and Targetome of GLI2 in SHH Subgroup Medulloblastoma. Developmental cell *48*, 167-183.e165.

Yoshino, S., Etoh, Y., Konishi, Y., Iwaki, T., Okada, H., Nishida, T., Imai, T., Isobe, K., Itoh, S., and Tamiya, T. (2011). A case of medullomyoblastoma. Pediatrics international : official journal of the Japan Pediatric Society *53*, 399-402.

Youn, H.S., Kim, T.Y., Park, U.H., Moon, S.T., An, S.J., Lee, Y.K., Hwang, J.T., Kim, E.J., and Um, S.J. (2017). Asxl1 deficiency in embryonic fibroblasts leads to cellular senescence via impairment of the AKT-E2F pathway and Ezh2 inactivation. Scientific reports *7*, 5198.

Yue, F., Bi, P., Wang, C., Shan, T., Nie, Y., Ratliff, T.L., Gavin, T.P., and Kuang, S.J.N.c. (2017). Pten is necessary for the quiescence and maintenance of adult muscle stem cells. *8*, 1-13.

Yuzyuk, T., Fakhouri, T.H., Kiefer, J., and Mango, S.E. (2009). The polycomb complex protein mes-2/E(z) promotes the transition from developmental plasticity to differentiation in C. elegans embryos. Developmental cell *16*, 699-710.

Zhan, X., Shi, X., Zhang, Z., Chen, Y., and Wu, J.I. (2011). Dual role of Brg chromatin remodeling factor in Sonic hedgehog signaling during neural development. Proceedings of the National Academy of Sciences of the United States of America *108*, 12758-12763.

Zhang, J., Haider, S., Baran, J., Cros, A., Guberman, J.M., Hsu, J., Liang, Y., Yao, L., and Kasprzyk, A. (2011a). BioMart: a data federation framework for large collaborative projects. Database : the journal of biological databases and curation *2011*, bar038.

Zhang, J., Walsh, M.F., Wu, G., Edmonson, M.N., Gruber, T.A., Easton, J., Hedges, D., Ma, X., Zhou, X., and Yergeau, D.A.J.N.E.J.o.M. (2015). Germline mutations in predisposition genes in pediatric cancer. *373*, 2336-2346.

Zhang, L., He, X., Liu, X., Zhang, F., Huang, L.F., Potter, A.S., Xu, L., Zhou, W., Zheng, T., Luo, Z., *et al.* (2019). Single-Cell Transcriptomics in Medulloblastoma Reveals Tumor-Initiating Progenitors and Oncogenic Cascades during Tumorigenesis and Relapse. Cancer Cell *36*, 302-318.e307.

Zhang, P., Chen, Z., Li, R., Guo, Y., Shi, H., Bai, J., Yang, H., Sheng, M., Li, Z., Li, Z., *et al.* (2018). Loss of ASXL1 in the bone marrow niche dysregulates hematopoietic stem and progenitor cell fates. Cell discovery *4*, 4.

Zhang, W., Hong, M., Bae, G.U., Kang, J.S., and Krauss, R.S. (2011b). Boc modifies the holoprosencephaly spectrum of Cdo mutant mice. Disease models & mechanisms *4*, 368-380.

Zhou, Q., and Melton, D.A. (2008). Extreme makeover: converting one cell into another. Cell stem cell *3*, 382-388.

Zhu, B., Ramachandran, B., and Gulick, T. (2005). Alternative pre-mRNA splicing governs expression of a conserved acidic transactivation domain in myocyte enhancer factor 2 factors of striated muscle and brain. The Journal of biological chemistry *280*, 28749-28760.

Zhu, G., Rankin, S.L., Larson, J.D., Zhu, X., Chow, L.M., Qu, C., Zhang, J., Ellison, D.W., and Baker, S.J. (2017). PTEN Signaling in the Postnatal Perivascular Progenitor Niche Drives Medulloblastoma Formation. Cancer research *77*, 123-133.

Zindy, F., Nilsson, L.M., Nguyen, L., Meunier, C., Smeyne, R.J., Rehg, J.E., Eberhart, C., Sherr, C.J., and Roussel, M.F. (2003). Hemangiosarcomas, medulloblastomas, and other tumors in Ink4c/p53-null mice. Cancer research *63*, 5420-5427.

Zuckermann, M., Hovestadt, V., Knobbe-Thomsen, C.B., Zapatka, M., Northcott, P.A., Schramm, K., Belic, J., Jones, D.T., Tschida, B., Moriarity, B., *et al.* (2015). Somatic CRISPR/Cas9-mediated tumour suppressor disruption enables versatile brain tumour modelling. Nature communications *6*, 7391.

Zurawel, R.H., Chiappa, S.A., Allen, C., and Raffel, C. (1998). Sporadic medulloblastomas contain oncogenic beta-catenin mutations. Cancer research *58*, 896-899.